DOKUZ EYLÜL UNIVERSITY

GRADUATE SCHOOL OF NATURAL AND APPLIED SCIENCES

OPTIMIZATION OF SHIP DIESEL GENERATORS TO IMPROVE THE ENERGY EFFICIENCY AND POWER MANAGEMENT

by

Onur YÜKSEL

February, 2022

İZMİR

OPTIMIZATION OF SHIP DIESEL GENERATORS TO IMPROVE THE ENERGY EFFICIENCY AND POWER MANAGEMENT

A Thesis Submitted to the

Graduate School of Natural and Applied Sciences of Dokuz Eylül University

In Partial Fulfillment of the Requirements for the Degree of Doctor of

Philosophy in Marine Engineering, Marine Transportation Systems Engineering Program

by

Onur YÜKSEL

February, 2022

İZMİR

Ph.D. THESIS EXAMINATION RESULT FORM

We have read the thesis entitled **"OPTIMIZATION OF SHIP DIESEL GENERATORS TO IMPROVE THE ENERGY EFFICIENCY AND POWER MANAGEMENT"** completed by **ONUR YÜKSEL** under supervision of **ASST. PROF. DR. BURAK KÖSEOĞLU** and we certify that in our opinion it is fully adequate, in scope and in quality, as a thesis for the degree of Doctor of Philosophy.

…….

Asst. Prof. Dr. Burak KÖSEOĞLU

Supervisor

……..	……...
Asst. Prof. Dr. Mustafa NURAN	Prof. Dr. Efendi NASİBOĞLU
Thesis Committee Member	Thesis Committee Member
……..	……...
Assoc. Prof. Dr. Hakan DEMİREL	Assoc. Prof. Dr. Görkem KÖKKÜLÜNK
Examining Committee Member	Examining Committee Member

Prof. Dr. Okan FISTIKOĞLU
Director

Graduate School of Natural and Applied Sciences

ACKNOWLEDGMENT

I would like to thank my supervisor Burak KÖSEOĞLU, as well as Efendi NASİBOĞLU and Mustafa NURAN, for their guidance throughout this thesis.

Thank you to my parents and my wife, Sevil YÜKSEL, for constantly listening to me rant and talk things out, and for the sacrifices you have made for me to pursue a PhD degree.

I would like to thank a fellow marine engineer Ömürcan YILDIZ for his help for ensuring data collection and my coworkers Olgun KONUR and Süleyman Aykut KORKMAZ for their contributions and support.

Onur YÜKSEL

OPTIMIZATION OF SHIP DIESEL GENERATORS TO IMPROVE THE ENERGY EFFICIENCY AND POWER MANAGEMENT

ABSTRACT

The gradual reduction and minimization of air polluting gases originating from ships is the focus of priorly the International Maritime Organization and the maritime industry. In this context, intensive work is being done on various improvements and innovations on propulsion and electricity generation facilities that produce harmful gases on ships. In particular, the support of the ship power distribution system with alternative energy systems and the optimization of these systems has the potential to contribute to the reduction of polluting gases originating from the facility. In this thesis, a system proposal that can be quickly applied to the ship power generation facility has been studied. An analysis of how much fuel saving will be achieved in cases where the battery set to be added to the system is charged using generators or waste heat system has been conducted. To perform this analysis, the mathematical model of the ship diesel generator system was created using Python and MATLAB, using the operational data taken from the ship and the technical specifications of the generators. The simulation models the load distributions of diesel generators according to the changing electricity needs and determines their fuel consumption depending on the generator loads. The validation of this model was carried out with the data taken from the ship and the outputs of the tests performed by the manufacturer. Various multi-criteria decision-making methods were used in the selection of the most suitable battery system. The economic performances of the systems were also compared, and the future fuel savings were estimated using regression algorithms. The proposed systems have the potential to provide fuel savings of up to 8,618% when the generators are charging, and up to 18,145% when the waste system is used. In 20 years, 6888.969 t can be saved by utilization of the proposed system.

Keywords: Marine diesel generators, mathematical modeling, multi attribute decision making, regression analysis, ship emissions, economic analysis.

ENERJİ VERİMLİLİĞİ VE GÜÇ YÖNETİMİNİ GELİŞTİRMEK İÇİN GEMİ DİZEL JENERATÖRLERİNİN OPTİMİZASYONU

ÖZ

Gemilerden kaynaklı hava kirletici gazların kademeli olarak azaltılarak en az seviyeye indirilmesi, Uluslararası denizcilik örgütü başta olmak üzere, denizcilik sektörünün odak noktasıdır. Bu bağlamda, gemiler üzerinde zararlı gazların üretilmesini sağlayan itki ve elektrik üretim tesisleri üzerinde çeşitli iyileştirmeler ve yenilikler üzerinde yoğun olarak çalışılmaktadır. Özellikle gemi güç dağıtım sisteminin alternatif enerji sistemleri ile desteklenmesi ve bu sistemlerin optimizasyonu tesisten kaynaklı kirletici gazların azaltmasına katkı sağlama potansiyeline sahiptir. Bu tezde gemi elektrik üretim tesisine hızlı bir şekilde uygulanabilecek bir sistem önerisi üzerinde çalışılmıştır. Sisteme eklenecek batarya setinin jeneratörler veya atık ısı sistemi kullanılarak şarj edildiği durumlarda ne kadar yakıt tüketimi tasarrufu sağlanacağının analizi gerçekleştirilmiştir. Bu analizi gerçekleştirmek için gemiden alınmış operasyon verileri ve jeneratörlerin teknik özellikleri kullanılarak, gemi dizel jeneratör sisteminin matematik modeli Python ve MATLAB kullanılarak oluşturulmuştur. Simülasyon, dizel jeneratörlerin değişen elektrik ihtiyacına göre yük dağılımlarını modellemekte ve jeneratör yüklerine bağlı olarak yakıt tüketimlerini belirlemektedir. Bu modelin doğrulaması gemiden alınan veriler ve üretici firmanın gerçekleştirdiği testlerin çıktıları ile gerçekleştirilmiştir. En uygun batarya sisteminin seçiminde çeşitli çok kriterli karar verme yöntemleri kullanılmıştır. Sistemlerin ekonomik performansları da karşılaştırılmış ve gelecekteki yakıt tasarrufu miktarları regresyon algoritmalar kullanılarak tahmin edilmiştir. Jeneratörlerin şarj ettiği durumda %8,618'e kadar, atık sistemi kullanıldığında %18,145 oranına kadar yakıt tasarrufu sağlama potansiyeli bulunmaktadır. Önerilen sistemin kullanılması, 20 yıllık periyotta 6888,969 t yakıt tasarrufu sağlamaktadır.

Anahtar kelimeler: Gemi dizel jeneratörleri, matematik modelleme, çok kriterli karar verme, regresyon analizi, gemi emisyonları, ekonomik analiz.

CONTENTS

Ph.D. THESIS EXAMINATION RESULT FORM……ii
ACKNOWLEDGEMENTS……iii
ABSTRACT……iv
ÖZ……v
LIST OF FIGURES……vii
LIST OF TABLES……xi

CHAPTER 1 - INTRODUCTION.....1

1.1 Motivation.....3
1.2 Objectives.....3
1.3 Data Collection.....4
1.4 Thesis Outline.....5

CHAPTER 2 - BACKGROUND AND LITERATURE REVIEW 6

2.1 Marine Diesel Engines 7
2.2 Synchronous Generators.....8
2.3 Literature Review.....13
2.3.1 Studies Focus on Calculation and Prediction of Fuel Consumption or Emissions Onboard.....13
2.3.2 Studies Focus on Alternative Energy and Hybrid Applications Onboard.21
2.3.3 Studies Focus on the Optimization of Hybrid System Onboard.....25

CHAPTER 3 - METHODOLOGY AND MODEL DESCRIPTION 31

3.1 Ship Power Distribution System Model Description.....32
3.2 Multi-attribute Decision-Making Methods.....35
3.2.1 Technique for Order of Preference by Similarity to Ideal Solution (TOPSIS) 37

3.2.2 Multi-Objective Optimization on the Basis of Ratio Analysis (MOORA). 39
3.2.3 Preference Ranking Organization Method for Enrichment of Evaluations (PROMETHEE) 40
3.2.4 Determination of Criteria Weights 43
3.3 Hybrid Ship Power Distribution Plant Model Description 45
3.4 Emission Calculation 56
3.5 Fuel Consumption Estimation Algorithms 56
3.5.1 Time Series Analysis 56
3.5.2 Ordinary Least Squares Regression 59
3.5.3 Support Vector Regression 61
3.5.4 Artificial Neural Networks 62
3.5.5 Model evaluation and data standardization 63
3.6 Economic Analysis 64

CHAPTER 4 - RESULTS AND DISCUSSIONS 66

4.1 Model Validation 66
4.2 Outcomes of the Ship Power Distribution System Model 72
4.3 Outcomes of the Hybrid Ship Power Distribution System Model 77
4.4 Results of Fuel Consumption and SoH Prediction 85
4.4.1 Results of the Fuel Consumption Prediction 85
4.4.2 Results of the SoH Prediction 94
4.5 Results of the Economic Analysis 95

CHAPTER 5 - CONCLUSIONS 99

REFERENCES 104

LIST OF FIGURES

Page

Figure 2.1 Simplified ship power distribution system 6
Figure 2.2 Simplified phasor diagram of a synchronous generator 10
Figure 2.3 Time dependent semi logarithmic fault plot of the AC component 13
Figure 3.1 Power distribution system modeling and FC estimation workflow 31
Figure 3.2 Ship hybrid power distribution system modeling and FC estimation workflow 32
Figure.3.3 The algorithm scheme of the mathematical model. 35
Figure.3.4 The algorithm scheme of the battery selection program. 36
Figure 3.5 TOPSIS method flow diagram 37
Figure 3.6 PROMETHEE method flow diagram 41
Figure 3.7 Weighting techniques classification 44
Figure 3.8 Charge curve of battery 1 47
Figure 3.9 Discharge curve of battery 1 47
Figure 3.10 Charge and discharge curves of batteries 2,3 and 4 48
Figure 3.11 Charge and discharge curves of batteries 5 and 6 48
Figure 3.12 Aging curve of battery 1 48
Figure 3.13 Aging curve of batteries 2 and 3 49
Figure 3.14 Aging curve of battery 4 49
Figure 3.15 Aging curve of battery 5 49
Figure 3.16 Aging curves of battery 6 50
Figure 3.17 Algorithm scheme of the model when generators charge the batteries 50
Figure 3.18 Diagram of ship hybrid electric distribution system when generators charge batteries 50
Figure 3.19 Circuit diagram for batteries 1, 2, 3, 4, 6 51
Figure 3.20 Circuit diagram of the battery 5. 51
Figure 3.21 Exhaust flow diagram of the WHRS 53
Figure 3.22 Working diagram of the WHRS 53

Figure 3.23 Diagram of ship hybrid electric distribution system when WHRS charge batteries 54
Figure 3.24 Algorithm scheme of the model when WHRS charges the batteries 55
Figure 3.25 Circuit diagram for batteries 1, 2, 3, 4, 6 with WHRS charge 55
Figure 3.26. Circuit diagram of the battery 5 with WHRS charge. 55
Figure 3.27 SVR Example 61
Figure 3.28 ANN structure 63
Figure 3.30 IFO 380 prices 65
Figure 3.31 MGO prices 65
Figure 4.1 Measured and calculated line voltage comparison 67
Figure 4.2 Test and calculated generator output power comparison. 68
Figure 4.3 Frequency drop of the generator 1 vs power 68
Figure 4.4 Frequency drop of the generator 2 vs power. 69
Figure 4.5 Frequency drop of the generator 3 vs power. 69
Figure 4.6 Power of generator 1 vs total system load 70
Figure 4.7 Power of generator 2 vs total system load 70
Figure 4.8 Power of generator 3 vs total system load. 71
Figure 4.9 Frequency drop of the system vs increasing total system load 71
Figure 4.10 Theoretical induced power vs armature current in the generator 72
Figure 4.11 Internally generated voltage vs armature current in the generator. 73
Figure 4.12 Brake-specific fuel oil consumptions of prime movers regarding engine rpm. 73
Figure 4.13 Fuel oil consumptions of prime movers depending on engine rpm. 74
Figure 4.14 Transmitted power of prime mover vs engine load. 74
Figure 4.15 Transient current behavior when a fault occurs at the terminals of the generator. 75
Figure 4.16 The distribution of utilization hours according to operation modes 76
Figure 4.17 The distribution of FC according to operation modes 76
Figure 4.18 Total emissions from the plant 77
Figure 4.19 The distribution of FC regarding operation modes for each battery combination with generator charge 82

Figure 4.20 The distribution of FC regarding operation modes for each battery combination with WHRS charge 84
Figure 4.21 FC of the normal operation regarding operation hours 86
Figure 4.22 ACF and PACF plots of the hourly FC data 87
Figure 4.23 Analogy of actual and predicted data for ARIMA (0, 2, 2) 88
Figure 4.24 Analogy of actual and predicted data for OLS regression 88
Figure 4.25 Analogy of actual and predicted data for SVR regression 88
Figure 4.26 Analogy of actual and predicted data for ANN 89
Figure 4.27 Analogy of FC actual and predicted data for hybrid plant combinations. 91
Figure 4.28 Analogy of SoH actual and predicted data for OLS. 94
Figure 4.29 EPC of each combination 96
Figure 4.30 LEC of each combination 96
Figure 4.31 PBP of each combination 97

LIST OF TABLES

Page

Table 2.1 Summary table of the FC calculation and prediction studies 18
Table 2.2 Summary table of studies that covers hybrid ship power and propulsion systems 24
Table 2.3 Summary table of studies that covers hybrid system optimization on marine vessels 28
Table 3.1 General information about the generator. 33
Table 3.2 Operational modes used in the model. 34
Table 3.3. Preference functions 42
Table 3.4 Specifications of batteries 45
Table 3.5 Charge and discharge hour combinations 46
Table 3.6 Power production from DG WH 52
Table 3.7 Power production from ME WH 52
Table 3.8 EF (g emission/ g fuel) 56
Table 3.9 Characteristics of the ACF and the PACF of AR and MA processes 58
Table 4.1 Emissions from diesel generators according to operation modes. 77
Table 4.2 Weight calculation results with objective weighting methods 79
Table 4.3 Top three selections of MADM methods. 79
Table 4.4 Battery combinations used in the plant 79
Table 4.5 FC and FS of the hybrid plant when batteries are charged by generators. . 81
Table 4.6 FC and FS of the hybrid plant when batteries are charged by WHRS. 81
Table 4.7 FS regarding operation modes when generators charge batteries 81
Table 4.8 Emissions from the hybrid plant with C1 generator charging 82
Table 4.9 Emissions of the hybrid plant with C2 generator charging 82
Table 4.10 Emissions of the hybrid plant with C3 generator charging 83
Table 4.11 Total emissions and ER of combinations with generator charging 83
Table 4.12 FS in regard of operation modes when the WHRS charge batteries 83
Table 4.13 Emissions of the hybrid plant with C1 WHRS charging 84
Table 4.14 Emissions of the hybrid plant with C2 when the WHRS charging 85

Table 4.15 Emissions of the hybrid plant with C3 when the WHRS charging.....85
Table 4.16 Total emissions and ER of combinations with WHRS charging.....85
Table 4.17 Results of the ARIMA order search.....87
Table 4.18 Model evaluation metrics and one-year FC predictions.....89
Table 4.19 Emission estimation of OLS.....90
Table 4.20 Performance metrics of OLS for hybrid plant FC estimation.....91
Table 4.21 FC and FS of each combination in future periods.....91
Table 4.22 Emissions from the hybrid plant in the future periods with different battery and charging combinations. 92
Table 4.23 Emission reductions of hybrid plants in the future periods with various battery and charging combinations.....93
Table 4.24 Performance metrics of OLS for SoH Prediction and battery life regarding combinations 94
Table 4.25 Fuel, investment, and maintenance costs of combinations.....95
Table 4.26 Profits and losses of combinations during the system lifetime.....97

CHAPTER 1
INTRODUCTION

Greenhouse gases (GHG) is the major cause of the climate change which is a substantial problem for the globe. Since the source of the GHG is usage of fossil fuels, the systems that lowers or prevents this usage becomes essential in every industrial sector (Yan, 2021). Maritime sector has a massive impact on the global warming because ships and ports take major actions to transport the cargo around the world. In fact, maritime transportation ensures over 85% of global trade that causes a remarkable amount of air pollution (UNCTAD, 2018; Eyring et al., 2005; Sirimanne et al., 2019). To procure the control over the shipping emissions, International Maritime Organization (IMO) sets limits to the specific pollutants sourced by marine vessels. These limits are mandatory and published in Annex 6 of the International Convention for the Prevention of Pollution from Ships (MARPOL). For instance, limit of Sulphur Oxide (SO_x) emissions lowered to 0.5% from 3.5% outside specified emission control areas (ECA) on 1 January 2020. The limit is firmer in ECA, which is 0.1%. These amendments can provide environmental and health advantages for the globe since SO_x causes the acid rains. These restrictions caused an increment of very low Sulphur fuel oil (VLSFO) usage on board. Some vessels implemented SO_x treatment technologies such as scrubber systems (IMO, 2019). Nitrogen oxides (NO_x) emissions are aimed to reduce as well. Since 1 January 2016, IMO has made compulsory reduction of the NO_x limit of 3.4 g/kWh for engines with 130 rpm or lower and 2 g/kWh if the engine speed is 2000 rpm or higher. These regulations are also made necessary the application of NO_x reduction technologies on board (IMO 2, 2019). Carbon oxides (CO_x) have been an issue for the world for a long time and both IMO and European Commission collect fuel consumption (FC) data from ships over 5000 gross tonnages to detect mainly carbon oxides (IMO3, 2019; EC, 2020). Carbon oxides are CO and CO_2, the former can be prevented with an efficient combustion in marine diesel engines. Decreasing of CO_2 can be ensured with low FC or using an alternative fuel to petroleum-based fuels. Although studies on the alternative fuels for diesel engines show very high potential, they require a retrofit on the current engines on ships. Therefore, lowering fuel consumptions is most applicable method and it can be ensured with an energy

management strategy for the ships. IMO made mandatory The Energy Efficiency Design Index (EEDI) was for new ships and the Ship Energy Efficiency Management Plan (SEEMP) for all ships to ensure the energy management on board (IMO2, 2020; Seddiek & Elgohary, 2014). The energy efficiency increment and FC reduction are an up-to-date topic among marine industry so, there are various studies about the subject. Ship operation adjustments such as, route, trim optimization and reducing length of ballast legs can be applied to existing ships. Optimization and application of emission control strategies and alternative methods such as shortening the port stay time, optimization of navigation speed according to optimal engine speed are also applied and studied. Some researchers concentrate on waste heat recovery systems to reduce FC and improve energy efficiency. In addition, there are numerous research about various fuel changes, electric-propulsion, hull, or propeller design optimization and adding an alternative energy source to the existing system. The first two requires retrofit or new building of the ship, but effects on last one can be seen faster and it can be applied to existing ships easily (Nishida et. al., 2011; Norstad et. al., 2011; Xie, 2011; Shao et. al., 2012; Motley et. al., 2012; Baldi et. al., 2015; Attah & Bucknall, 2015; Zhu et. al., 2017; Nuchturee, Li & Xia, 2020; Frangopoulos, 2020).

One of the major sources of the electrical energy production is using synchronous machines (Boldea, 2015). Especially, in the marine vessels they are widely used and in most of the commercial ships driven by diesel engine as the prime mover for three-phase electric generation. The number of generators on board can change with dimension and electrical needs of the ship. Typically, three generators are used in most of the commercial vessels and according to the type of the operation, number of running generators can vary. For example, in the most of ships, when the ship on the route without tank heating or any additional operation, one generator can be enough for the electrical supply. However, operations like cargo handling or tank heating require much more energy and all the generators are running while carrying out such operations. The prime mover of the synchronous machine can burn types of fuel oil or marine diesel oil on board ships (McGeorge, 1998). Marine diesel generators are continuous emission producers that causes, particularly air pollution, especially near

urban and port areas. That's why, efficiency improvements which can reduce the FC of the system, gains substantial significance (Dragović et al. ,2018).

1.1 Motivation

As mentioned above, viable and quick applications that can lower the FC of marine diesel engines are the focus of the maritime sector. Specially, reducing air pollution in the areas which are close to the port is significant from environmental and health aspects. Lowering the FC of the ship electricity generation system or marine diesel generators plant aids this purpose.

Creating a detailed mathematical model of the system has a crucial importance for this topic, because the shipping companies won't allow modifying their vessel's systems. This model can be used to analyze the additions such as energy storage units, alternative energy sources or waste heat recovery systems (WHRS) to the plant. In the literature there is a lacking such an elaborative and real-time based model for simulating marine diesel generators plant considering operation modes and times that has been the primary motivation of this thesis.

1.2 Objectives

The objectives of the thesis were:

- To create a comprehensive mathematical model of the marine diesel generators that involves load sharing with varying system needs, using real-time ship data.
- To determine emission production of the plant for specified date range.
- To predict future FC and emissions using the outputs of the mathematical model.
- To analyze battery pack addition to the plant using various charging strategies.
- To select the optimum energy storage configuration, charge-discharge rates and number of parallel sets by taking into battery price, weight and fuel-saving ratios consideration.

- To assess the emission reduction (ER) of the strategies for current time range and the future.
- To analyze the economic performance of the proposed configurations.

1.3 Data Collection

To model the ship electricity generation plant, the required data was taken from 50000 DWT oil/chemical tanker. The operational and technical data for construction of the simulation was gathered between 02.03.2020 and 27.05.2020. Port calls, cargo transfer and type information and position history data were obtained from MarineTraffic (2021). The mathematical simulation was developed in MATLAB and Python environment and validated using the data obtained from the ship. The plant comprises of three equivalent HIMSEN/MAN marine diesel generators with rated 1050 kW power. Gathered data were listed as:

- Port calls and position history of the ship between 06 December 2019 and 07 June 2021.
- Generator technical specifications such as, rpm, full load, no load and system frequencies, stator-rotor currents, excitation currents, load angles, load dispatches, powers, voltages, field current, power factor, efficiency, rated field current, armature phase winding resistance, field winding resistance, stator winding connection type, speed and voltage drop.
- Generator manuals, data sheet and specific FC curves.
- Working hours and maintenance schedule.
- Governor tests, parallel running tests, open and short circuit tests.
- Ship electrical schemes and electrical load test results.
- Operational data, such as, exhaust temperatures, l/o pressure and temperatures, cooling water pressure and temperatures, the fuel pressure, temperature and type.
- Pumps, heater, and other electrical components' electrical motor specifications.
- Cargo transfer pump rates.

1.4 Thesis Outline

The following chapter ensures a fundamental knowledge about working principle, types and application areas of marine diesel engines and synchronous alternators which are the main parts of the marine diesel generators. A literature review on FC reduction methods of marine diesel engines and FC estimation of marine vessels was also included.

Third chapter describes the model specifications and equations, of the marine diesel generators plant model. Firstly, the essential specifications of ship electricity generation plant were indicated. Secondly, the fundamental equations that forms the mathematical simulation were demonstrated. Thirdly, the programing logic and working principles of the simulation were described. Fourthly, emission calculation method was introduced. Specifications of appropriate batteries that can be used in the plant were shown fifthly. The battery combination selection algorithms and data set construction were indicated sixthly. The hybrid model logic and charging strategies were introduced seventhly. Finally, chapter includes the equations and working principles of prediction algorithms used to predict FC and battery life.

Fourth chapter involves the results and discussion of the analysis. Firstly, the model validation process was proposed, and validation metrics were outlined. The outputs of the simulation were indicated. Battery selection process outputs and FC reduction of the charging strategies were demonstrated. Results of prediction algorithms and economic analysis were also devoted in this chapter.

The last chapter the conclusions of the thesis were depicted, limitations and recommendations for the future studies were mentioned.

CHAPTER 2
BACKGROUND AND LITERATURE REVIEW

The chapter provides a foundational understanding of the operating principles, kinds, and applications of marine diesel engines and synchronous alternators, which are the most important components of marine diesel generators. A literature review on marine diesel engine FC reduction strategies and marine vessel FC calculation was also included.

Ship electricity generation plant consists of marine diesel generators which comprise a prime mover and a synchronous generator. The plant also has the main switchboard, which is a metal box that takes power from the diesel generator (DG) and distributes it to other machinery. Bus Bars serve as a load carrier and enable the movement of cargo from one location to another. Circuit breakers that operate as switches and are in a dangerous state can be tripped to prevent failure and accidents. Fuses are used as machine safety devices. Transformers are used to increase or decrease voltage. A step-down transformer is utilized in the distribution system to provide power to the lighting system. Large auxiliary gear receives high-voltage power from circuit breakers. Miniature circuit breakers and supply fuses are used for smaller supply circuits (Taylor, 1996). Figure 2.1 depicts the simplified ship electrical power distribution system scheme.

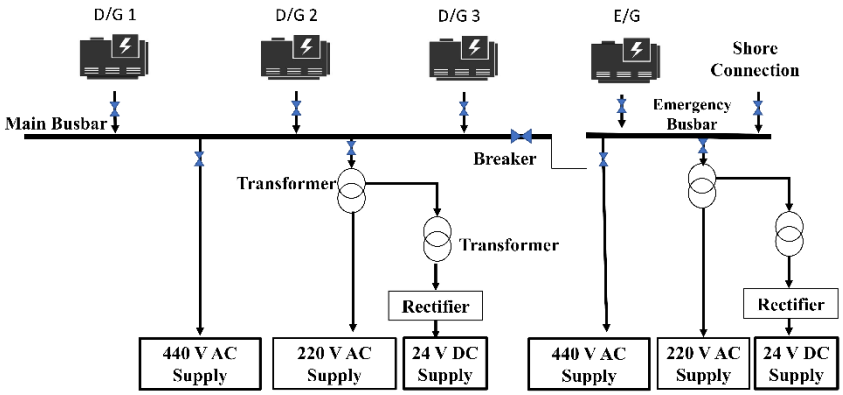


Figure 2.1 Simplified ship power distribution system (Adapted from Cahyagi & Koenhardono, 2018, Oways, 2019)

The plant generally composes of three equivalent DG to meet system electrical needs. In case of a malfunction occurs in the DG plant, an emergency generator (E/G) is automatic starts and ensures power to required equipment to run the DG plant again (McGeorge, 1998).

2.1 Marine Diesel Engines

The term prime mover is used to describe the main power source that rotates the rotor of the alternator to generate three-phase electricity. Diesel engines are the most used prime mover on commercial ships. Marine diesel engines can produce the work with two or four strokes. The low-speed engine has a range of speeds between 70 and 120 rev/min, and they are two-stroke engines used in the main propulsion plant of the ship. The medium speed marine diesel engines' speed range is between 120 to 1200 rev/min, and they produce power in four strokes. Four-stroke medium-speed marine diesel engines are preferred as the prime mover of the alternator to generate electricity onboard. Their working principle resembles the gasoline engine. In the four-stroke, intake, compression, power, and exhaust strokes can be carried out with the engine. The air is emitted and pressurized in the cylinder during the intake and compressed e compression strokes respectively. When the temperature of the compressed air is reached the desired limit, the fuel is sent into the cylinder in pulverized form for better ignition. The power stroke is achieved with the ignition of the fuel. After the power stroke, exhaust gases formed with the combustion of the fuel are removed from the cylinder during the exhaust stroke. The high-speed marine diesel engine revolution is higher than 1400 rev/min (Nichols & Williams, 2009; Woodyard, 2009).

In the mathematical model, brake-specific FC data are gathered from look-up tables provided by the manufacturer of the engine, accordingly, the load of the engine. The power and torque transmitted to the synchronous generator are calculated using the stroke, the bore and the break mean effective pressure values also gathered from the manufacturer. Equation 2.1 to 2.3 (Pulkrabek, 2004) explains the calculation process of the power and torque of the diesel engine.

$$V_d = \pi*\left(b^2/4\right)*s \quad (2.1)$$

where V_d is displacement volume, b is the bore of the piston and s is the stroke.

$$P = (V_d*n*bmep*N/1000)*\eta_t \quad (2.2)$$

where P is the transmitted power, n is the number of the cylinders which is 6 for this engine, bmep is the brake mean effective pressure and N is the number of firing strokes which can be calculated with the division of rpm to 120 for this engine and finally η_t is the transmission efficiency.

$$\tau = P/2*\pi*n*1000 \quad (2.3)$$

where τ is the transmitted torque of the engine.

2.2 Synchronous Generators

The world electricity production has been supplied by generators and they can be classified as synchronous, induction, and parametric. In the ship electricity generation plant, synchronous generators produce AC power (Boldea, 2015; McGeorge, 1998). Synchronous generators or alternators are the devices that convert the mechanical power to alternating current (AC) electrical power. The exciting current applied to rotor windings creates a magnetic field. Then, the motion provided by the prime mover rotates the rotor and that creates a rotating magnetic field inside the generator. Induction of three-phase AC is ensured by this field. Two kinds of windings exist in the generator. The first one is called field windings which generate the prior magnetic field. The second is named as stator or armature windings that produce the voltage. The rotor is a huge electromagnet, and it can have either salient or non-salient poles (Chapman, 2005; Krause et al. 2002; Boldea, 2015).

The equations to construct the mathematical model of the synchronous generators are demonstrated in this chapter. The magnetic field of the rotor indicates

which direction it returns. The relation between magnetic field, revolution speed, and stator electrical frequency (f_e) can be indicated with Equation 2.4 (Chapman 2005).

$$f_e = n_m \times p/120 \tag{2.4}$$

In Equation 2.4 n_m represents the rpm of the rotor and P typifies pole numbers. The induced voltage in a generator (E_A) can be written as:

$$E_A = K \times \omega \times \phi \tag{2.5}$$

where ϕ is the magnetic flux, K is a design coefficient, when ω is given as electrical radian/seconds it can be shown as follows:

$$K = N_c/\sqrt{2} \tag{2.6}$$

and if ω is given as mechanical radian/seconds it becomes:

$$K = N_c * P/\sqrt{2} \tag{2.7}$$

where N_c is the number of turns in the generator. E_A is directly proportional to flux and speed. Phase voltage V_ϕ is not equal to E_A because of internal losses. Phase voltage is illustrated in Equation 2.8.

$$V_\phi = E_A - jX_S I_A - R_A I_A \tag{2.8}$$

where I_A is armature current, R_A armature resistance, and X_s is synchronous reactance.

Terminal voltage (V_T) equals phase voltage (V_ϕ) if the phases Δ connected. For Y-connected phases, V_T equals $\sqrt{3V_\phi}$. The power converted from mechanical to electrical in generator (input power- P_{in}) is expressed in Equation 2.9

$$P_{in} = \tau_{app}\omega_{in} = 3E_A I_A \cos\gamma \quad (2.9)$$

where τ_{app} is the torque and ω_{in} represents the angular speed of the engine. The phase angle between E_A and I_A is denoted as γ. The difference between input power and output power gives us generator losses. The output power of a synchronous generator can be expressed with line variables (shown in Equation 2.10) and phase variables (shown in Equation 2.11). The reactive power formula is illustrated through both line and phase variables in Equations 2.12 and 2.13 respectively (Chapman, 2005; Krause et al. 2002; Boldea, 2015). Figure 2.2 shows the simplified phasor diagram of a synchronous generator whose armature resistance is neglected (Chapman 2005).

$$P_{out} = \sqrt{3}V_T I_L \cos\theta \quad (2.10)$$

$$P_{out} = 3V_\phi I_A \cos\theta \quad (2.11)$$

$$Q_{out} = \sqrt{3}V_T I_L \sin\theta \quad (2.12)$$

$$Q_{out} = 3V_\phi I_A \sin\theta \quad (2.13)$$

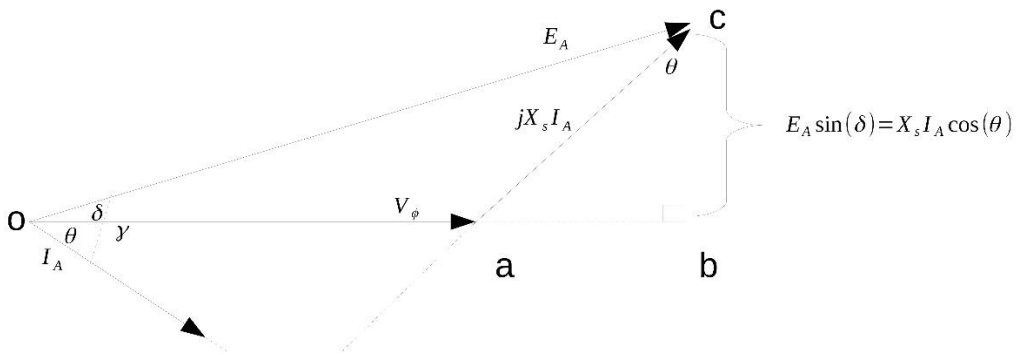


Figure 2.2 Simplified phasor diagram of a synchronous generator (Adapted from Chapman, 2005)

According to the phasor diagram of the generator, the power can be written as in the Equation 2.14.

$$P = 3V_\phi \sin(\delta)/X_s \quad (2.14)$$

Induced moment (τ_{ind}) in a synchronous generator can be obtained by regulating $P = \tau_{ind}\omega_i$equation. An alternative expression for the induced moment can be gathered by the multiplication of magnetic fields. Equations 2.15 and 2.16 show the induced moment different expressions.

$$\tau_{ind} = 3V_{\phi}E_A\sin(\delta)/(\omega_m X_s) \quad (2.15)$$

$$\tau_{ind} = kB_R B_{net}\sin(\delta) \quad (2.16)$$

where B_R represents the rotor magnetic field induced, B_{net} typifies the net magnetic field, which is the difference between stator and rotor fields, and δ symbolizes the angle between the net and rotor magnetic field.

The synchronous reactance is the ratio of induced armature voltage and armature current shown in Equation 2.17.

$$X_s = E_A/I_A \quad (2.17)$$

The voltage regulation (VR) of the generator can be found from Equation 2.19:

$$VR = ((V_{nl}-V_{fl})/V_{fl})x100\% \quad (2.18)$$

where V_{nl} symbolizes no-load voltage and V_{fl} represents the full load voltage. When the load increases, the speed of the prime mover decreases. The speed drop (SD) of the prime mover can be found from Equation 2.19:

$$SD=((n_{nl}-n_{fl})/n_{fl})\times100\% \quad (2.19)$$

where n_{nl} typifies no-load speed and n_{fl} represents the full load speed of the generator. Equation 2.20 represents the frequency power relation. S_p is the slope of the curve in Figure 4b and has a unit of kW/Hz or mW/Hz. Power is represented as P; no-load

frequency is denoted f_{nl} and system frequency is f_{sys} (Chapman, 2005; Krause et al. 2002; Boldea, 2015).

$$P = s_p*(f_{nl}-f_{sys}) \tag{2.20}$$

If two equivalent generators are run parallel in the system, the total power equals the addition of each generator's power. The formula is the same for the reactive powers. Equations of the total power and reactive power of the system are represented as Equations 2.21 and 2.22, respectively.

$$P_{tot}= P_{load}=P_{G1}+P_{G2} \tag{2.21}$$

$$Q_{tot}= Q_{load}=Q_{G1}+Q_{G2} \tag{2.22}$$

Figure 2.3 illustrates the semi-logarithmic plot of the fault component of the alternating current component versus the time graph. The figure explains the transient behavior of the synchronous generator. RMS current through the transient time is named as transient current represented by the symbol of I'. Steady state is current denoted by the symbol of I_{ss} and equals the ratio of armature voltage and synchronous reactance. The sub transient current is denoted by the symbol of I'' so, then RMS magnitude of the current at any time after a fault occurs at the terminals of the generator is:

$$I(t)=(I''-I')e^{\frac{-t}{T''}}+(I'-I_{ss})e^{\frac{-t}{T''}}+I_{ss} \tag{2.23}$$

where T'' represents the time parameter. The sub-reactive and reactive reactance are given in Equations 2.24 and 2.25 respectively (Chapman, 2005; Boldea, 2015).

$$X''=E_A/I'' \tag{2.24}$$

$$X'=E_A/I' \tag{2.25}$$

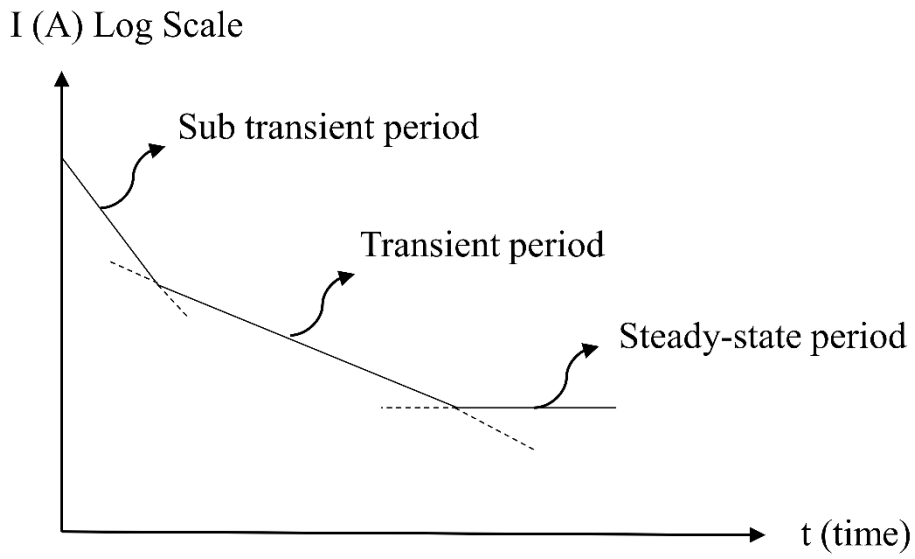


Figure 2.3 Time dependent semi logarithmic fault plot of the AC component (Adapted from Chapman, 2005)

2.3 Literature Review

The studies related to this thesis are examined under three different sections. The first subsection involves the studies that calculate or estimate the FC or emissions of the marine vessels. The second composes of the articles which study hybrid systems on board to reduce FC or GHG. The last includes the research that focus the optimization of the hybrid systems and energy management systems on marine vessels.

2.3.1 Studies Focus on Calculation and Prediction of Fuel Consumption or Emissions Onboard

Kesgin & Vardar (2001) computed GHG from marine vessels in Istanbul and Canakkale straits using AIS data with a mathematical model (MM). Cooper (2003) analyzed ships' exhaust emissions at berth. Emission measurements are the source of the data from the main and auxiliary engines of six various ships. Endersen et al. (2005) calculated shipping-related Sulphur dioxides (SO_2) using a fuel-based method. Endresen et al. (2007) evaluated the historical process of shipping FC. Perez et al. (2009), developed a methodology to predict marine vessel emissions using Automatic Identification System (AIS) data.

Hulskotte & Van der Gon (2010) performed a study that computes the FC and air pollutants due to ships at berth using onboard survey data. Miola & Ciuffo (2011) offered an alternative approach to estimate pollutants from ships and evaluated the reliability of current methods. Prpić-Oršić & Faltinsen (2012) supplied a method to predict shipping speed loss and related CO_2 emissions for a container ship on the North Atlantic route. Yau et al (2012) proposed a model which estimates emissions from ocean-going ships in the Hong Kong region using data gathered from AIS. Bilgili et al. (2014) compared various marine vessel sourced emission forecasting methods and reduction techniques for a bulk carrier using the emission footprint. Two different approaches were used in the study to estimate emissions which are FC and engine power methodologies.

Winnes et al. (2015) calculated GHG emissions using AIS and ship technical data from ships, then analyzed reduction techniques of GHG emission from ships in coastal regions. They analyzed three various scenarios which are “Alternative Fuel”, “Ship Design” and “Operation” at the Port of Gothenburg. Tichavska & Tovar (2015) built a model based on data obtained from the AIS and the Ship Traffic Emission Assessment Model (STEAM). Their model has calculated emissions produced from ferries and cruise vessels in the port. Bilgili & Celebi (2015) conducted a study that predicts emission from cargo ships using a calculation method that involves the footmark of annual emission and dimensions of the ship.

Prpić-Oršić et al. (2016) provided a detailed method to ensure reliable estimations of FC, CO_2 emission and ship speed in various sea conditions. A statistical approach to estimating a ship's FC, and speed curves was proposed by Bialystocki & Konovessis (2016). Using the noon report data, Bal Beşikci et al. (2016) built an Artificial Neural Network (ANN) to investigate the association between engine revolutions per minute (rpm) and outside influences. Chang (2016) investigated the association between carbon emission production and shipping deadweight tonnage.

Styhre et al. (2017) created a model that computes GHG resulted from shipping activities in several ports. Cepowski & Drozd (2017) presented a study that engages in FC predictions of container ships. They created a curve-fitting model using software based on wave and ship service conditions. Mersin, Alkan, & Mısrlıoğlu (2017) proposed a novel technique fır computing FC and displacement of the ship. They improved the equation of FC related to navigation speed by taking into consideration of the varying displacement of the ship. Anan, Higuchi, & Hamada (2017) developed an artificial intelligence methodology to enhance the fuel efficiency of ships using the operational data obtained from ships. Their data and model involved the relation between FC and sea conditions. The application of the novel data collection and statistical approach leads to successful FC estimations of ships with a 5% or less error rate. Kim et al. (2017) provided a statistical approach to predict the FC of container ships using the operational data. Partial Least Squares (PLS) regression was used to find the relations between FC, rpm, temperature, pressure, and power of the engine. Lepore et al. (2017) analogized the regression methods for the prediction of shipping CO_2 emissions using the data gathered from a Ro-Pax ship. The Least Absolute Shrinkage and Selection Operator (LASSO) regression performed well in different scenarios in their evaluation.

Kee et al (2018) used the multiple linear regression (MLR) technique to forecast the speed curve and the FC of tugboats. Curves also were used to monitor and measure the performance of an operating ship. Simonsen, Walnum, & Gössling (2018) performed a work that demonstrates a model used for predicting the FC and the energy utilization of cruise ships. The data was gathered from AIS and comprise ships that sail around Norway. Demirci & Karaguzel (2018) assessed the FC of fishing vessels and their emission production in İskenderun bay. They collected data from 34 various fishing vessels to build the calculation model. Wang et al. (2018) used LASSO regression to estimate the ship FC. Results showed that the LASSO method demonstrated successful performance.

Ekmekçioğlu (2019) conducted a study that estimates shipping emissions in Izmir and Mersin ports. Karagiannidis et al. (2019) created an ANN model based on noon-

report data collected from the ship for 18 months. The Feed-Forward ANN (FNN) was built to predict the FC of the ship including various scenarios and it was programmed in Python language. Tillig & Ringsberg (2019) worked up a model that involves environmental forces and moments to estimate the FC of a ship. The simulation comprised four degrees of freedom (DOF) which are heel, surge, yaw, and drift. The results showed that enhanced simulation gave better outputs compared to the 1 DOF model. Hu et al. (2019) used Gaussian Process Regression (GPR) and the Back-Propagation ANN (BPNN) machine learning methods to estimate the FC of a navigating ship. They compared two techniques and despite GPR's higher coefficient of determination (R^2) score BPNN was found preferable due to its remarkably less running time. Li et al. (2019) performed a study using Broad Learning System (BLS) regression to forecast the FC of Ro-Ro ship. BLS gave a satisfactory performance on the operational data gathered from the ship according to the results. It is stated that BLS can be useful in real-time FC estimation because of its speed. Safaei, Ghassemi, & Ghiasi (2019) developed an MLR model to estimate the FC of four different very large crude carriers (VLCC). The data were obtained from noon reports and AIS. Capezza et al. (2019) performed a study that aims to track and estimate the ship's FC. The proposed model ensured both the fuel-saving and assisting fault identification for a Ro-Pax ship.

Işıklı et al. (2020) proposed the usage of Response Surface Methodology (RSM) to construct a predictive model which captures the complex relationships. They estimated FC sourced by maritime transportation using RSM. An ANN model was presented by Le et al. (2020) used a regression model to forecast the FC of ocean-going container ships. The information was gathered at a huge container terminal in Korea. Liu & Duru (2020) devised a probabilistic Bayesian prediction (BP) system that estimates shipping emissions using AIS data to track ship movements. To anticipate the ship's power and FC, Farag, & Ölçer (2020) employed ANN and multi-regression approaches. The performance of different regression techniques for estimating ship FC was compared by Uyanik et al. (2020). Reis et al. (2020) used the actual data collected from a Ro-Pax to design and evaluate two feature-oriented models for estimating shipping CO_2 emissions. Using RSM, Li et al. (2020) attempted to optimize the exhaust emissions

from a marine dual-fuel engine. Kim & Roh (2020) constructed a ship FC prediction model based on ISO 15016:2015. They improved the methodology and compared it with the gray box methodology built on real-time data. The outcomes of the study depicted that the offered technique can be a useful tool to forecast the FC of a ship.

Moreira, Vettor, & Soares (2021) built an ANN structure to estimate the FC and the ship speed on a specific route. The data collection was ensured on board during the operation. Ekmekçioğlu, Ünlügençoğlu, & Çelebi (2021) developed a model to predict emission originating from container ships in Turkish ports. Zhu et al. (2021) researched to predict the FC of a passenger ship accurately. They collected data from multiple sources related to the ship used the combination of ANN, Support Vector Regression (SVR), and LR for estimations. Kim et al. (2021) developed an ANN model that uses operational data to estimate the FC of a container ship. Zhou et al. (2021) compared Random Forest (RF), ANN, Lasso, and Lasso regression algorithms and regression support vector machines (SVM) ensured the Bayesian hyperparameter tuning of the models to estimate the FC of a ship considering maritime conditions. Hu et al. (2021) constructed a model that aims to estimate the FC of container ships using the data collected from sensors. Their model is the combination of the extremely RF, randomized tree (ET), Xgboost (XGB), and MLR. The offered model has a lower standard deviation and higher accuracy according to their results. Tien- Tien-Anh, T. (2021) built a hybrid model that composes of the combination of Monte Carlo (MC) simulation and ANN to estimate the FC of a bulk carrier's main engine (ME). Karagiannidis & Themelis (2021) performed a study that aimed to provide reliable predictions for the FC and speed loss of a ship. They constructed a data-based propulsion model for the ship and used Feed-Forward Neural Networks (FNN) to procure the estimations. Yan et al. (2021) built a gradient boosting regression tree (GBRT) model using Python programming language for the FC predictions. The data was obtained from the monitoring, reporting, and verification (MRV) system of the European Union (EU). Lee, Roh, & Kim (2021) used FNN to estimate the ship power to minimize the FC. The data involves environmental and operational data. Ji (2021) built a Gaussian process regression (GPR) model for estimating the FC and emission

production. Hyperparameter optimization was ensured with Bayesian optimization. Table 2.1 summarizes the mentioned studies with citation and method information.

Table 2.1 Summary table of the FC calculation and prediction studies

Reference	Method	Results
Kesgin & Vardar (2001)	MM	353.625 t/yr for Istanbul and 347.221 t/yr for Canakkale Strait were estimated. Transit ships were responsible for 51% of emissions.
Cooper (2003)	MM	The emission equation that uses DWT can be a reliable tool for ferries. The chemical tanker had a substantial change in power requirements when loading and emptying where the power consumption doubled.
Endresen et al. (2007)	MM	Due to larger and more effective ships, CO_2 emissions per tonne decreased dramatically.
Endersen et al. (2007)	MM	The method given here was useful for updating worldwide SO_2 emissions from the maritime sector on an annual basis in an easy and precise manner. It's also useful for analyzing SO_2 trends and evaluating the impact of various emission control measures.
Perez et al. (2009)	MM	The usage of AIS data provided an enhanced accuracy of emission calculation.
Hulskotte. & Van Der Gon, (2010).	LR	Emission production ratios of ship types: 30 % tankers, 25 % containers, 20% Ro-Ro and ferries in Rotterdam Harbor.
Miola & Ciuffo (2011)	MM	An analysis method that enables the efficient usage of existing data was presented.
Prpić-Oršić & Faltinsen (2012)	MM	The suggested method enables improved machinery selection and more accurate forecasting of navigation time, FC, and GHG from the ME.
Yau et al (2012)	MM	Emissions from the modeled contributes 0.07 % NO_x, 0.05 % SO_2, and 0.06 % PM_{10} to the world's total maritime air pollutants.
Bilgili et al. (2014)	MM, method comparison	Total emissions were 10115.7 and 9213.7 tons for two different FC approaches. Three different results were obtained for the engine power approach: 11503.1, 11191.2, and 11546.4 tons.
Winnes et al. (2015)	MM	In a business-as-usual scenario, ship GHG in the port is expected to rise by 40% by 2030. The ‘Operation' scenario had the greatest lowering, with GHG emissions 10% less than the BAU level.
Tichavska & Tovar (2015)	MM, STEAM	The highest emission shares in passenger shipping. Distressed emission areas at the source are seen in passenger terminals.
Bilgili & Çelebi (2015)	MM	Derived formulas based on ship dimensions for emission prediction can be useful during the navigation or predesign phase.
Prpić-Oršić et al. (2016)	MM	The suggested strategy's outcomes could improve a critical aspect of marine technology, namely, clean ship design and shipping, which entails lower FC and GHG emissions while also ensuring a considerably safer voyage for the crew, and the ship itself.

Table 2.1 continues

Bialystocki & Konovessis (2016).	MM, LR	A simple and practicable approach that has high accuracy was presented based on the noon report data.
Bal Beşikci et al. (2016)	ANN	ANN can be trained effectively and accurately to learn and predict the relationship between ship FC and input parameters.
Chang (2016)	Cointegration test	DWT, energy consumption, and carbon emission variables have a distinct relationship in the 1980-2006 period.
Styhre et al. (2017)	MM	The "at berth" mode accounts for around half of all emissions in ports. The amount of emissions that can be reduced hinges on how frequently the ship enters the port.
Cepowski & Drozd (2017)	Curve fitting	The convergence function given in the paper could be useful for estimating container ship FC while weather routing is considered. Furthermore, the study demonstrated the link between a container carrier's FC and the length of time from its last moorage.
Kim et al. (2017)	PLS	The proposed method gave a satisfactory performance.
Lepore et al. (2017)	LASSO	The most influential elements on the response of LASSO were found to be voyage duration, power diversity between shaft alternators, and final draught.
Kee et al. (2018)	MLR	The suggested system was verified with previous operational data, demonstrating that it can save up to 37.1% on fuel.
Simonsen et al. (2018)	MLR	Based on a passenger count of 643, the ship emitted 91.9 kg CO_2 per voyager day. The second cruise produced 151.5 kg CO_2 per person assuming number of passengers are 1200, whereas the last ship contributed 111.6 kg CO_2 per capita day if 2139 passengers were participated the voyage.
Demirci & Karaguzel (2018)	MM	In terms of FC, the fishing vessel had a high variance. This height difference was due to considerably varying engine power on the same sized fishing craft. The vessel's structure, the ME model and year, the age of the ship, the maintenance routine of the ship, and long transmission features are all elements that influence FC.
Wang et al. (2018)	LASSO	The advantages of the presented method over other techniques were verified. The method was an enhancement to predict FC.
Ekmekçioğlu (2019)	MM	As a result, total NO_x, SO_2, CO_2, VOC, PM, and CO emissions of Port of İzmir were estimated as 900 tons/year, 589 tons/year, 45320.5 tons/year, 49.7 tons/year, 77.7 tons/year and 36.9 tons/year, respectively. For the Mersin Port mentioned emissions were computed as 1998 tons/year, 1339 tons/year, 102330 tons/year, 114.5 tons/year, 178.5 tons/year, and 82.5 tons/year, respectively.
Karagiannidis et al. (2019)	FNN	The outcomes suggested that using appropriate data pre-processing, is likely to improve the model's performance.
Tillig and Ringsberg (2019)	MM	The enhanced simulation with 4 DOF gave better outputs compared to the 1 DOF model.
Hu et al. (2019)	GPR, BPNN	Despite GPR's higher R^2 score, BPNN was found preferable due to its remarkably less running time
Li et al. (2019)	BLS	BLS gave a satisfactory performance on the operational data gathered from the ship according to the results. It is stated that BLS can be useful in real-time FC estimation because of its speed

Table 2.1 continues

Safaei et al. (2019)	MLR	The independent, and dependent parameters had a strong association, according to the findings. As a result, the derived equation accurately estimated vessel fuel consumption under all different conditions was in good consistency with actual FC data.
Capezza et al. (2019)	PLS	The presented PLS approach is valuable not only to marine engineers and shipping businesses but also to international agencies responsible for enacting CO_2 emission monitoring legislation.
Işıklı et al. (2020)	RSM	RSM adaptation performed well for the FC estimation. Draught, Speed, and RPM were the key factors that determine the FC.
Le et al. (2020)	ANN	The outcomes offered that using large container ships is more efficient both environmentally and economically.
Liu & Duru (2020)	BP	The method was shown to have a satisfactory alignment with a 95% confidence level, making it suitable for generating ship emission estimates.
Farag & Ölçer (2020)	ANN	The model depicts certain outcomes of the voyage FC estimation under different sea conditions with 99.6% accuracy.
Uyanık et al. (2020)	ANN, SVM, RF, KNN, LASSO, RIDGE	MLR and RIDGE has R^2 of 0.999 with low root mean square and mean absolute errors, are used to predict real FC data under the effect of various outer variables.
Kim and Roh (2020)	MM	The outcomes of the study depicted that the offered technique can be a useful tool to forecast the FC of a ship.
Moreira et al. (2021)	ANN	The findings produced with the ANN model indicate high accuracy in both predicting the vessel's speed and FC.
Ekmekçioğlu et al. (2021)	MM	The study's emission prediction algorithms can be used to simulate ship-sourced air contamination and predict pollutants from container vessels if their GRT is known. According to the GRT at Turkey's ports, the average error margins for container ships were at acceptable levels.
Zhu et al. (2021)	SVR, ANN, LR	Alongside of the traditional parameter finding technique, the accuracy was improved by 8.5 (LR), 0.35 (SVR), and 51.5% (ANN), using the proposed method.
Kim et al. (2021)	ANN, MLR	ANN models performed the best performance. The quality of ANN models' fit is between 0.9709 and 0.9936.
Zhou et al. (2021)	ANN, SVM, RF	The suggested model can thus serve as an important reference for predicting FC, as Bayesian optimization for hyper-parameter tuning can effectively increase the prediction accuracy.
Hu et al. (2021)	ET, RF, XGB, MLR	The offered model had a lower standard deviation and higher accuracy according to their results
Tien-Anh, T. (2021)	ANN, MC	The proposed model was more accurate than prior models around energy management on marine vessels.
Karagiannidis & Themelis (2021)	FNN	FC and speed loss were estimated successfully for the specified dataset. Model accuracy was dependent on filtering and preparation of data.
Yan et al. (2021)	GBRT	The performance of the estimation models is valid, with the average R^2 of various models at 0.78
Lee et al. (2021)	FNN	By applying four different methods, the accuracy of the FNN model was increased
Ji (2021)	GPR	The promising results are consistent with the validation data, demonstrating the proposed models' high efficacy and resilience.

2.3.2 Studies Focus on Alternative Energy and Hybrid Applications Onboard

Ashari & Nayar (1999) presented dispatch strategies for photovoltaics (PV)- diesel-battery hybrid power systems. They developed a computer program for an optimal dispatch plan to predict long-term energy performance and cost calculation.

Kusakana & Vermaak (2014), conducted a study about optimization of hybrid multisource system operation and proposed an approach that meets reliable load demand and minimum life cost requirements. Elsayed & Mohammed (2015) presented a study that compares hybrid energy storage systems used on marine vessels. They modeled and analyzed various possible hybrid system combinations and found out that battery-flywheel combinations can lead to higher efficiency. Lan et al. (2015) conducted an article that provides a technique to figure out optimum dimensions of the PV system, energy storage system, and DG. They investigated five operation modes and for different cases. Ovrum & Bergh (2015) performed research that models and analysis a hybrid battery system for ship crane operations. Their results show that the hybrid system can lead to a 30% lower FC and CO_2 emission. Bellache et al. (2015) conducted a study that evaluates an energy management strategy (EMS) based on a frequency approach for a hybrid diesel-electric boat propelled by a variable speed generator (VSDG) and lithium-ion batteries. Giannoutsos & Manias (2015) applied a system as a new installation in a tanker's energy system. Then, they compared experimental outputs to the former condition to illustrate the effect of optimized DG operation on FC. Results show that yearly energy consumption of the vessel's power distribution system was decreased 18.3% and FC was remarkably lowered by 20.3%. Tang et al. (2015) presented a novel multi-energy source-based energy and power managing system for a hybrid ship system. The method aimed to reduce FC and emission while enhancing energy efficiency.

Lundh et al. (2016), suggested a methodology for prediction of specific FC of each generator to facilitate exact efficiency and to optimize the plant with forecasted FC. Results depicted that their method provides 4-6% fuel saving (FS) for a large cruise ship. Lan et al. (2016) simulated and analyzed a flywheel storage system to ensure the

stability of the PV power outputs on a large oil tanker. Various operation modes and ship rolling effects were considered during the analysis. Results showed that a flywheel system can improve the quality of the produced power and can ensure more stable PV system. Leloup et al. (2016) built a simulation of the ship propulsion system with kites and calculated the system's FC.

Jia & Dong (2017) conducted a study about ship power plant simulation using MATLAB and Labview software. Mathematical modeling of prime mover, synchronous generators, governor, exciter, and load are constructed in MATLAB Simulink. The model is directed with an interface created in Labview software. The simulation results gave an accurate analysis of the ship's electrical power production system.

Bassam et al. (2018) studied a hybrid dsipatch system of a passenger ship. The system involved the addition of proton exchange membrane (PEM) fuel cells to the propulsion system. They developed an EMS for the hybrid system. A novel multi-scheme EMS was presented which uses the combination of multiple EMS control strategies. The modeling was ensured in MATLAB/Simulink program and the results demonstrated that energy and hydrogen consumptions can be reduced 8% and 16.7% with the suggested strategy.

Peralta et al (2019), analyzed a hybrid system with Li-on batteries and DGs with various scenarios. They used HOMER (Hybrid Optimization Model for Multiple Energy Sources) software to simulate the system. By the installation involving the diesel engines and batteries, the most noticeable CO_2 reduction potential is 8.7%. Lana et al. (2019) presented a modeling method for hybrid power distribution systems and energy storage components' sizing. The developed methodology ensures fuel efficiency and optimal sizing for system components. Roh et al. (2019) performed a paper that compares their electric propulsion system with present power sources on the test station. The system constructed by the authors consists of hybrid power systems and a DG. The hybrid system produced 70-74% less CO_2 emissions compared to the conventional system.

German–Galkin et al. (2020) performed a study on ship hybrid grid systems using a wind and DG combination. They conducted a systematic analysis to observe possible usage scenarios of the system. Karatug & Durmusoglu (2020) conducted a study that incorporates the projection and assessment of a PV system, DG, and shaft generator on a Ro-Ro ship. Their performance analysis predicted that a 7.76% energy efficiency increase and a 7.38% fuel consumption reduction. Cheng et al. (2020) conducted an article that evaluates the applicability of wind and solar energy usage on ship rolling mechanisms and power systems. The ship electricity system involving alternative energy was constructed using a simulation program. The results illustrated that the rolling movement of the ship can cause power fluctuations in the solar and wind power grid. To prevent this phenomenon battery usage in the system can be a solution.

Fan et al. (2021) evaluated solutions that lower the carbon emission for ships operated inland. They analyzed four various scenarios using two different situations using Life Cycle and Life Cycle Cost Analyses. The results showed that for small canal container ship battery power scenario produced 14.5% less CO_2 and 17.78% lower costs than classical diesel configuration. For the 6700 DWT bulk carrier, the cost is 39.15% and the total emission is 33.44 % lower than the diesel setup. Gaber et al. (2021) conducted a study that performs and designs an improved EMS for the ship electric system using an adaptive neuro-fuzzy inference system (ANFIS) using MATLAB. The hybrid system consisted of PEM fuel cells with the total power of 12.5 kW. The simulation results were verified with experimental results. The results depicted that ANFIS EMS has an advantage over traditional EMS in terms of performance. The outcomes of the study demonstrated that ANN is a suitable method for such applications. Kistner, Bensmann, & Hanke-Rauschenbach (2021) performed an analysis that includes the usage of solid oxide fuel cells (SOFC), batteries, and supercapacitors in marine vessels. They worked on two scenarios whether batteries or super capacitors were required for the operation. To meet the dynamic fluctuations of the ship power, the results indicated that SOFC with energy storage equipment gives desirable outcomes. Wang, Yang, & Xiao (2021) presented an EEDI computation technique for hybrid ships. They used a 7500 DWT bulk carrier which has a hybrid propulsion unit as an example. The outcomes of the paper depicted that the presented

method is realistic and can be useful in scientific research. Table 2 depicts the summary of the mentioned studies about hybrid ship power and propulsion system applications.

Table 2.2 Summary table of studies that covers hybrid ship power and propulsion systems

Reference	Method	Results
Ashari & Nayar (1999)	Comparison of three dispatch strategies for PV-diesel-battery configuration with a simulation.	Working the inverter according to a scenario that considers battery aging, DG FC, and load profile results in a lower system operation cost.
Kuskana & Vermaak (2014)	MM of a hybrid diesel-alternative energy system and its optimization.	Time-independent operation strategies can be the optimal solution.
Elsayed & Mohammed (2015)	MM of energy storage configurations for marine vessel and their comparison.	The battery-flywheel combination can lead to higher efficiency
Ovrum & Bergh (2015)	MM and analysis of a hybrid battery system for ship crane operations.	A 30% reduced FC and CO_2 emission
Bellache et al. (2015)	A simulation of VSDG and battery. EMS based on frequency approach.	Proposed EMS meets the dynamic responses, lowers fluctuations and battery sizes.
Giannoutsos & Manias (2015)	EMS and DG FC optimization	DG annual energy consumption and FC are reduced by 18.3% and 20.3%.
Tang et al. (2015)	EMS for hybrid ship system	PEMS can reduce ship FC remarkably.
Lundh et al. (2016)	FC estimation and optimization of a diesel-electric ship.	4-6% FS for a large cruise ship.
Lan et al. (2016)	Simulation and evaluation of a high-speed flywheel storage grid to ensure the PV stability.	The system can improve the power quality and stability of the PV system
Leloup et al. (2016)	Analytical modeling of kite usage as auxiliary propulsion in a tanker ship.	For 9.77 ms^{-1} wind velocity 10 %, for 15.68 ms^{-1} up to 50% FS.
Jia & Dong (2017)	Ship power plant simulation using MATLAB and Labview software	The simulation results gave an accurate analysis of the ship electrical power production system
Bassam et al. (2018)	A novel EMS approach was presented for a PEM/diesel propulsion system for ships.	Energy and hydrogen savings of 8% and 16.7%
Peralta et al (2019)	Analysis and simulation of DG and Li-on batteries.	CO_2 reduction potential up to 8.7%.
Lana et al (2019)	Modeling for the hybrid power distribution system and determination of energy storage components' sizes	The developed methodology ensures fuel efficiency and optimal sizing for system components.
Roh et al (2019)	Comparison of the hybrid propulsion system with the traditional propulsion system.	70-74% less CO_2 emissions

Table 2.2 continues

Qui et al (2019)	Economic analysis of PV systems integrated with the ship electricity grid.	PV system can provide cost reduction and environmental benefits
German–Galkin et al. (2020)	Modeling and evaluation of hybrid ship electrical system	The presented strategy in this study not only improves the combined system's energy efficiency but also minimizes dangerous exhaust component emissions to the environment and increases the engine's longevity and dependability.
Karatug & Durmuşoglu (2020)	Design and analysis of a PV system, DG, and shaft generator on a Ro-Ro ship	7.76% energy efficiency increment and 7.38% FC reduction
Cheng et al. (2020)	Simulation and analysis of the applicability of wind and solar energy usage on ship the rolling mechanisms and power systems using PSCAD/EMTDC software	The results illustrated that rolling movement of the ship can cause power fluctuations in the solar and wind power grid. To prevent this phenomenon battery usage in the system can be a solution.
Fan et al. (2021)	Evaluation of solutions that lower the carbon emission for ships operated inland using LCA and LCCA	For small container ship battery power scenario produced 14.5% less CO_2 and 17.78% lower costs For the 6700 DWT bulk carrier the cost is 39.15% and total emission is 33.44 % lower
Gaber et al. (2021)	Design of a smart EMS for ship power system supported by green energy sources using ANN	The outcomes of the study demonstrated that ANN is a suitable method for such applications.
Kistner et al. (2021)	Evaluation of usage of solid oxide fuel cells (SOFC), batteries, and supercapacitors in marine vessels.	SOFC with energy storage equipment combination gives desirable outcomes.
Wang et al. (2021)	A novel EEDI computation technique for hybrid ships.	The technique is realistic and can be useful in scientific research.

2.3.3 Studies Focus on the Optimization of Hybrid System Onboard

Radan et al. (2005) presented an optimization study to ensure minimization of the total FC and enhance blackout resistance of vessels using dynamic positioning by optimizing the load-dependent star tables. Their method involves efficient usage of the fast load reduction systems and outlines of the batteries to control the inertia of the electricity distribution system.

Al-suod et al. (2015) proposed an algorithm that ensures the selection of the optimal parameters for generators based on daily statistical data. The data were collected automated control system power plant.

Baldi et al. (2016), applied mixed-integer linear programming (MINLP) to solve the load allocation problem and they used a present power plant that includes a hybrid

plant for the comparison. They achieved 3% savings because of the optimization. Wen et al. (2016) analyzed that ship effects of the swinging to the allocation of energy storage systems which consist of PV/diesel, on an oil tanker. They developed an optimization algorithm that considers swinging action taken from ship swinging platform.

Haseltalab & Negenborn (2017) presented a power management estimation algorithm for all-electric marine vessels' electricity distribution scheme. Kumar & Fozdar (2017) performed a study that uses particle swarm optimization (PSO) to detect optimum dimensions of PV-battery- diesel ship power system in a tanker. They compared different scenarios using various types of PSO. Lai & Illindala (2017) studied integration and designing measures of batteries in a ship dc hybrid power generation system. They used General Algebraic Modeling System (GAMS) to optimize the model and the results depicted that a substantial advancement can be achieved with the planning of an energy storage system onboard.

Al-Falahi et al. (2018) presented a review on recent technologies of AC ship microgrids related to control and power management strategies. Ancona et al. (2018), built an optimization framework hinged on a genetic algorithm to detect optimal operating points with minimum fuel consumption of the VSDG plant by adjusting the load distribution of the marine electricity generation system. Trivyza, Rentizelas, & Theotokatos (2018) constructed a multi-objective decision support methodology for hybrid ship power systems and sustainably increment. Non-dominated Sorting Genetic Algorithm II (NSGA-II) was used for a multi-objective optimization problem. Results indicated that, for various ship types and hybrid systems, a combination of cost-effectiveness and low impact on the environment has a key role in the decision process.

Dolatabadi, A., Ebadi, R & Mohammadi-Ivatloo (2019) presented stochastic programming for the size optimization of a hybrid marine electricty system, energy storage systems, the DG, and PV panels. Scenario analysis was carried out with a Monte Carlo sampling approach with five different load conditions. Jaurola et al. (2019) presented a literature review that contains the design and optimization of power

management in marine vessels. Qui et al. (2019) conducted an economic analysis on PV systems adjoint with the ship power grid. Their mathematical model predicted solar irradiation for six different routes. Techno-economic analysis showed that PV systems can provide cost reduction and environmental benefits. Ghenai et al. (2019) studied a performance evaluation and design optimization of a hybrid ship electrical system on a cruise ship that works in Stockholm, Sweden. Their hybrid system consists of PV panels, PEM fuel cell, and DG and according to calculations made by the mathematical model, a 9.84% reduction in greenhouse gases can be ensured by the system.

Bolbot et al. (2020) conducted a study on cruise ship power plants and their optimization. Their study aimed to find out the optimum power plant configuration for cruise ships with various fuel types. The study put forward emissions, safety, and employment requirements in the life-cycle assessment. The results of the study illustrated that dual fuel and natural gas applications have the advantage in case of lifetime costs and emissions.

Gaber et al. (2021) presented a smart EMS for ship power systems supported by green energy sources. They controlled the multi-sourced system using ANN to meet the equivocalness of the hybrid power system. The model determined which source can be used for specified conditions. Lu, Wang, & Xiao (2021) optimized the EMS for a hybrid ship propulsion system that involves PV, wind turbine, and energy storage units using a multi-objective differential evolution framework based on decomposition and multi-strategy mutation (MODE-DMSM) algorithm. The results showed that green energy support to the ship propulsion system with an optimized EMS can reduce the emissions remarkably.

Table 2.3 Summary table of studies that covers hybrid system optimization on marine vessels

Reference	Method	Results
Radan et al. (2005)	An optimization of load-dependent start tables using a simulation for dynamic positioning vessels.	The vessel can operate with a closed bus tie to save as much fuel as possible while maintaining blackout prevention and operability.
Al-suod et al. (2015)	State machine-based simulation and optimization of the ship power system. Statistical analysis.	The algorithm minimizes the FC and maximizes the DG time density.
Baldi et al. (2016)	Load allocation optimization using MINLP	3% FS
Wen et al. (2016)	Modeling and optimization of ship swinging effects on the allocation of hybrid ship power system	The swinging affects the EMS, and the optimization algorithm helps to ensure high efficiency and lower GHG.
Haseltalab & Negenborn (2017)	EMS optimization with Model Predictive Control (MPC) for an all-electric ship.	The algorithm predicted accurately the required power
Kumar & Fozdar (2017)	PSO for optimal sizing the hybrid ship power system	PSO provides an optimal EMS for the selected system.
Lai & Illindala (2017)	Dynamic modeling and GAMS optimization of the hybrid ship power system.	The dynamic model assists in coping with load uncertainties. The findings showed that this is a key factor in shipboard dc hybrid power system EMS planning.
Al-Falahi et al. (2018)	Review on EMS optimization on board.	Meta-heuristic optimization methods like PSO and GA produce better results than traditional methods when it comes to EMS optimization.
Ancona et al. (2018)	Load allocation optimization of the ship power plant. Comparison of five different strategies	Yearly reduction of CO_2 up to 20%
Trivyza et al. (2018)	Multi-objective decision support using NSGA II for ship power systems	SCR, EGR, Dual fuel engines have specific advantages in reducing emissions.
Dolatabadi et al (2019)	Stochastic programming for the size optimization of a hybrid ship power system.	The entire cost of PV panels goes up by roughly 16%, but fuel and pollution costs go down by about 5%.
Jaurola et al (2019)	Review on EMS optimization for marine vessels	The duty cycle of a vessel has a remarkable effect on the viability of deploying a hybrid power system that can be determined using numerical optimization in a maritime vessel.
Ghenai et al (2019)	Design optimization of a hybrid ship electrical system on a cruise vessel	A 9.84% reduction in GHG
Bolbot et al. (2020)	Modeling of cruise ship power plants and their optimization	Dual fuel and natural gas applications have the advantage in case of lifetime costs and emissions
Gaber et al. (2021)	Design of an improved EMS for ship electric system	ANFIS EMS has the advantage over traditional EMS in terms of performance
Lu et al. (2021)	Optimization of EMS for a hybrid ship propulsion system using MODE-DMSM.	Green energy support to the ship propulsion system with an optimized EMS can reduce the emissions remarkably

The literature review of the thesis was divided into three main categories which are studies focus on the calculation or estimation of air pollutants and reduction of FC, emissions with the integration of renewable energy sources to current marine systems and optimization of hybrid systems on the marine vessels. The outcomes of the first category depicted that ferries, Ro-Ro, cruise, and container vessels were the major preferred ship types for the studies. The main reason for this phenomenon could be easier monitoring for these kinds of ships. Tankers and dry bulks were also analyzed in some studies, and their one specific route was selected generally for the analysis due to the same concern. The studies before 2016 chiefly used numerical simulations and calculations on the other hand, after 2016, articles involved machine learning algorithms. Several types of linear regression algorithms were used to predict FC. However, especially after 2019, deep learning algorithms and more complex machine learning methods gained popularity. ANN and its types are the most favored among all. SVR was also become a frequently used algorithm to estimate emissions from ships. The studies fundamentally concentrated emission from ME or overall FC. Some articles used AIS, or FC data gathered from the ship for their model and others made their calculations considering environmental factors, ship dimensions, and ME properties. The results of the second category demonstrated that PV, wind, and fuel cells were the most preferred alternative energy source additions to ship main or auxiliary machinery to reduce FC. The researchers also provided analyzes involving super capacitor, battery, flywheel energy storage, and VSDG usages and applications. The strategies substantially were applied to cruise ships because of their large plants. Especially, studies on ship power generation plants preferred to work on cruise ships because of the excess number of generators and the area to add the alternative energy equipment. Ferries and Ro-Ro ships were also chosen by researchers due to mentioned reasons. Some studies were carried out container vessels and they offered to place energy storage units in containers. Tankers and dry bulks are rarely preferred for these kinds of applications and generally, calculations were ensured for their specific routes. The third category focused on the usage of the optimization algorithms on the marine power systems. EMS optimization of the hybrid systems, sizing and design optimization, and load allocation optimization of the ship power distribution systems

are main attention-grabbing subjects on this topic. The preferred ship types are again ferries and cruise vessels due to similar causes mentioned above.

This thesis aims to build a comprehensive mathematical model of an oceangoing oil/chemical tanker's electricity generation plant. Using the model, FC and emission production of the marine diesel generators are calculated. The simulation involves load-sharing characteristics to meet various operational loads. Calculations are ensured between 06.12.2019 and 07.06.2021 including every major navigation and port activity of the selected ship. By benchmarking several machine learning methods, time-based predictions of the FC are performed and the most efficient regression method for the data is determined. After that, the hybridization of the system is assessed by adding energy storage units to the simulation. Six different battery configurations are evaluated, and the most optimum combinations are selected using different multi-attribute decision making (MADM) algorithms. Choosing criteria are weight, cost, and fuel-saving of the battery configuration. The weights of the criteria are determined using the Entropy method. The configuration involves C-rates, the number of parallel units, and the battery cell type. After the determination of the energy storage unit setup, two different charge source options are added to the simulation and analyzed. The first one is to use generators for charging. Peralta et al. (2019) offered this fast applicable method for a container ship. This study evaluated for conditions of tanker ships. They offered to install the energy storage unit in a container, in a tanker because of limited space, the weight is added to selection criteria. The second charging source is waste the heat recovery system (WHRS) which uses ME and DG waste heat (WH) to generate electricity and charge the generators. FS and ER potentials of both strategies are discussed, and future forecasts are ensured with the selected regression algorithm. The feasibility of the selected battery systems and charging strategies for this ship are analyzed with economic analysis and discussed.

CHAPTER 3
METHODOLOGY AND MODEL DESCRIPTION

The chapter depicts the structure and logic of the mathematical model of the ship's power distribution system. System description of the base and hybrid model, energy storage equipment specifications, MADM methods for battery selection, algorithm schemes of charging strategies, WHRS system structure, emission calculations, working principles of the algorithms used in FC estimation, and economic analysis foundations are the main topics for the section. Figure 3.1 demonstrates ship power distribution model construction processes that consist of data collection, modeling, and FC estimation. Figure 3.2 depicts the hybrid ship electricity generation plant simulation processes.

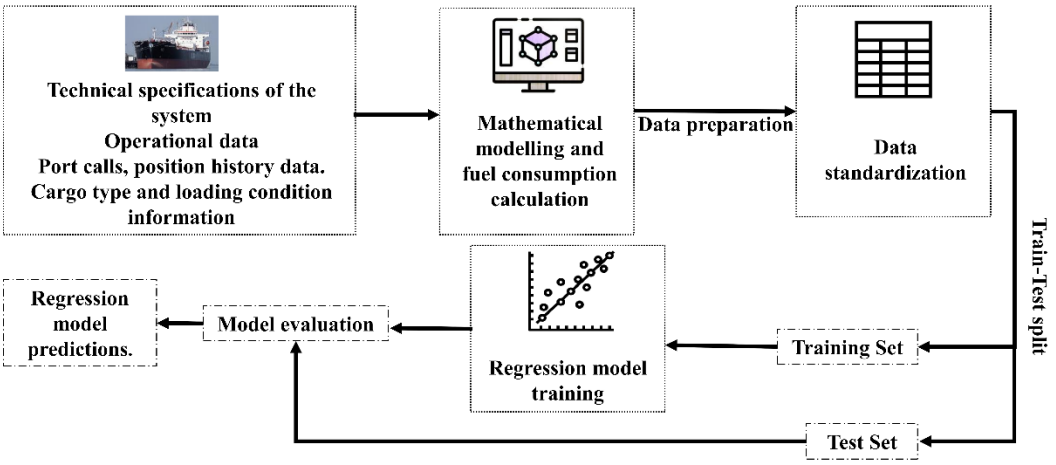


Figure 3.1 Power distribution system modeling and FC estimation workflow

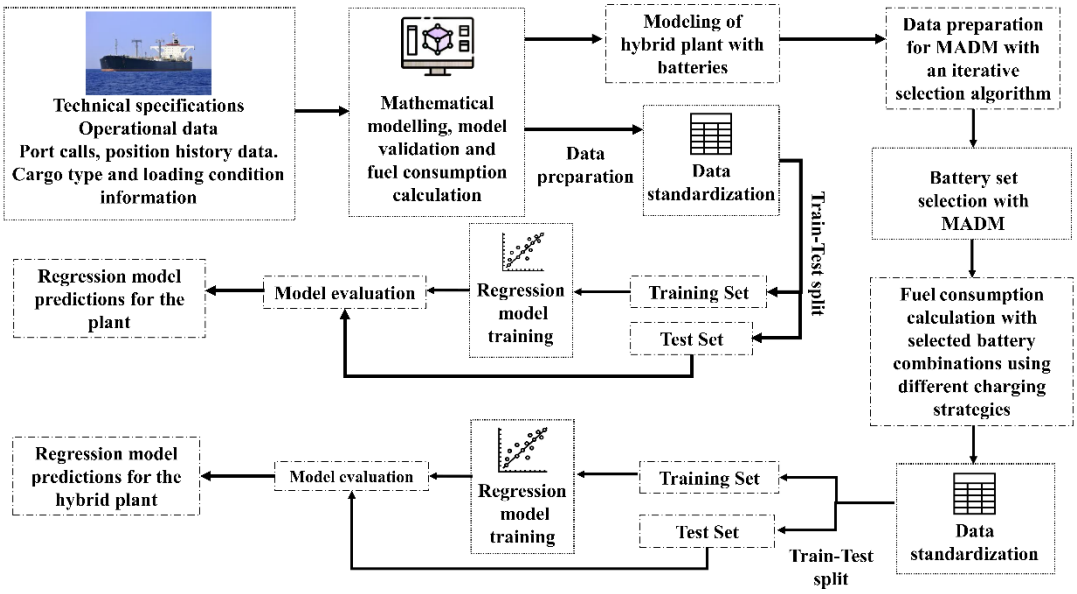


Figure 3.2 Ship hybrid power distribution system modeling and FC estimation workflow

3.1 Ship Power Distribution System Model Description

The mathematical model consists of three main components which are synchronous generator, prime mover, and electrical load. The ship trial tests of synchronous generator taken during the data collection phase provided data which include load tests, governor tests, parallel running tests, open circuit, and short circuit tests. During navigation, the prime mover uses heavy fuel oil (HFO), and during harbor and port operations, it uses marine gas oil (MGO). The ship's fuel records supplied the fuel parameters. The engine manufacturer's look-up tables gave brake-specific FC data for the prime mover in the numerical model. Using the manufacturer's stroke, bore, and bmep values, the torque, and power transferred to the synchronous generator were computed. Table 3.1 demonstrates the general specifications of the alternator and the prime mover.

Table 3.1 General information about the generator

Prime Mover	
Engine MCR	960 kW
Rpm	900
Generator MCR	900 kW
L/O Temp. Inlet	66
Valve Clarence	0.5 mm
Ambient Air Temperature	25
Ambient Air Pressure	1 bar
MDO Lower Calorific Value	42700 kJ/kg (10200 kcal/kg)
Cooling water for air cooler	25
Cylinder Bore (mm)	210
Piston Stroke (mm)	320
Swept Volume per Cylinder (dm3)	11.1
Piston Mean Speed (m/s)	9.6
Compression Ratio	17:1
Mean Effective Pressure (bar)	24.1
Alternator	
Output Capacity	1312.5 KvA
Voltage	450 V
Frequency	60 Hz
Poles	8
Variation of Generator Voltage	2.50%
Voltage Adjust	5%
Power Factor	0.8 Lagging

The data sets are interpolated using Python language to create look-up tables from the manufacturer's data. Python's Scipy library provides a function named interp1d and using this function provides one-dimensional interpolation of the data. Type of the interpolation can be adjusted using the function parameters and linear interpolation gave the most efficient application for the data. In the model, the load section is based on the selection of the operation mode which ensures the operational load and operational current. Operational load in kW and operational current are among parameters which are gathered from electrical load analysis of the ship. The datasheet is taken from the commercial ship and the analysis had been carried out in the shipyard. There are six operational modes in the model and users can select each of them. In addition, the model enables to enter alternative load values as well. Table 3.2 shows the available operational modes, their loads, and operational currents.

Table 3.2 Operational modes used in the model

Operation Mode	Operation Number	Load	Current
Sea Gong	1	850.6	1364.152
Sea Gong with Tank Heating	2	1195.7	1917.607
At Port	3	1122	1799.410
At Cargo Handling	4	1781.5	2857.085
At Harbor	5	571.3	916.224
At Harbor with Tank Heating	6	863	1384.038

Operational current is the required current that is to be produced by the synchronous generators. According to load and the current, the model makes a comparison with the active power of generators calculated in the synchronous generator section. This analogy determines the number of generators for the selected operational mode. According to the number of generators, the model includes the operation of the synchronous generators of the ship by order. The user can specify the order of generators, filling the generator sequence section. Using this section, the model fills a binary array if the generator is running its value 1, if not 0. Then, the control array is checked so, frequency, speed drop, the slope of the power curve calculations can be carried out of the running generators. After that, again using the control array and number of generators data, system frequency, power, load, and current requirement of each generator are calculated. Using the calculated load percentage of each generator, power of the prime mover, armature currents, internally generated voltages, line voltages, voltage regulation percentages, synchronous power output, brake specific fuel consumptions are determined. Brake-specific fuel consumption values are interpolated from manufacturer data and synchronous machinery data are calculated using the equations given in chapter 2. Brake-specific fuel consumption yields the fuel consumption in kg per hour and emissions produced by the generator also in kg per hour. Figure 3.3 illustrates the algorithm scheme of the model.

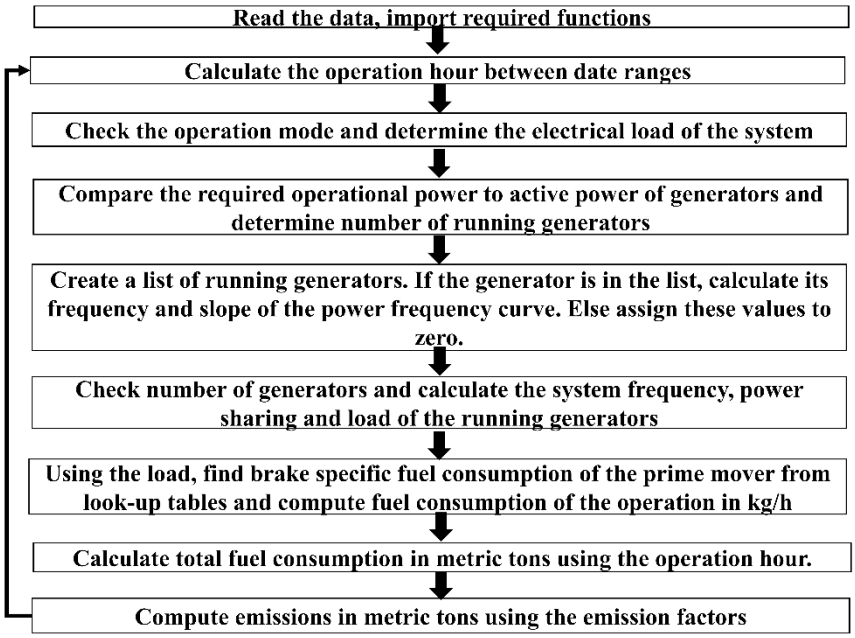


Figure.3.3 The algorithm scheme of the mathematical model

3.2 Multi-attribute Decision-Making Methods

To select the ideal number of the batteries, battery brand, C-rates for charging and discharging processes, multi-criteria decision-making (MCDM) methods are used, and their outputs compared. The data sets for the methods are prepared using an iterative model selection algorithm that makes the model work with every combination. The stop criterion of the iteration is determined by the battery weight limit set at a low level, which is 0.002 times of the DWT since to not affect the ME FC and the low weight and volume applications can be applied quickly and flawlessly to the commercial ships (American Bureau of Shipping, 2013). The algorithm initially calculates the FC of the regular marine diesel generator operation without batteries in total hours equals the summation of charge hours (CH) and discharge hours (DH). It also determines the fuel-saving ratio and removes the combinations that supply saving lower than 1%. The algorithm's final outputs are used to determine the best combination accordingly, fuel-saving ratio, battery total cost, and weight parameters. Figure 3.4 depicts the working scheme of the selection algorithm.

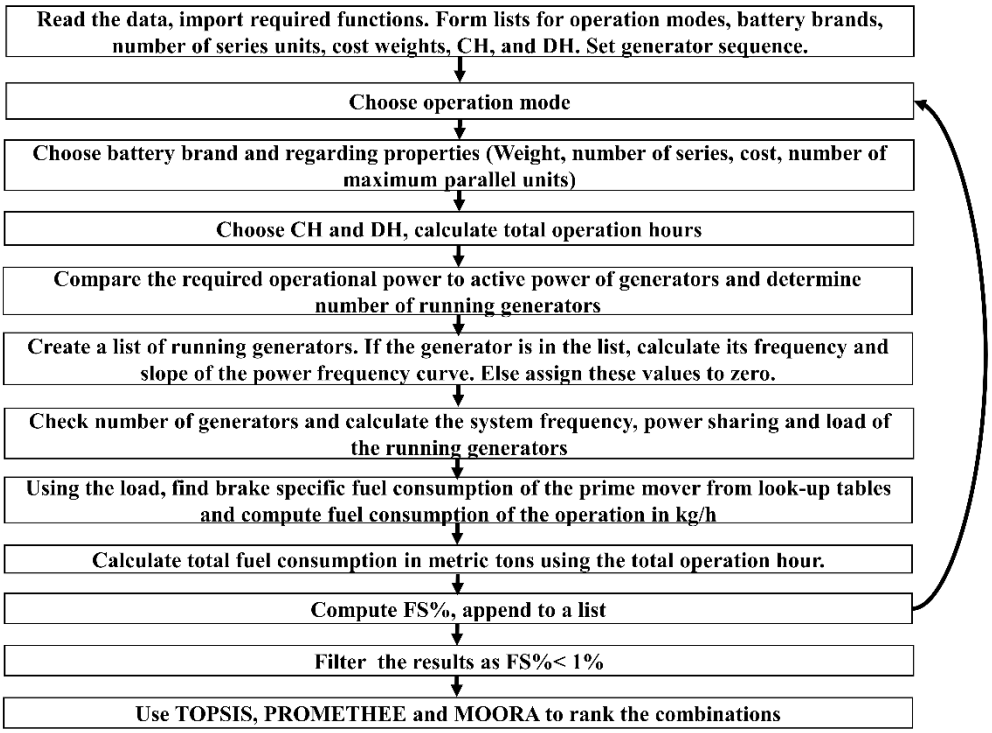


Figure.3.4 The algorithm scheme of the battery selection program

The data is formed for the first scenario (generator charge) and combination determination is done with this scenario only because it is a worst-case scenario compared to the second scenario (WHRS charge). To rank the effectiveness of combinations, MCDM techniques are an effective methodology. The goal of MCDM is to rank multiple possibilities by evaluating and assigning a value. MCDM can be split into two maim sections which are multi-attribute decision making (MADM) and multi-purpose decision making (MPDM). MADM refers to a challenge that entails evaluating and grading a set of attributes and selecting the best option. MPDM, on the other hand, is concerned with determining the best option based on a variety of factors (Phua & Minowa, 2005). In this thesis, some of the well-known MADM methods are used to determine the ideal battery combinations for our hybrid ship electrical generation plant. The methods which are well-known among both academia and industry used in the thesis can be listed as follows:

- Technique for Order of Preference by Similarity to Ideal Solution (TOPSIS)
- Multi-Objective Optimization on the Basis of Ratio Analysis (MOORA)

- Preference Ranking Organization Method for Enrichment of Evaluations (PROMETHEEII)

3.2.1 Technique for Order of Preference by Similarity to Ideal Solution (TOPSIS)

TOPSIS is one of the MADM methods and it is gaining importance for both academic communities and private corporates. The technique was presented by Hwang and Yoon in the year of 1980, and it has been widely used in many different industries. The main principle of the method is based on positive and negative ideal solutions. The nearest distance to the positive ideal solution (PS) or the furthest distance to the negative ideal solution (NS) leads to the detection of the best alternatives. PS is the solution that makes the cost criterion minimum and the benefit criterion maximum. NS has the opposite effect compared to PS. TOPSIS method calculates the distances to PS and NS and finds the ideal and non-ideal solutions. The method requires at least two decision options. TOPSIS method gives ideal solutions with a simple algorithm and its results are easy to understand (Cheng-Min & Wang, 2001; Soba & Eren, 2011). Figure 3.5 illustrates the steps of the technique.

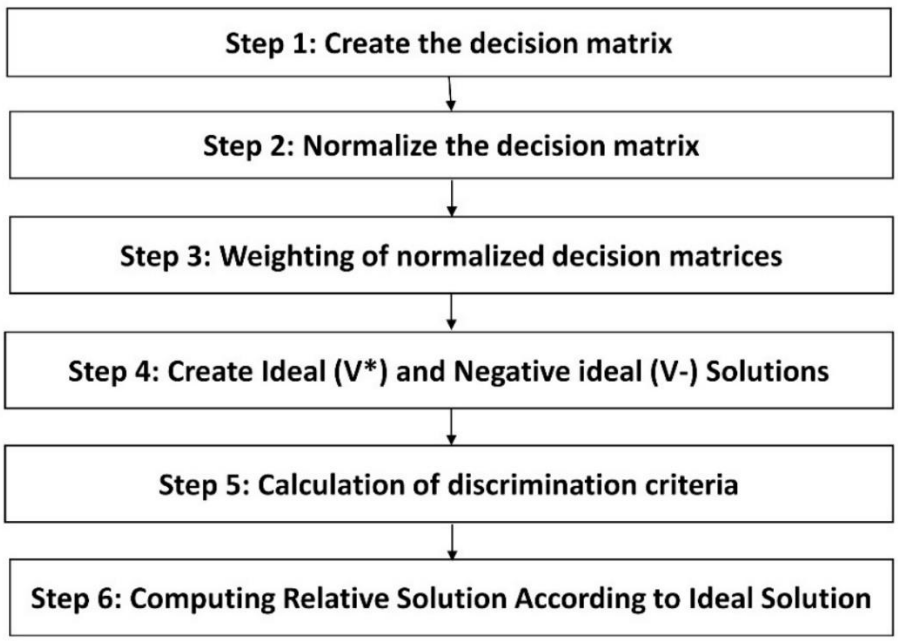


Figure 3.5 TOPSIS method flow diagram (Soba & Eren, 2011; Gökdalay, 2009)

The steps of the method are as follows (Soba & Eren, 2011; Gökdalay, 2009; Ecer, 2007):

- The first step of the method is to form a decision matrix. The matrix was created using the iterative selection algorithm. Equation 3.1 shows the decision matrix. The second step is the normalization of the decision matrix. Equation 3.2 explains the normalization process.

$$\begin{bmatrix} r_{11} & \dots & r_{1m} \\ . & . & . \\ r_{n1} & ..... & r_{nm} \end{bmatrix} \tag{3.1}$$

$$r_{ij} = \frac{d_{ij}}{\sqrt{\sum_{k=1}^{n} d_{kj}^2}} \tag{3.2}$$

- The third step is to create a weighted decision matrix (V). To form this, we multiply the decision matrix with its weights. The fourth step is to get PS (V^*) and NS (V^-). If the evaluation criteria are the benefit type, PS is the maximum value in the V matrix. On the other hand, if the criterion is the cost type, PS becomes the minimum value in the V matrix. Equation 3.3 illustrates the positive and a negative solution set.

$$\begin{aligned} V^* &= \{v_1^*, v_2^*, \dots, v_m^*\} \\ V^- &= \{v_1^-, v_2^-, \dots, v_m^-\} \end{aligned} \tag{3.3}$$

- In the fifth step, the Euclidean distance PS and NS of each value is calculated. Equation 3.4 shows the calculation. S_i^* and S_i^- are PS and NS distances respectively. Finally, in the last step, the relative closeness coefficient (C_i^*) is computed and the data can be ranked using it. Equation 3.5 is the formula to calculate the coefficient.

$$S_i^* = \sqrt{\sum_{j=1}^{m} \left(v_{ij} - v_j^*\right)^2}, \; i=1,2\dots,n \tag{3.4}$$

$$S_i^- = \sqrt{\sum_{j=1}^{m} \left(v_{ij} - v_j^-\right)^2}, \; i=1,2\ldots,n$$

$$C_i^* = \frac{S_i^-}{S_i^- + S_i^*} \tag{3.5}$$

3.2.2 Multi-Objective Optimization on the Basis of Ratio Analysis (MOORA)

MOORA was initially introduced by Brauers & Zavadskas in 2006 and it is a widely used MADM method in various areas. The technique consists of a weighted normalization that considers whole decision choices and criteria. Simple application, less computing time, less mathematical operations, and high reliability make MOORA a preferred method. Four different forms of MOORA can be listed (Kundakci, 2016):

- Ratio
- Reference point
- Full multiplicative
- Importance factors

In the study, ratio, and reference point forms of MOORA are used. The MOORA-Ratio assumes that each criterion has an equal value. The steps of MOORA-Ratio (Kundakci, 2016; Brauers & Zavadskas, 2006; Özbek, 2015):

- **Step 1**: Form a decision matrix.
- **Step 2**: Normalize the decision matrix with Equation 3.6
- **Step 3**: Create weighted normalized decision matrix (v_{ij}) with the multiplication of weights (w_j) to the normalized matrix (Equation 3.7).
- **Step 4**: Calculate the performance of decision choices with Equation 3.8 and obtain preference values (y_i^*)
- **Step 5**: Sort the y_i^* values in descending order.

$$x_{ij}^{*}= \frac{x_{ij}}{\sqrt{\sum_{j=1}^{n} x_{ij}^{2}}} \quad (3.6)$$

$$v_{ij}=x_{ij}^{*}*w_{j} \quad (3.7)$$

$$y_{i}^{*}= \sum_{j=1}^{g} v_{ij} - \sum_{j=g+1}^{n} v_{ij} \quad (3.8)$$

MOORA-Reference Point steps can be listed as (Kundakci, 2016; Brauers & Zavadskas, 2006; Özbek, 2015):

- **Step 1**: Form a decision matrix.
- **Step 2**: Normalize the decision matrix with Equation 3.6
- **Step 3**: Create weighted normalized decision matrix (v_{ij}) with the multiplication of weights (w_j) to the normalized matrix (Equation 3.7).
- **Step 4**: Determine a reference point (r_{ij}) for each criterion. If the value is beneficial, the maximum of the data is taken as a reference point, if not, the minimum value is selected.
- **Step 5:** Calculate the distance from the reference point with Equation 3.9. Find the highest value for each alternative with Equation 3.10 and sort them in descending order.

$$d_{ij}=r_{i}-x_{ij}^{*} \quad (3.9)$$

$$P_{i}=\min_{i}(\max_{j} d_{ij}) \quad (3.10)$$

3.2.3 Preference Ranking Organization Method for Enrichment of Evaluations (PROMETHEE)

J.P. Brans invented the PROMETHEE I (partial ranking) and PROMETHEE II (full ranking), which were first introduced in 1982 at a conference held by R. Nadeau and

M. Landry at the Université Laval in Québec, Canada (Brans & De Smet, 2016). PROMETHEE allows to obtain both partial and certain priorities so, detailed analysis can be ensured. Figure 3.6 shows the workflow scheme of the method.

In the first step, the decision-maker must determine the decision points, evaluation factors, and weights thus, the dataset is formed. To assess evaluation factors and show the internal relationship, the decision-maker must select a preference function (step 2). Table 3.3 shows six different preference functions. In the Table, q is the indifference value, p is the certain choice limit, s is the standard deviation also the difference between p and q. q .is the maximum difference and p is the smallest value between evaluation criteria and decision points (Şenkayas & Hekimoğlu, 2013).

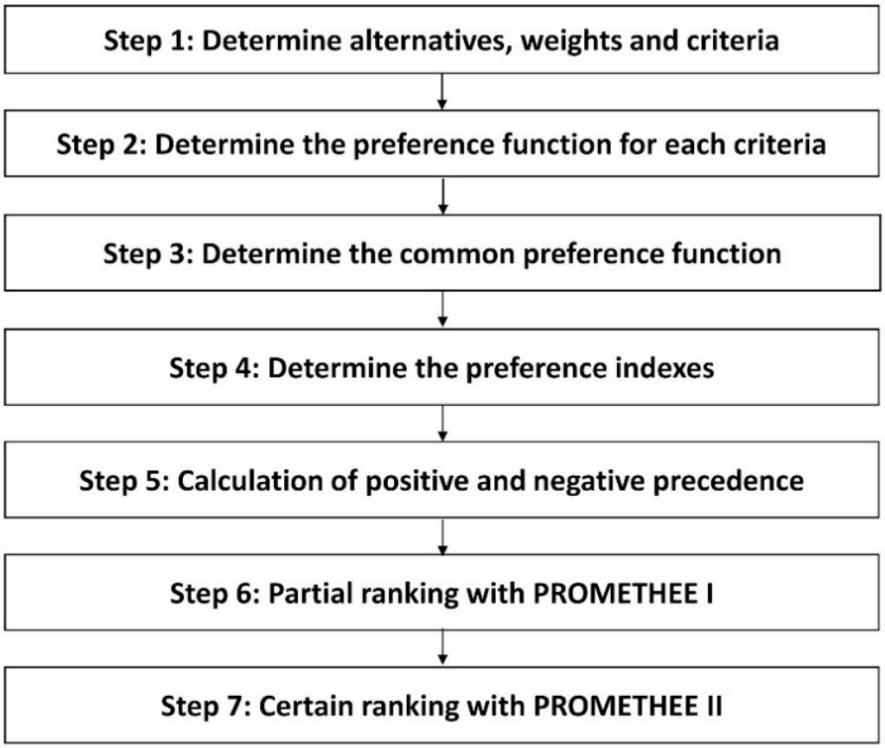


Figure 3.6 PROMETHEE method flow diagram (Brans & De Smet, 2016)

Table 3.3 Preference functions (Brans & De Smet, 2016; Şenkayas & Hekimoğlu, 2013)

Generalized criterion	Function	Parameter
Usual Criterion	$P(x)=\begin{cases}0 & x<0\\ 1 & x>0\end{cases}$	-
U- Shape Criterion	$P(x)=\begin{cases}0 & x<q\\ 1 & x>q\end{cases}$	q
V- Shape Criterion	$P(x)=\begin{cases}0 & x<0\\ \frac{x}{p} & 0\leq x<p\\ 1 & x>p\end{cases}$	p
Level Criterion	$P(x)=\begin{cases}0 & x<q\\ \frac{1}{2} & q\leq x<p\\ 1 & d>p\end{cases}$	p, q
Gaussian Criterion	$P(x)=\begin{cases}0 & x<q\\ 1-e^{\frac{-x^2}{2s^2}} & d>q\end{cases}$	s

If the decision-maker does not have an assessment criterion, the preference function must be the usual criterion. If the decision-maker chooses to use his/her choices for decision points, with a higher value than set points decided by her/him, the function is the Second Type (U type). The third type (V-shape) has the same characteristics, but it does not ignore the values below the decision points. If a specific set of values will decide the decision maker's choices for an assessment factor, the function should be Type Four (level). In terms of an evaluation factor, if the decision-maker is willing to use her/his choice for decision sets with above-average parameters, the function should be a Type Fifth (linear) preference function. If the diversion values of the regarding assessment factor parameters from the average will be the key factor in the decision maker's choice, the function should be the sixth Type (Gaussian) (Brans & De Smet, 2016; Şenkayas & Hekimoğlu, 2013). In this study, the usual criterion was selected because of the aforementioned reasons.

A pairwise comparison between each evaluation factor and decision points must be ensured in step 3. Equation 3.11 illustrates the prevalant preference function when A and B show the two different decision points. Equation 3.12 determines preference indexes using common preference functions.

$$P_{(A,B)} = \begin{cases} 0 & f(A) \leq f(B) \\ p[f(A)-f(B)] & f(A) > f(B) \end{cases} \quad (3.11)$$

$$\pi(A,B) = \sum_{i=1}^{k} (w_i P_i(A,B)) \quad (3.12)$$

In step 5 positive (φ^+) and negative (φ^-) superlative degrees are calculated using Equations 3.13 and 3.14. In the formula, "x" shows the decision points except for A.

$$\varphi^+ = \frac{1}{n-1} \sum \pi(A,x) \quad (3.13)$$

$$\varphi^- = \frac{1}{n-1} \sum \pi(x,A) \quad (3.14)$$

In step 6 partial ranking is determined with PROMETHEE 1. The algorithm ensures the pairwise comparison of positive (φ^+) and negative (φ^-) superlative degrees and find out which decision point is superior. Finally, in the seventh step, using PROMETHEE 2, an exact ranking of the decision points can be resolved. Priority degrees can be calculated with Equation 3.15 and sorted in descending order. According to the formula if $\varphi(A) > \varphi(B)$, alternative A is superior (Brans & De Smet, 2016; Behzadian et. Al. 2010; Şenkayas & Hekimoğlu, 2013).

$$\varphi(A) = \varphi^+(A) + \varphi^-(A) \quad (3.15)$$

3.2.4 Determination of Criteria Weights

Weight determination is a crucial issue that affects the results directly for an MCDA study. There are several weighting methods to overcome this challenge. The methods can be divided into three main categories which are subjective, objective, and integrated. Subjective methods involve expert opinions and decision-makers. They

decide the importance of each criterion based on their previous experiences. On the other hand, during objective weighting, decision-makers do not have a role, the data is used to determine the weights. Objective methods are useful when experts' opinions are non-reachable (Odu, 2019; Zardari, Shirazi, & Yusop, 2015). For this reason, in this thesis, several objective weighting methods were applied to data and the most suitable weighting method was Entropy Method for the MCDA. Figure 3.7 shows these methods and their sub-categories. Entropy, Criteria Importance Through Intercriteria Correlation (CRITIC), and Standard Deviation methods are tried and compared. As a result, the Entropy Method is a more reasonable choice for this data set.

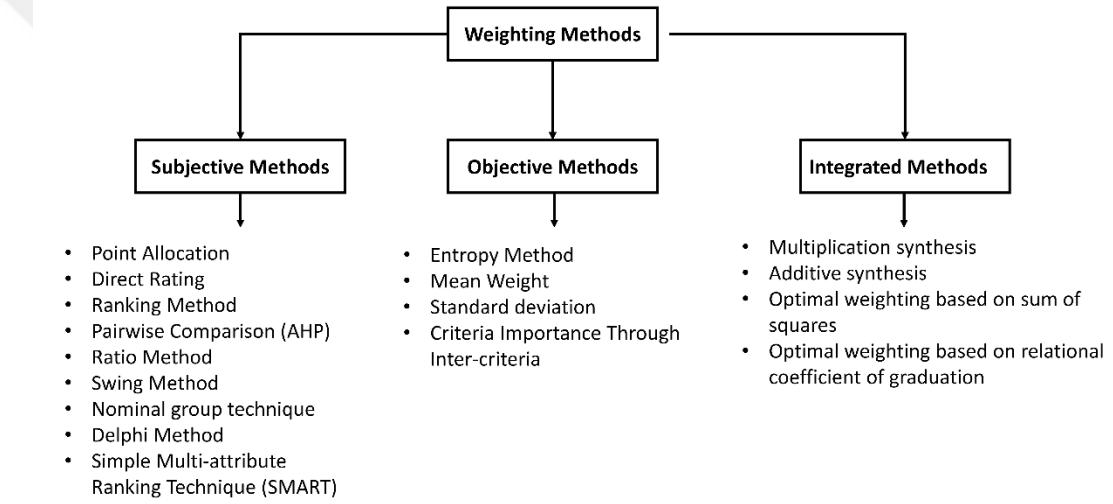


Figure 3.7 Weighting techniques classification (Odu, 2019)

Since the Entropy Method is chosen to weigh the criteria, its logic is discussed. Shanon (1948) introduced the Entropy Method, and It has a wide range of several kinds of applications including engineering (Zou, Yi, & Sun, 2006). The working steps of the method can be listed as:

- **Step 1:** Normalization of the decision matrix is ensured using Equation 3.16. In the equation x_{ij} is the decision point to be normalized and r_{ij} normalized data points. m is the number of alternatives.

$$r_{ij} = \frac{x_{ij}}{\sum_{i=1}^{m} x_{ij}} \tag{3.16}$$

- **Step 2:** Compute the entropy using Equation 3.17.

$$e_j = -\frac{1}{\ln m}\sum_{i=1}^{m} r_{ij} \ln r_{ij}\,,\ j=1,2,\ldots n \tag{3.17}$$

- **Step 3:** Compute the weight factor with Equation 3.18.

$$w_j = \frac{1-e_j}{\sum_{j=1}^{n}(1-e_j)}\ \ j=1,2,\ldots n \tag{3.18}$$

3.3 Hybrid Ship Power Distribution Plant Model Description

The model investigates high-voltage batteries and battery cells that can run in parallel with a ship's electrical power plant. Lithium-ion batteries were chosen for the study because they do not have a memory effect and had higher specific energy and voltage (Saxena et al., 2016; Peralta et al., 2019). Each battery's specs are listed in Table 3.4. The model's data was provided by technical datasheets, and the costs were guaranteed by dealers. The prices are valid for 07.06.2021. For one cell, the parameters of batteries 1 to 4 are given.

Table 3.4 Specifications of batteries (Panasonic, 2021; Molicel, 2018; LGChem, 2014; PowerXtra, 2021; Tesla, 2019; LGResu, 2021)

Battery No	Capacity (Ah)	Voltage (V)	Series Number	Weight (kg)	Cost ($)
1	3.35	3.6	320	0.048	11.83
2	3.5	3.6	320	0.048	11
3	3.5	3.6	320	0.049	7
4	3.2	3.7	320	0.05	5.5
5	56.25	240	2	114	8900
6	23.25	400	2	97	5250

The best battery, the number of parallel sets, CH, and DH are all determined by an iterative selection method. The algorithm runs the hybrid model on various operation modes with several battery combinations using the charging with generators scenario and determines the plant's fuel consumption for one cycle of each battery. At the same time, the FC of the generators without batteries is calculated in total hours equals the

summation of CH and DH. The fuel-saving ratio is calculated and the combinations that affect the fuel-saving ratio below 1% are eliminated. The constructed data set is used to determine the best combinations with the MADM methods mentioned above. CH and DH are selected according to the limits in the batteries' technical datasheets. Table 3.5 illustrates the CH and DH combinations.

Table 3.5 Charge and discharge hour combinations (Panasonic, 2021; Molicel, 2018; LGChem, 2014; PowerXtra, 2021; Tesla, 2019; LGResu, 2021)

Total Hour	CH	DH
16	8	8
12	8	4
12	4	8
11	3	8
11	8	3
9	6	3
9	3	6
8	4	4
7	3	4
7	4	3
6	3	3

There are two scenarios to charge batteries and the first one is charging with generators. The second strategy involves a WHRS to charge batteries during the navigation and to extend the discharge time of the batteries during the port and harbor operations. The determined battery combinations are used in the mathematical model and their effect is compared. The model is an adjusted version of the previous model used to simulate the marine diesel generator operation. Battery voltages are determined using state of charge (SoC) formulae and voltage curves obtained from the batteries' technical specifications. Figures, 3.8, 3.9, 3.10, and 3.11 illustrate charge and discharge curves used to calculate voltage from SoC. The state of health (SoH) of a battery is determined by the ratio of actual capacity (C_{act}) to initial capacity (Omar et al, 2014). Equations based on the number of cycles and capacity curves are used to calculate C_{act}. Figures 3.12, 3.13, 3.14, 3.15, and 3.16 depict the aging curves of the batteries used to determine the SoH. The charging protocol is constant current, constant voltage, and the discharging protocol is constant current, constant voltage, and variable C rates are employed. To avoid increasing inner resistance and to improve battery life, the SoC range for the model is between 20% and 80%. When the SoH approaches 80%, batteries are thought to need replacement (Saxena et al., 2016).

Figure 3.17 shows the algorithm scheme of the model when the generator charging strategy is applied. Figure 3.18 illustrates the diagram of the electrical distribution system with batteries for this charging scenario. Figures 3.19 and 3.20 depict simplified circuit diagrams involving batteries, inverters, and converters. Selected inverter and converter inlet voltages are calculated using the technical data sheets (SMA, 2021).

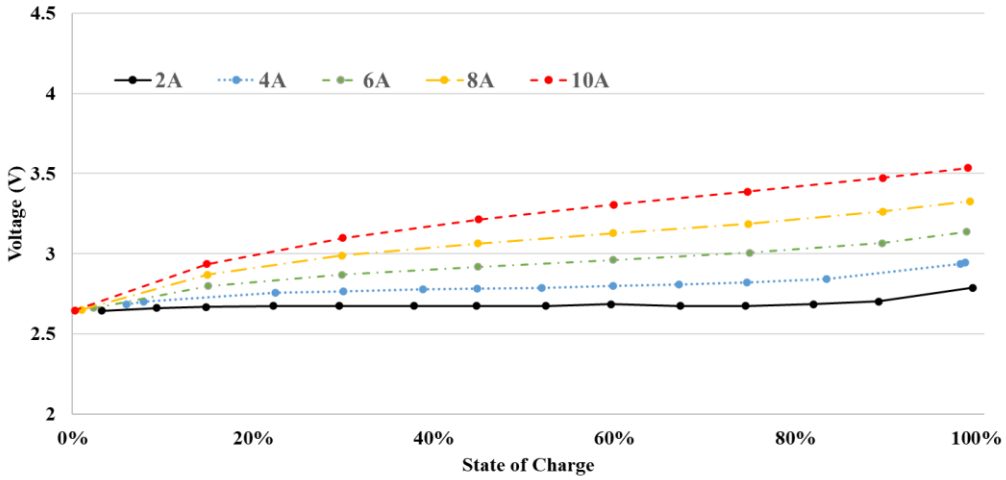


Figure 3.8 Charge curve of battery 1 (Panasonic, 2021)

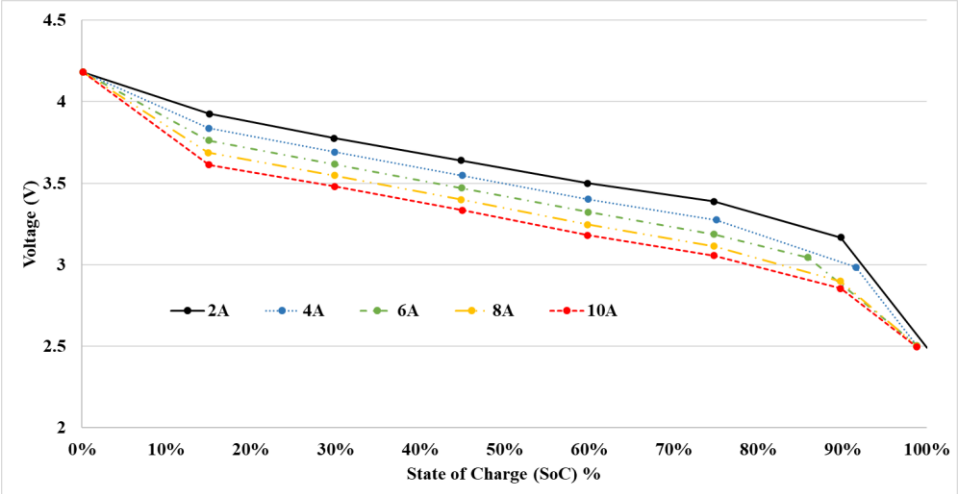


Figure 3.9 Discharge curve of battery 1 (Panasonic, 2021)

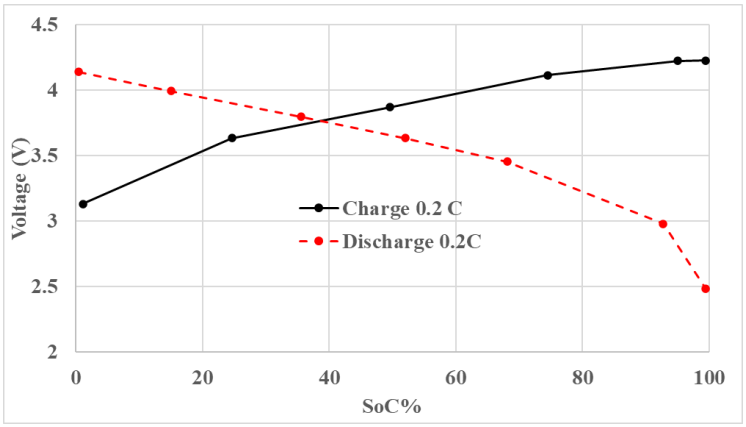


Figure 3.10 Charge and discharge curves of batteries 2,3 and 4 (Molicel, 2018; LGChem, 2014; PowerXtra, 2021)

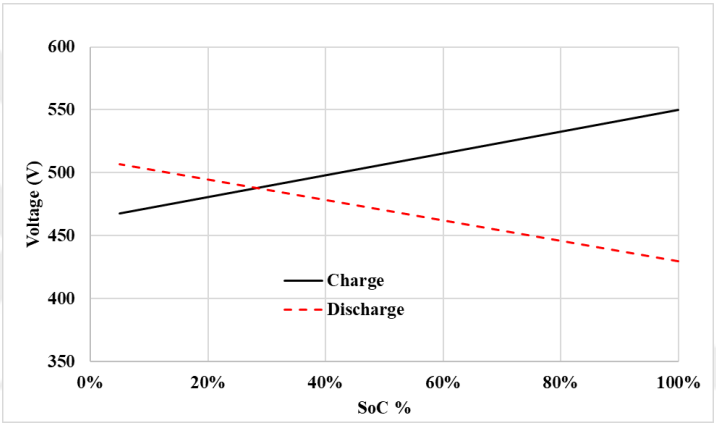


Figure 3.11 Charge and discharge curves of batteries 5 and 6 (LGResu, 2021)

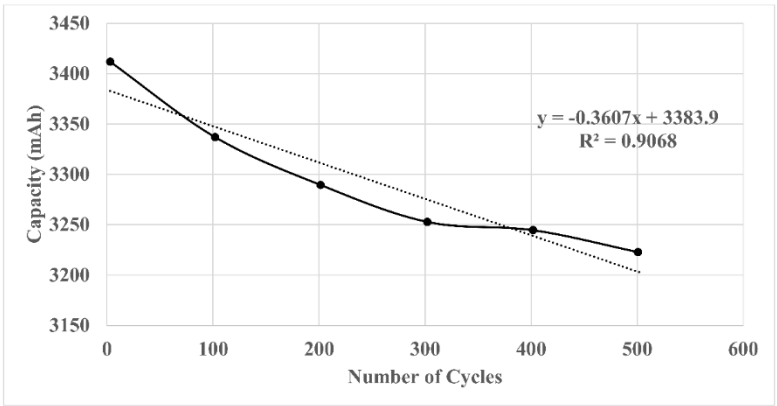


Figure 3.12 Aging curve of battery 1 (Panasonic, 2021)

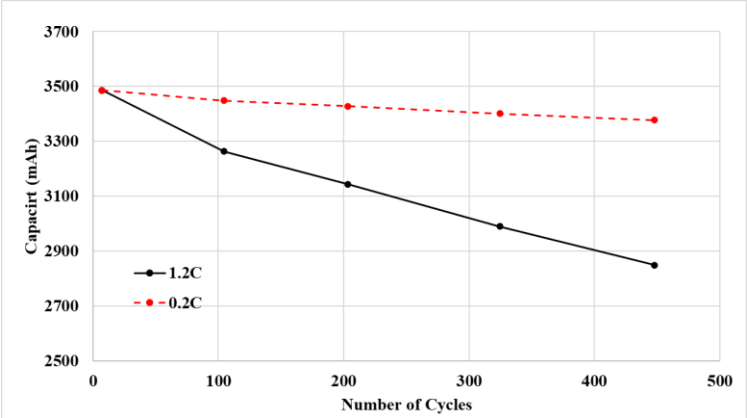


Figure 3.13 Aging curve of batteries 2 and 3 (Molicel, 2018; LGChem, 2014)

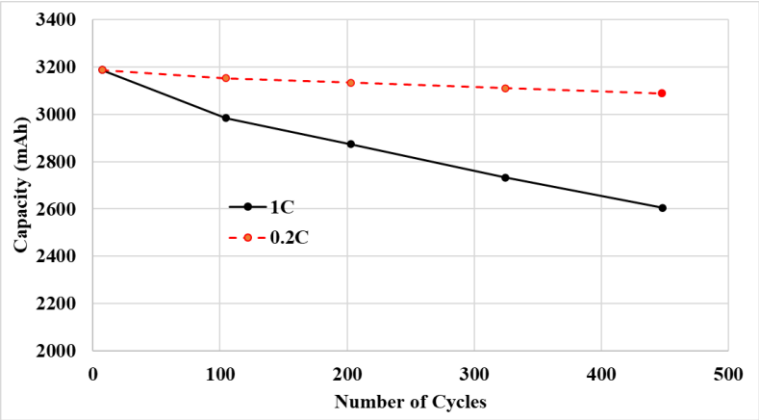


Figure 3.14 Aging curve of battery 4 (PowerXtra, 2021)

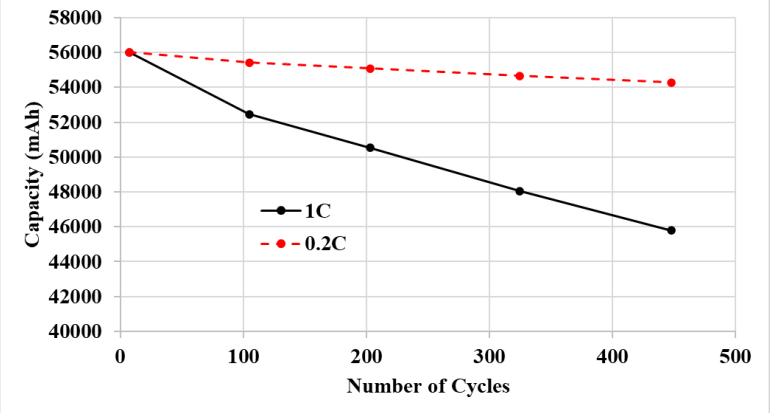


Figure 3.15 Aging curve of battery 5 (Tesla, 2019)

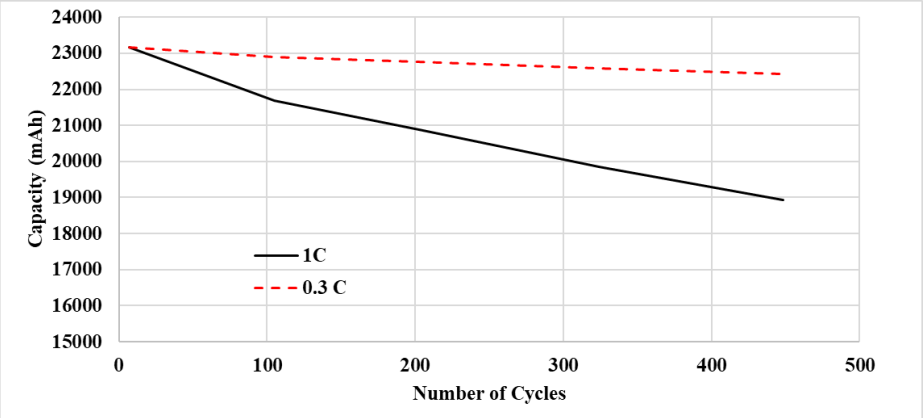


Figure 3.16 Aging curves of battery 6 (LGResu, 2021)

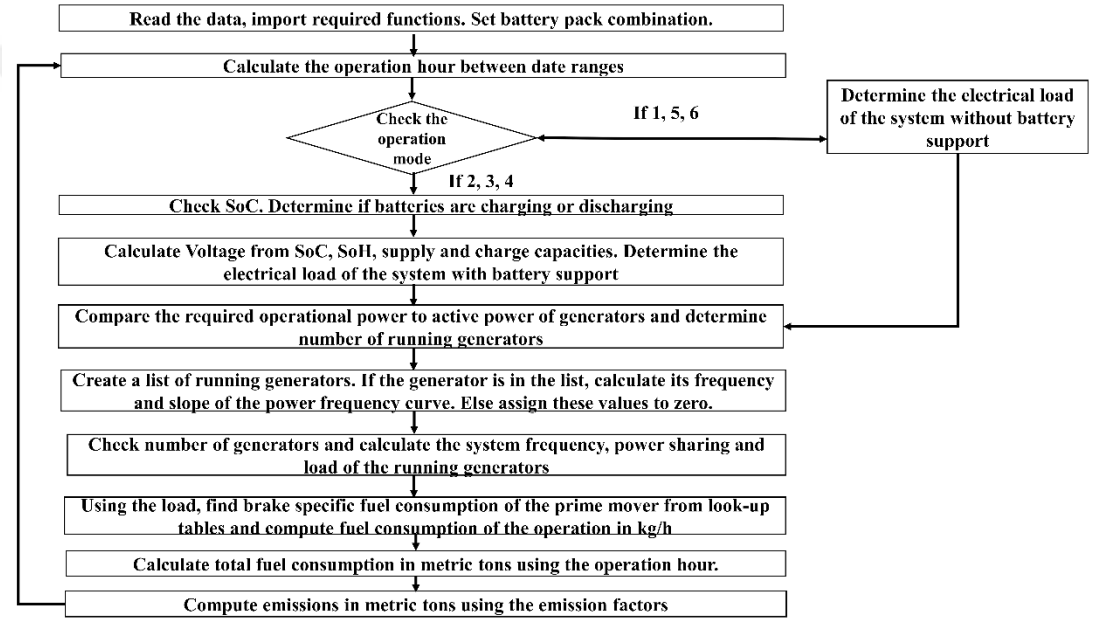


Figure 3.17 Algorithm scheme of the model when generators charge the batteries

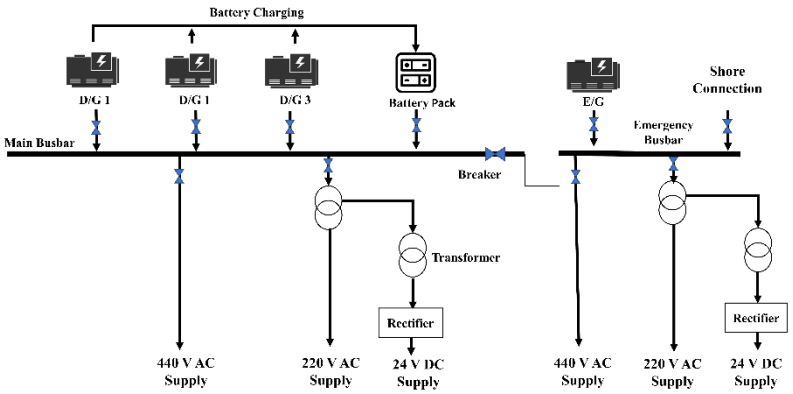


Figure 3.18 Diagram of ship hybrid electric distribution system when generators charge batteries (Adapted from Cahyagi & Koenhardono, 2018, Oways, 2019)

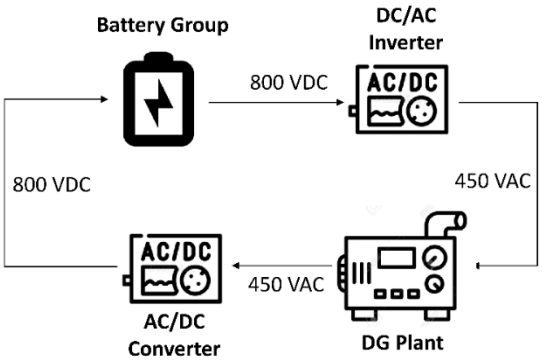


Figure 3.19 Circuit diagram for batteries 1, 2, 3, 4, 6

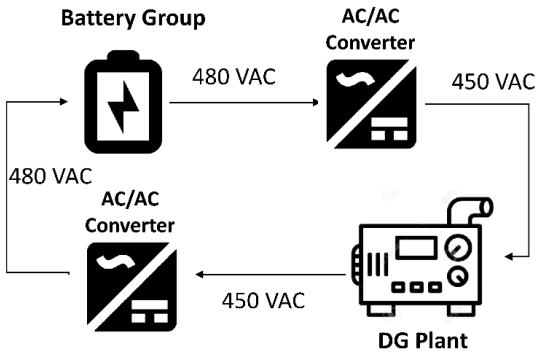


Figure 3.20 Circuit diagram of the battery 5

The second battery charging strategy uses a WHRS that generates electricity from the WH of the ME and DGs. To determine the electricity production capacity of the WH, required data of ME were obtained from M.A.N (2020). DG WH data were gathered from the ships that include technical sheets and operational information. Selected WHRS has a design award, and its efficiency (η_{WHRS}) can reach 14% (Cision, 2015). Table 3.6 indicates a generator's WH potential, and Table 3.7 is the potential for the ME. Calculations have been carried out using Equations 3.19 and 3.20. In Equation 3.19, $\dot{m}_{Ex}$ is exhaust mass flow rate, $T_{Ex,in}$ and $T_{Ex,out}$ are the inlet and outlet temperature in the turbine. W is the net produced power WHRS (Konur et al. 2020).

$$Q_{WH}=\dot{m}_{Ex}*c_p*(T_{Ex,in}-T_{Ex,out}) \quad (3.19)$$

$$W=Q_{WH}*\eta_{WHRS} \quad (3.20)$$

Table 3.6 Power production from DG WH. (M.A.N, 2020)

Load %	WH from DGs (kW)	Power from WHRS (kW)
10	121.07055	16.94988
25	286.02918	40.04409
50	446.76781	62.54749
75	598.95	83.853
100	718.74	100.6236

Table 3.7 Power production from ME WH (M.A.N, 2020)

Load %	Exhaust Flow Rate (kg/h)	WH from ME (kW)	Power from WHRS (kW)
100	14.7	1760.913	246.52782
95	14.2	1701.018	238.14252
90	13.7	1641.123	229.75722
85	13.2	1581.228	221.37192
80	12.6	1509.354	211.30956
75	12	1437.48	201.2472
70	11.4	1365.606	191.18484
65	10.8	1293.732	181.12248
60	10.1	1209.879	169.38306
55	9.4	1126.026	157.64364
50	8.6	1030.194	144.22716
45	7.9	946.341	132.48774
40	7.1	850.509	119.07126
35	6.2	742.698	103.97772
30	6.1	730.719	102.30066
25	5.4	646.866	90.56124
20	4.6	551.034	77.14476
15	3.9	467.181	65.40534
10	2.8	335.412	46.95768

Low-temperature heat is transformed into clean power by the WHRS Unit. The system is built for unrivaled efficiency within the operating temperatures, using the concepts of the Organic Rankine Cycle but at significantly decreased pressures. The module entails driving a flow that creates electricity utilizing a heat source (high pressure) and a cold sink (low pressure). Each module has an evaporator for transferring heat to the interior working fluid, a turbine-generator configuration for converting thermal energy to electric energy, and a cooling system for transferring heat from the system to the cooling water line (Climeon, 2021). Figure 3.21 demonstrates the exhaust flow diagram to the WHRS from sources. Figure 3.22 indicates the working principle of the system.

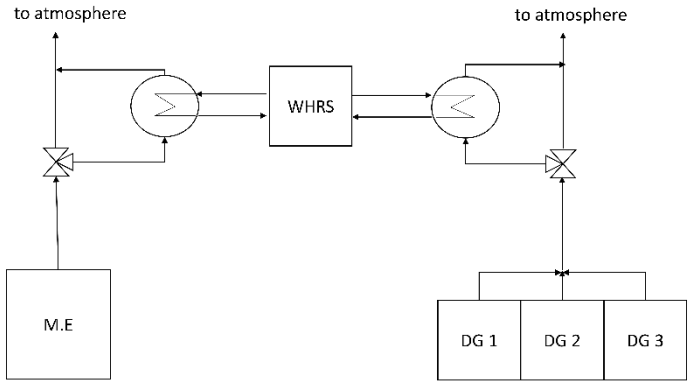


Figure 3.21 Exhaust flow diagram of the WHRS (Adapted from Konur et. al., 2020)

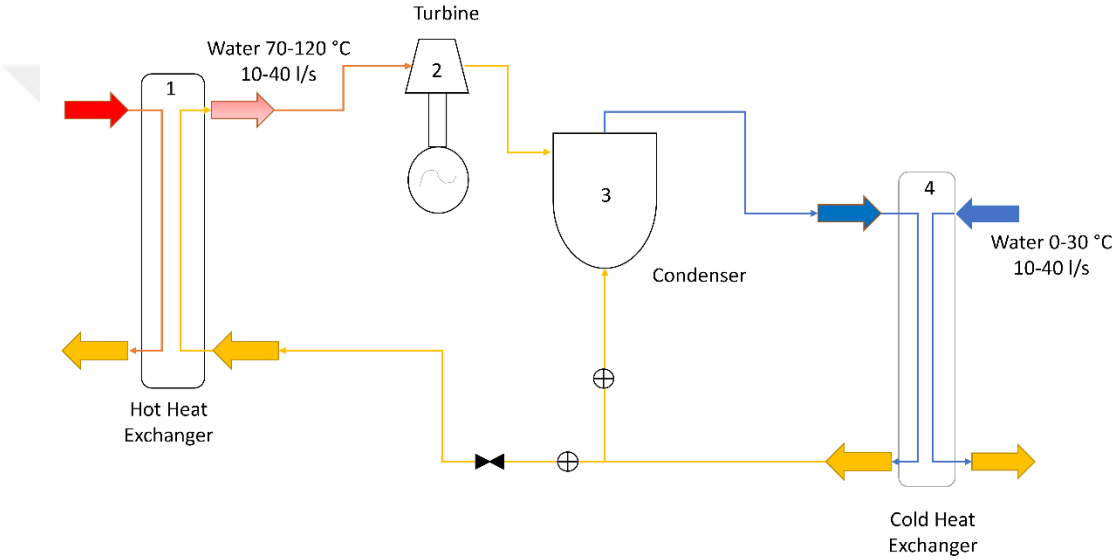


Figure 3.22 Working diagram of the WHRS (Adapted from Climeon,2021)

In the first component, the working fluid in the hot heat exchanger boils due to the heat from the heat source. After that, in the second stage, the vaporized working fluid goes through the turbine, which generates power by driving a generator. In the third phase, as the gas hits the cooled working fluid from the cold heat exchanger, the condenser turns it into liquid. The final stage closes the loop by distributing the liquid working fluid to the cold and hot heat exchangers (Climeon, 2021).

WHRS consists of a module that can provide 150 kW electricity for the hybrid plant, and it collects the exhaust waste of the diesel engines after the steam is produced in the exhaust boiler. Exhaust entering temperature at the WHRS inlet is assumed as 493 K and it is accepted to be reduced to 353 K. Sulfuric acid formation due to low

exhaust temperatures are assumed to be collected by the tanks placed in the WHRS configuration (Konur et al., 2020). Table 3.9 indicates that, even with slow-steaming loads (55-65%), ME has the potential to operate the one WHRS module. At least one generator WH is available for the operation. For these reasons, it is accepted that the WHRS supports the ship electric generation plant when the ME is running (operations 1 and 2), it provides 150 kW continuously. The electricity produced by WHRS using ME WH charges the batteries first if, SoC is below 20%. After that, it lowers the generator load during the navigation. When the ME is not working, the WH from working generators is used to support extending the discharge time of the battery set. It is also used to assist the generator load during the battery set charging. WH is calculated according to generator load without charge or discharge conditions. After that, charge power is calculated with battery charge power, WH support power, and the operation load. Figure 3.23 electric distribution system diagram when batteries are charged by WHRS. Figure 3.24 demonstrates the algorithm scheme of the model of the second scenario. Figures 3.25 and 3.26 demonstrate simplified circuit diagrams when the battery charge is ensured by WHRS, involving batteries, inverters, and converters.

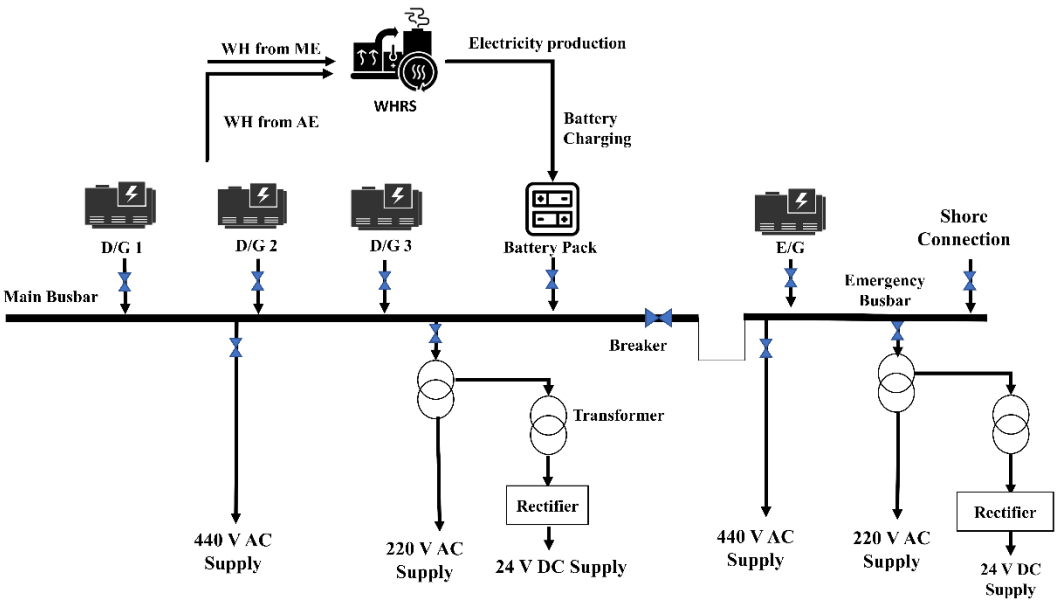


Figure 3.23 Diagram of ship hybrid electric distribution system when WHRS charge batteries (Adapted from Cahyagi & Koenhardono, 2018, Oways, 2019)

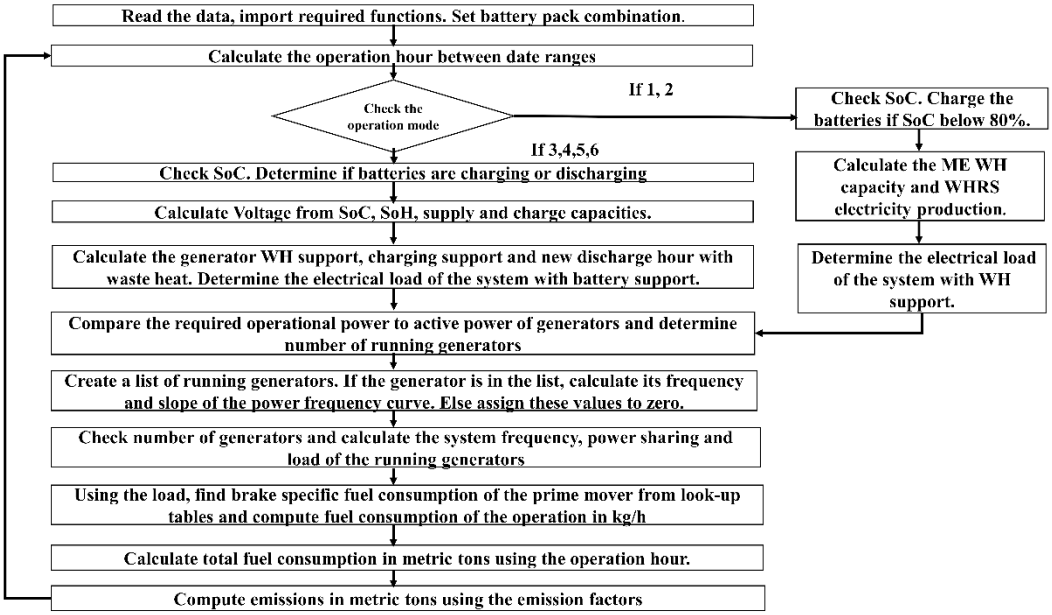


Figure 3.24 Algorithm scheme of the model when WHRS charges the batteries

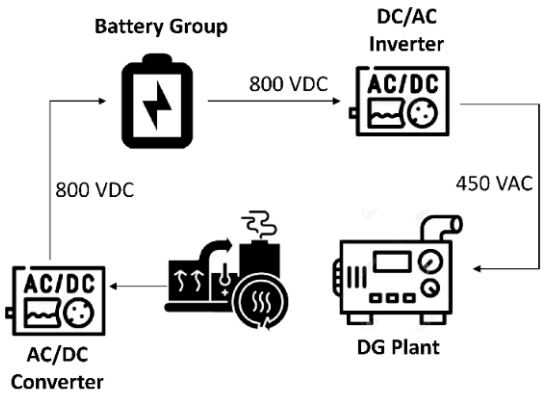


Figure 3.25 Circuit diagram for batteries 1, 2, 3, 4, 6 with WHRS charge

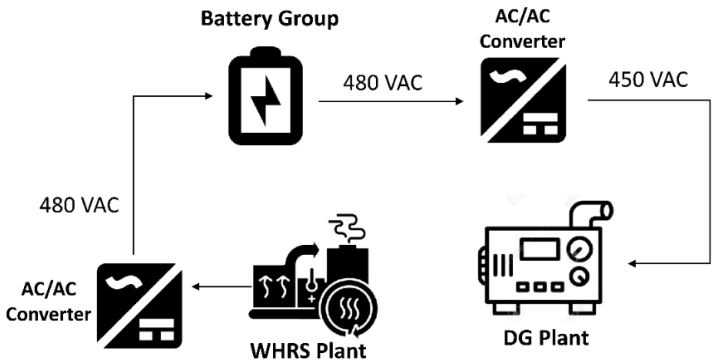


Figure 3.26 Circuit diagram of the battery 5 with WHRS charge

3.4 Emission Calculation

Ship emission calculations methods can be categorized into three different types. These are FC, energy, and engine power-based methods (Kuzu et al., 2021). Since the model calculates the FC from the plant, the first technique is applied to calculate emissions. Equation 3.21 presented by Trozzi (2010) uses emission factors (EF) to compute the total emissions (E) of a medium-speed diesel engine for each pollutant type (i). Table 3.8 illustrates EF proposed by IMO4 (2014).

$$E_i = \sum_k FC * EF_i \tag{3.21}$$

Table 3.8 EF (g emission/ g fuel) (Adapted from Kuzu et al., 2021; Trozzi, 2010; IMO4, 2014)

Pollutant	CO_2	CH_4	N_2O	NO_x	NMVOC	CO	PM_{10}	SO_2
EF MGO	3.206	0.00006	0.00015	0.0961	0.00308	0.00277	0.00097	0.01
EF HFO	3.114	0.00006	0.00015	0.0903	0.00308	0.00277	0.00278	0.025

3.5 Fuel Consumption Estimation Algorithms

Four different regression models provided future forecasts of the plant FC. Comparison between metrics of these models yielded to find the ideal estimation algorithm for the data set. Algorithms explained in this section that can be suitable to the data set can be listed as:

- Time series analysis using Auto-regressive integrated moving average (ARIMA).
- Ordinary least squares (OLS) regression.
- SVR
- ANN-FNN

The data standardization and model performance evaluation metrics are also explained in the section.

3.5.1 Time Series Analysis

Time series data can be expressed as quantitative values formed with chronological time stamps. The time series analysis in this thesis used the data formed in the

application. Time series analysis can be defined as a statistical approach that targets time series data or data with a trend. This analysis has been used to forecast in economics, politics, and environmental fields such as greenhouse gas amount forecast through time (Kirchgässner & Wolters, 2007; Shumway & Stoffer, 2017).

Seasonality is eligible for the time series data if repeating cycles or trends over time exist in the data. Stationary in the time series data means that statistical features of the data are not changing with time. If the data is nonstationary, it is recommended to apply an appropriate method that transforms the data to the stationary state. Detection of seasonality and stationarity can be done by plotting the time series data and examination of the statistical summary of the model. In addition, Augmented Dickey-Fuller (ADF) test can be applied to the data to check if it is stationary or not. In the ADF test, the p-value can determine the stationarity of the model. If the p-value is under 0.05, the data can be assumed stationary (Mills, 2019). These methods also provide us knowledge about our data is white noise or random walk. When the data is white noise, there is no relationship between observations in other words the data is comprised of random numbers with a mean of zero. The variance of all variables is the same and there is no correlation between variables Thus, white noise data cannot be predicted (Brownlee, 2017). Random walk time series is formed with data whose present variable is the addition or extraction of the previous value and some random step (Brownlee, 2017). Auto-correlation function (ACF) and partial autocorrelation function (PACF) are factors to decide the order of autoregressive (AR) and moving average (MA) series. They are also helpful to detect our data properties mentioned above. ACF is a metric that shows the autocorrelation between the current and lagged data. It determines the strength of the relationship between present and past values. PACF detects the correlation between residuals and lagged values. Order of AR (p) and order of MA(q) can be found with analysis of ACF and PACF plots. The number of lagged parameters in the model is denoted as p and MA distance size is denoted as q. Table 3.9 illustrates the behavior of ACF and PACF plots to detect the right model and orders (Brownlee, 2020; Mills, 2019; Salvi, 2019).

Table 3.9 Characteristics of the ACF and the PACF of AR and MA processes (Kirchgässner & Wolters, 2007)

Model	ACF	PACF
AR (p)	Tails off	Breaks off after lag p
MA (q)	Breaks off after lag q	Tails off
ARMA (p, q)	Tails off	Tails off

In the AR time series, past observations can be used to find the current value. Equation 3.22 shows the AR(p) model description (Mills, 2019; Salvi ,2019).

$$y_x = \alpha_1 * y_{x-1} + \alpha_2 * y_{x-2} + \ldots + \alpha_p * y_{x-p} + \epsilon_x \quad (3.22)$$

where y_x and ϵ_x values represent lags and white noise, respectively. In the MA model, the present data can be expressed with linearly combined past errors. Equation 3.23 describes the MA(q) model process (Salvi, 2019).

$$y_x = m_1 * \epsilon_{x-1} + m_2 * \epsilon_{x-2} + \ldots + m_p * \epsilon_{x-q} + \epsilon_x \quad (3.23)$$

A combination of the AR(p) and M(q) models give the ARMA (p, q). Equation 3.24 is the formula that describes the ARMA (p, q) process (Mills, 2019; Salvi, 2019).

$$y_x = m_1 * \epsilon_{x-1} + m_2 * \epsilon_{x-2} + \ldots + m_p * \epsilon_{x-q} + \epsilon_x \quad (3.24)$$

To ensure the stationary differencing the data is an applicable method. Autoregressive integrated moving average (ARIMA) models can apply the differencing automatically with the adjustment of the parameter d which is the non-seasonal differencing order (Brownlee, 2020).

Box-Jenkins method is a useful and effective guide when selecting the right model for the data and building the model. It was introduced by George Box and Gwilyn Jenkins in 1970. The method assumes the time series can be forecasted with ARMA for stationary models. If the data does not perform well with the ARMA models, using

an ARIMA model can fix the problem. The steps of the method can be listed as: (Box et. al., 2015; Brownlee, 2020).

- Identification
- Estimation
- Model Diagnostic Control
- Forecasting

Model order and type selection can be carried out using the Akaike Information Criteria (AIC) and the Bayesian Information Criteria (BIC). They have commonly used performance metrics both in statistics and time series analysis. AIC and BIC determine the model quality with the estimation of the model error. Both metrics penalize complex models, in other words, they tend to select simple models with minimum error rates. The lower AIC and BIC indicate better performance. Equations 3.25 and 3.26 are AIC and BIC formulas respectively (Fabozzi, et. al., 2014).

$$AIC= -2*\log L(\hat{\theta})+2*k \tag{3.25}$$

where θ model parameter vector, $L(\hat{\theta})$ likelihood of the maximum model estimation, k is the number of predicted parameters in the model.

$$BIC= -2*\log L(\hat{\theta})+k*\log n \tag{3.26}$$

where n is the number of observations, and the other parameters are denoted the same in the AIC formula.

3.5.2 Ordinary Least Squares Regression

OLS is a statistical evaluation technique that predicts the association between dependent and independent parameters by minimizing the sum of squares in the divergence between predicted and real variables of the dependent parameter set as a smooth curve (Encyclopedia, 2019). The method decides the regression line using the parameters β_0 and β_1 which are intercept and slope variables. OLS can achieve highly

accurate estimations with an easy computation and suitable data set. The predicted value $\hat{y}$ can be found with the determination of β_0 and β_1 and it depends on dependent parameter x. Equation 3.27 shows the estimation formula of $\hat{y}$ value.

$$\hat{y} = \beta_0 + \beta_1 x \tag{3.26}$$

The difference between estimated and observed values (y) are called residuals (r) and its computation is shown in Equation 3.27

$$r = y - \hat{y} \tag{3.27}$$

Different sums of squares are used in OLS. The first one is the total sum of squares (TSS) illustrated in Equation 3.28. TSS detects the mean changeability of the results.

$$TSS = \sum_{i=1}^{n} (y_i - \bar{y})^2 \tag{3.28}$$

where $\bar{y}$ is the sample mean of the results. TSS has two stages in an OLS regression model. The first stage is the model sum of squares (MSS), the second is the residual sum of squares (RSS) and they are demonstrated as Equations 3.29 and 3.30.

$$MSS = \sum_{i=1}^{n} (\hat{y}_i - \bar{y})^2 \tag{3.29}$$

$$RSS = \sum_{i=1}^{n} (y_i - \hat{y}_i)^2 \tag{3.30}$$

Minimization of the RSS is done by fitting the regression line. In the OLS, TSS = MSS + RSS. The determination coefficient (R^2) is a measure of how well the predictions are fitted. It will be between 0-1 and when it is close to 1 indicating a successful level of fit (Vittinghoff et al. 2006; Kasuya, 2019). Equation 3.31 shows the formulation of R^2.

$$R^2 = 1 - (RSS/TSS) \tag{3.31}$$

3.5.3 Support Vector Regression

The SVM algorithm's aim is to search a hyperplane in N-dimensional search space (N: feature number) that select between data points. SVMs are generally used for classification but, they can be utilized for regression problems as well and are named SVR. The method ensures a litheness to determine the allowable error rate in the problem, will search for a proper fitting line for the data (Sharp, 2020). SVR does not try to minimize the squared error instead it minimizes the coefficient vector. Constraints specified in the beginning, manage the error terms. Equations 3.32 the approximation of continuous function is depicted (Awad & Khanna, 2015).

$$y = f(x) = \langle w, x \rangle + b = \sum_{k=1}^{M} w_k x_k + b,\ y, b \in R,\ x, w \in R^M \tag{3.32}$$

The multiple parameter regression formula can be written as Equation 3.33. Equation 3.34 demonstrates the objective function and Equation 3.35 represents the constraints (Sharp, 2020).

$$f(x) = \begin{bmatrix} w \\ b \end{bmatrix}^T \begin{bmatrix} x \\ 1 \end{bmatrix} = w^T x + b,\ x, w \in R^{M+1} \tag{3.33}$$

$$\min_w \frac{1}{2} \|w\|^2 \tag{3.34}$$

$$|y_i - w_i x_i| \leq \varepsilon \tag{3.35}$$

where ε is the maximum error. Figure 3.27 demonstrates the planes of the SVR and approximation process.

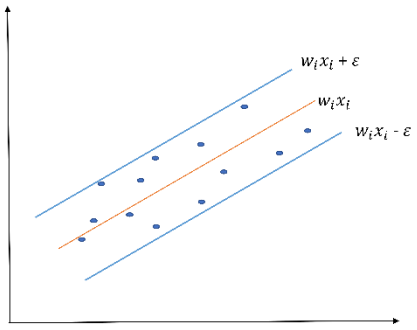


Figure 3.27 SVR Example (Adapted from Sharp, 2020)

3.5.4 Artificial Neural Networks

ANN is a deep learning method that is commonly utilized in classification and regression applications. The number of layers and neurons are critical components of ANN. Various experiments must be carried out to determine an appropriate number of neurons, layers, and the training-test split ratio (Oztemel 2016; Köseoğlu 2015). The number of layers, neurons, activation function, batch size, epochs, and optimizer were determined by the outcomes of Python trials. When compared to alternative activations, such as y=max, the Rectified linear unit (Relu) offers the best results with the data (0, x) as the transfer function of hidden layers. Because the data does not contain complex patterns or a substantial bias, more basic activation functions such as Relu can be used, reducing the ANN's training time (Dreyfus, 2005). The hyperbolic tangent sigmoid function is used in the output layer and its formula is depicted as Equation 3.36. Because of its efficiency, ease of implementation, and applicability for big datasets, the Adam optimizer is chosen to assemble the network (Kingma & Ba, 2014). 80% of the data is used as training data and 20 % of the is the test data to evaluate the performance of the network.

$$n_j = \left(\frac{2}{1+e^{-2Z}}\right) - 1 \tag{3.36}$$

where n_j is the output of the neuron. The term Z is calculated using Equation 3.37.

$$Z = \sum_{i=1}^{r} w_{ij} p_i + b_j \tag{3.37}$$

w_{ij} is the relation weights of the i_{th} neuron in the previous layers to j_{th} neurons. The output of the i_{th} neuron is p_i. Bias is b_j and r is the number of neurons (Najafi et al., 2018; Yüksel & Köseoğlu, 2019). Figure 3.28 depicts the structure of the ANN used in the study. Epochs are 50, the batch size is 10 in the model neuron numbers of each layer can be seen in the Figure. These values are determined as a result of many trials with the data and network.

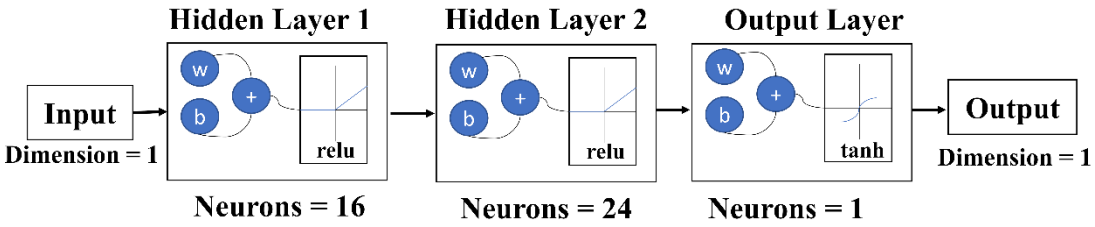


Figure 3.28 ANN structure

3.5.5 Model evaluation and data standardization

Data standardization is required to enhance the regression model performance meanwhile to accelerate the calculation speed. It is a way of scaling that transforms data into having a mean of zero and a standard deviation of one. Equation 3.38 indicates the process of data standardization. Each data point (x) is subtracted from the mean ($\overline{x}$) and then divided to the standard deviation (σ) (Trebuňa et al. 2014).

$$z = (x-\overline{x})/\sigma \tag{3.38}$$

The error rate is the difference between the model predictions and the real value, and it is used to evaluate the performance of models. In this thesis, because of their wide usages and comprehensibleness mean absolute error (MAE) and root mean squared error (RMSE) is used to determine the success of the model. The validity of the mathematical model of the ship power distribution plant is assessed with MAE since it is an understandable and dependable technique (Chai & Drexler, 2014; Willmott & Matsuura, 2005). MAE is a statistic that assesses the gap between actual and expected values without taking direction into account; a lower MAE indicates better prediction performance (Chai & Drexler, 2014). The regression algorithms' performance is evaluated with both MAE and RMSE. R^2 explained in the OLS section is also a valuable evaluation metric for regression algorithms and it is also used in their assessment. The analogy between three metrics ensures the evaluation is more reliable to prevent overfitting. Equations 3.39 and 3.40 indicate the MAE and RMSE formulation respectively. In the equations, n is the number of data points, y_p is the

computed or estimated value, y_t is the actual or true value and $\bar{y}$ is the mean (Chai & Drexler, 2014; Kasuya, 2019).

$$MAE=\frac{\sum_{i=1}^{n}\left|y_p-y_t\right|}{n} \tag{3.39}$$

$$RMSE=\sqrt{\frac{\sum_{i=1}^{n}(y_p-y_t)^2}{n}} \tag{3.40}$$

3.6 Economic Analysis

The economic model of the proposed hybrid system requires the total investment cost that involves the prices of batteries and the WHRS system. The battery price information is available on the dealer's website. In the thesis, the prices were gathered at 07.06.2021. WHRS price was found from Sachitanand (2017) and Pallis et al., (2021) as 2000 $/kW. To calculate electricity production price (c_{ele}) on board, average fuel prices of 20 bunker points between 06.12.2019 and 07.06.2021 were obtained from Ship&Bunker (2021). The plant consumes IFO380 during the navigation and MGO near the coastal areas. Figures 3.30 and 3.31 illustrate the price variations of the MGO and HFO respectively. Figures demonstrate a distinct fall in prices during pandemic conditions. Operation and maintenance costs are considered 1.5% of the investment cost (Wei et al., 2019). After the determination of costs, the capital recovery factor (CRF) presented in Equation 3.41 that turns the total current value to a flow of even annual payment at the annual interest rate (i = 5%) in the system life taken as 20 years and life span of batteries estimated according to SoH using the OLS (Yao et al., 2018; Tian et al., 2021).

$$CRF=\frac{i(1+i)^n}{(1+i)^n-1} \tag{3.41}$$

Levelized energy cost (LEC) is the stable electricity cost of the net power chosen as the indicator of economic analysis. LEC is calculated by using the total investment cost (C_{tot}), operation and maintenance costs (C_{om}), CRF, total electricity production

(W_{net}), and operation time (t). Equation 3.42 demonstrates the calculation of LEC. Payback periods (PBP) of systems are calculated using Equation 3.43 (Tian et al., 2021).

$$LEC = (CRF*C_{tot}+C_{om})/(W_{net}*t) \tag{3.42}$$

$$PBP = \frac{C_{tot}}{(W_{net}*t*c_{ele})-C_{om}} \tag{3.43}$$

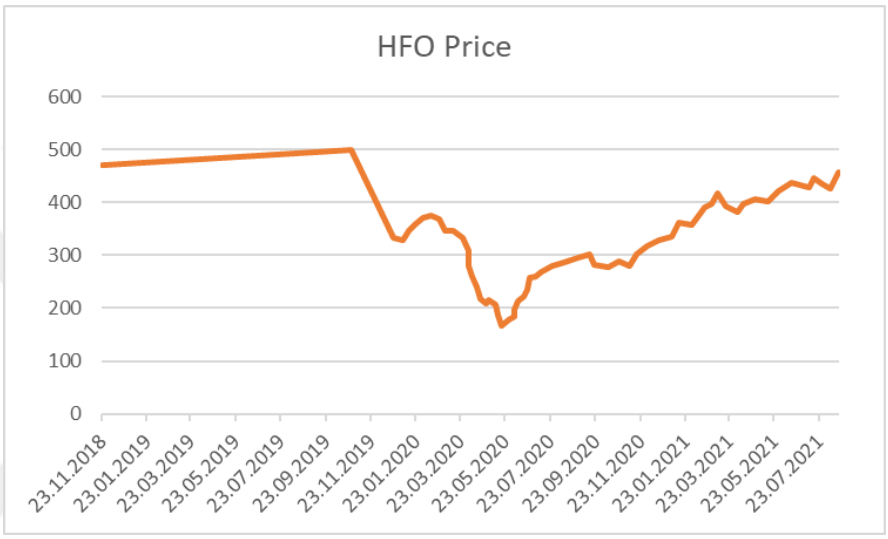


Figure 3.30 IFO 380 prices (Adapted from Ship&Bunker, 2021)



Figure 3.31 MGO prices (Adapted from Ship&Bunker, 2021)

CHAPTER 4
RESULTS AND DISCUSSIONS

The chapter indicates the results of the marine diesel generator's mathematical model, MADM algorithms, and hybrid system model. The validation of the mathematical model is illustrated and FC reduction of the hybrid system with different charging strategies is discussed in this section. Outcomes of emission reduction potential and economic evaluation of proposed systems are also demonstrated in the chapter.

4.1 Model Validation

Validation of the model has been a crucial issue since the analysis of the battery pack addition and power managements system optimization on the electrical system of the ship can give eligible and accurate results. Especially, parallel behavior and frequency variations of the generators hold a remarkable position while the connection of the battery pack is done. In addition, the results of the planned scenario analysis depend on an accurate model. Therefore, the parameters both calculated by the model and applicable at the manufacturer data sheet compared, and the error rate of the model was calculated. In addition, comparison graphics of measured and calculated values were presented in this section.

Figure 4.1 illustrates the analogy between measured and calculated line voltages of the synchronous generator. MAE of the line voltage calculation of the model is 0.000325. The error rate of the model line voltage prediction is successful according to the error rate calculation.

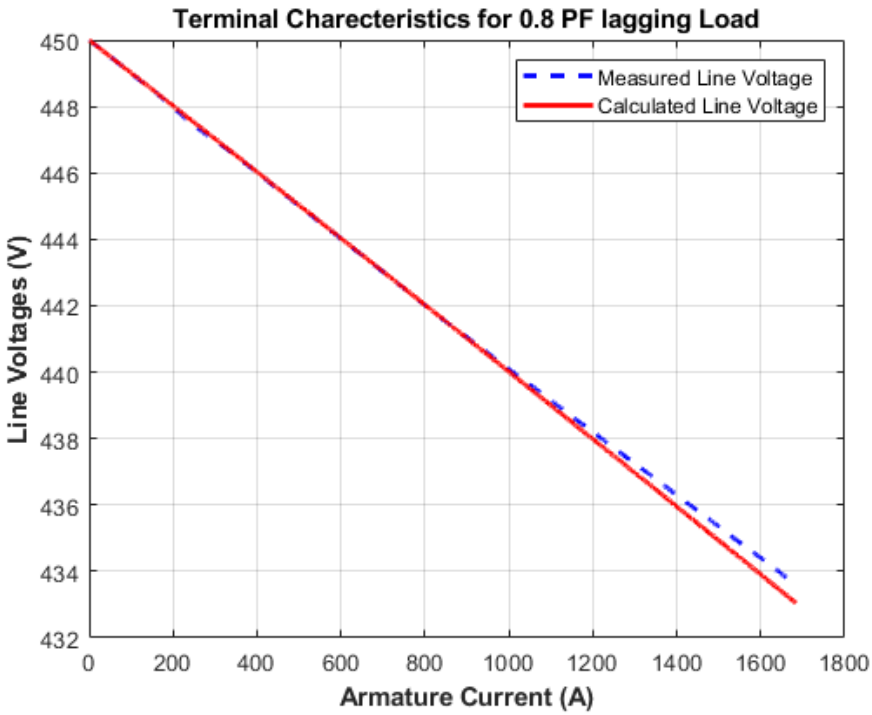


Figure 4.1 Measured and calculated line voltage comparison

Figure 4.2 depicts the benchmarking between the calculated and measured output power of the synchronous generators. MAE of this analogy is 0.0035 which is a small rate for this calculation. Figures 4.3, 4.4, and 4.5 represent an analogy between the frequency from governor test results and the frequency calculated by the model for generators 1, 2, and 3 respectively. The frequency calculation for generator 1 resulted in a MAE of 0.0034, for generator 2 MAE is 0.0039 and for generator 3 MAE is 0.004. The error rate is also in an acceptable range for this evaluation. Figures 4.6, 4.7, and 4.8 illustrate the comparison between the power-sharing according to the total system load taken from parallel running tests of each generator. Figure 4.9 demonstrates the frequency drop of the system depending on the total system load. Parallel running test done by the manufacturer, starts with stabilized system frequency which is 60 Hz. However, the model neglects the stabilization processes so, the error rate of the system frequency calculation could be higher. The error rate of the system frequency drop rate with the rising system power is 0.0099. The MAE of the power-sharing calculation for generator 1 is 0.0168, for generator 2 is 0.0095 and for generator 3 is 0.0102 which are also reasonable error rates.

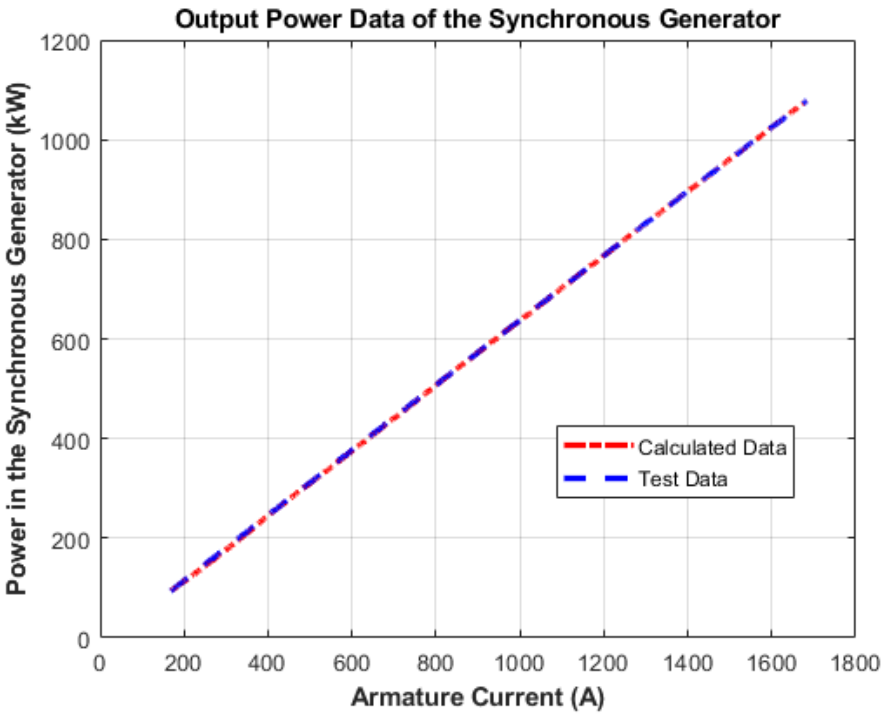


Figure 4.2 Test and calculated generator output power comparison

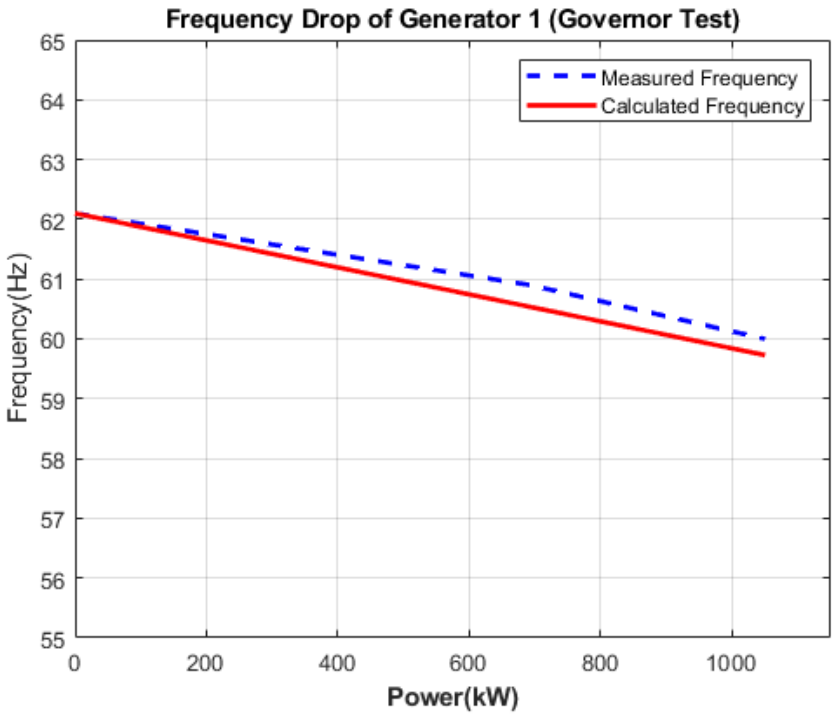


Figure 4.3 Frequency drop of the generator 1 vs power

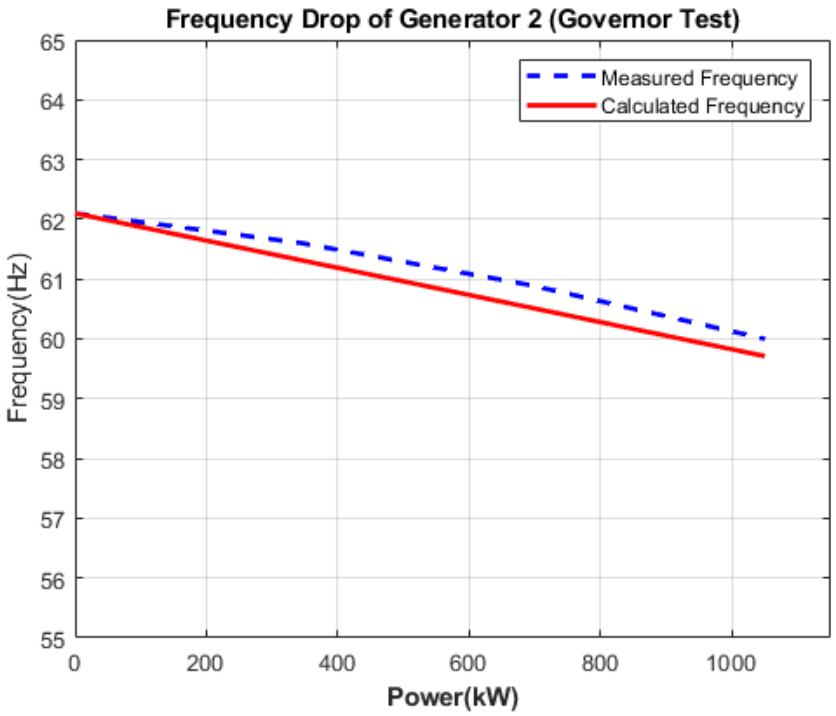


Figure 4.4 Frequency drop of the generator 2 vs power

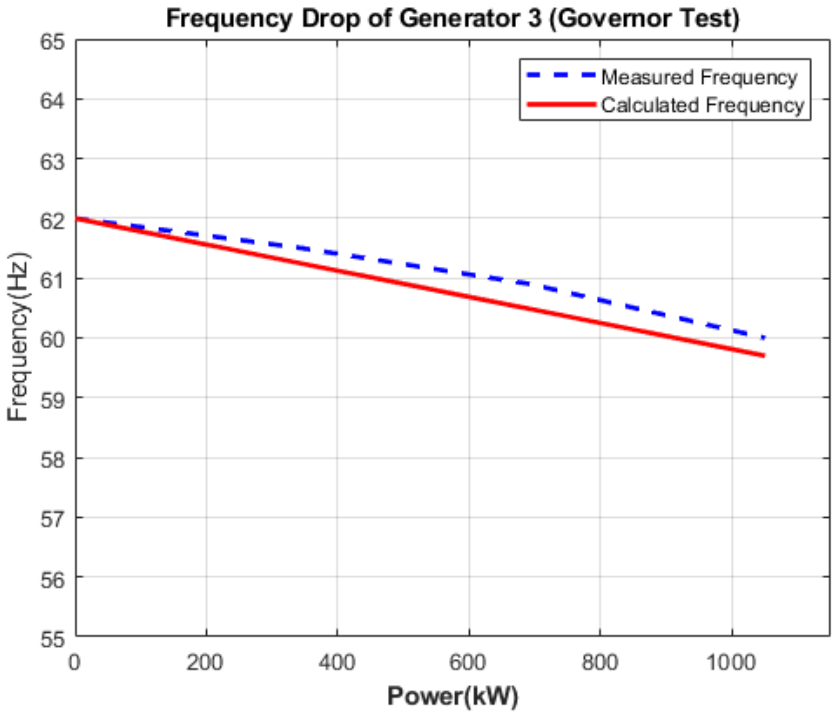


Figure 4.5 Frequency drop of the generator 3 vs power

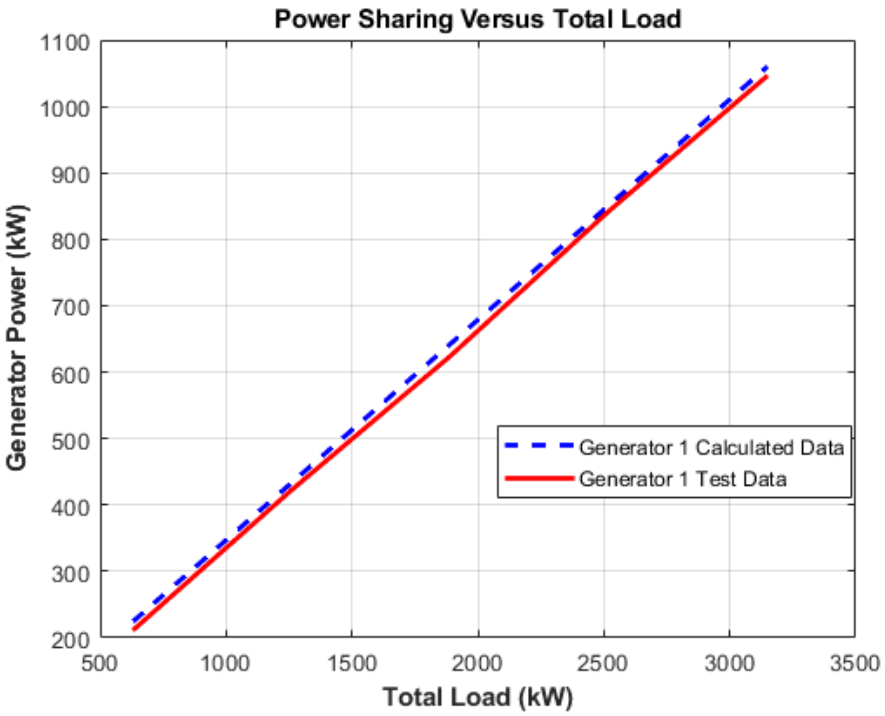


Figure 4.6 Power of generator 1 vs total system load

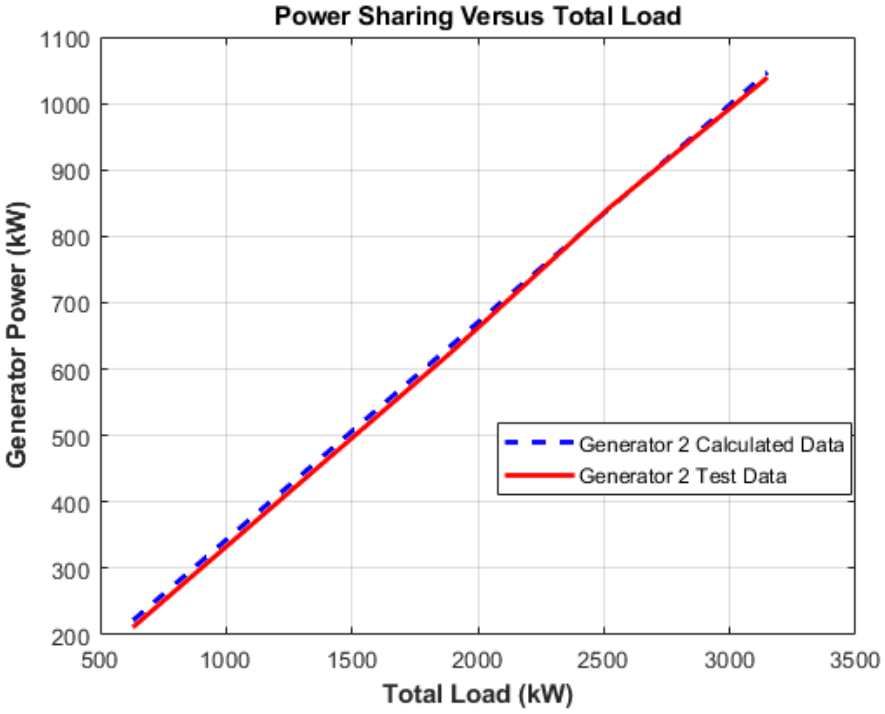


Figure 4.7 Power of generator 2 vs total system load

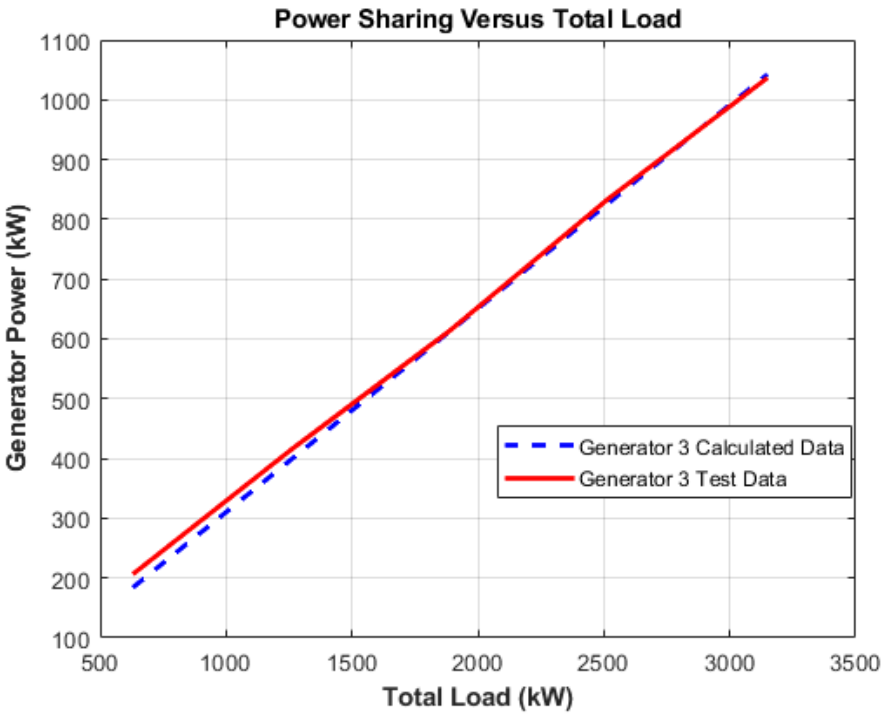


Figure 4.8 Power of generator 3 vs total system load

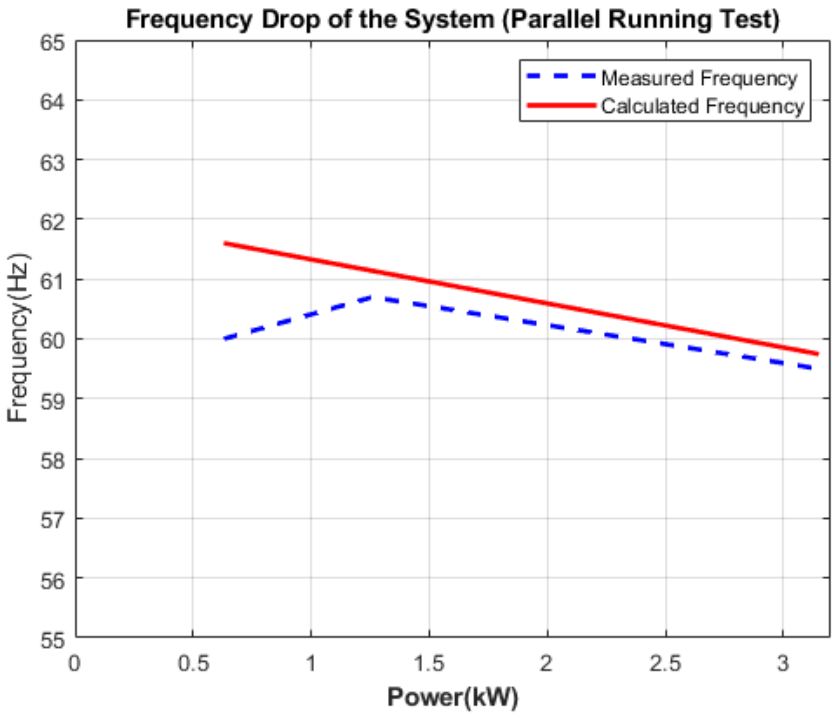


Figure 4.9 Frequency drop of the system vs increasing total system load

4.2 Outcomes of the Ship Power Distribution System Model

Outputs of the model are illustrated with figures. Figure 4.10 illustrates the theoretical induced power of the synchronous generator with a rising armature current. Figure 4.11 shows the relation between calculated internally generated voltage change depending on the armature current increment. Figure 4.12 indicates the relation between brake specific fuel consumption of the prime movers and the engine revolution per minute. Figure 4.13 shows the fuel consumption of each generator in kg/h according to engine revolution per minute. Transmitted power from the prime mover to synchronous generator varying with engine load graph is illustrated in Figure 4.14. Transmission efficiency is 0.9401 from the model calculation. Figure 4.15 shows the transient current behavior when a fault occurs at the terminals of the generator. When it is compared to Figure 2.3, transient, sub-transient, and steady-state regions can be observed for the alternator.

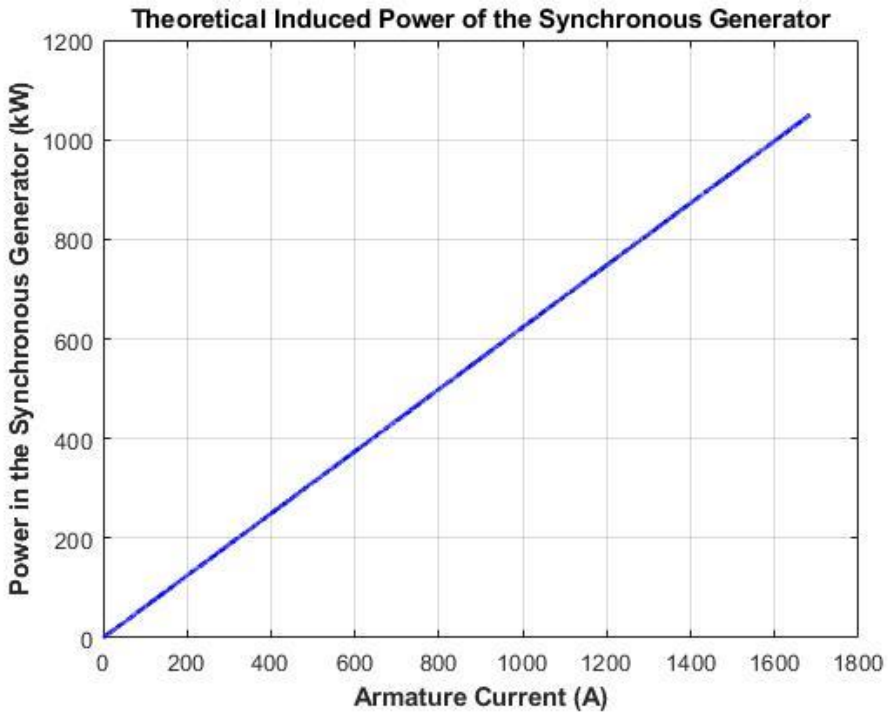


Figure 4.10 Theoretical induced power vs armature current in the generator

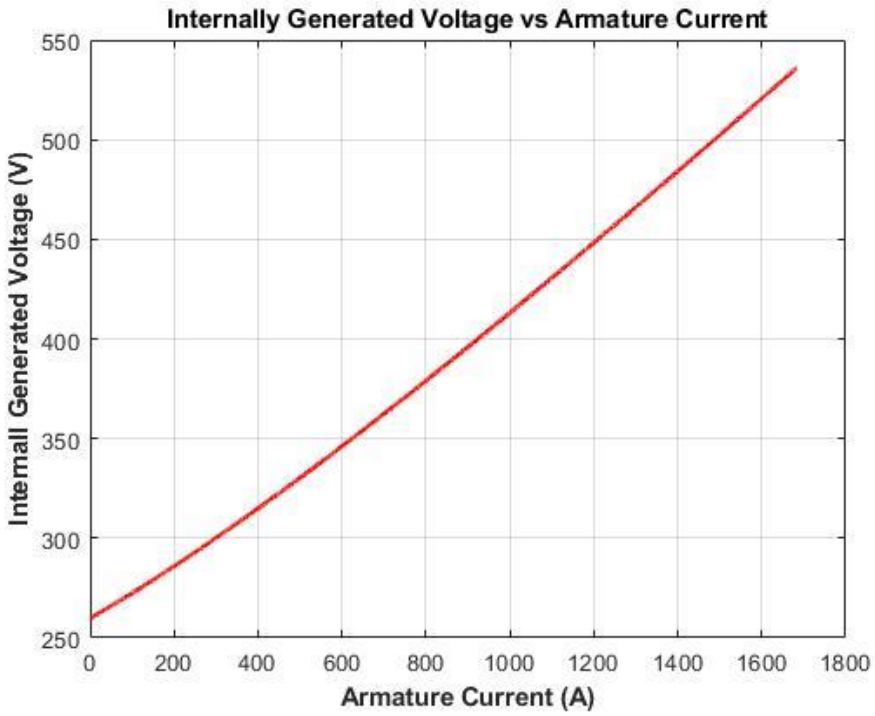


Figure 4.11 Internally generated voltage vs armature current in the generator

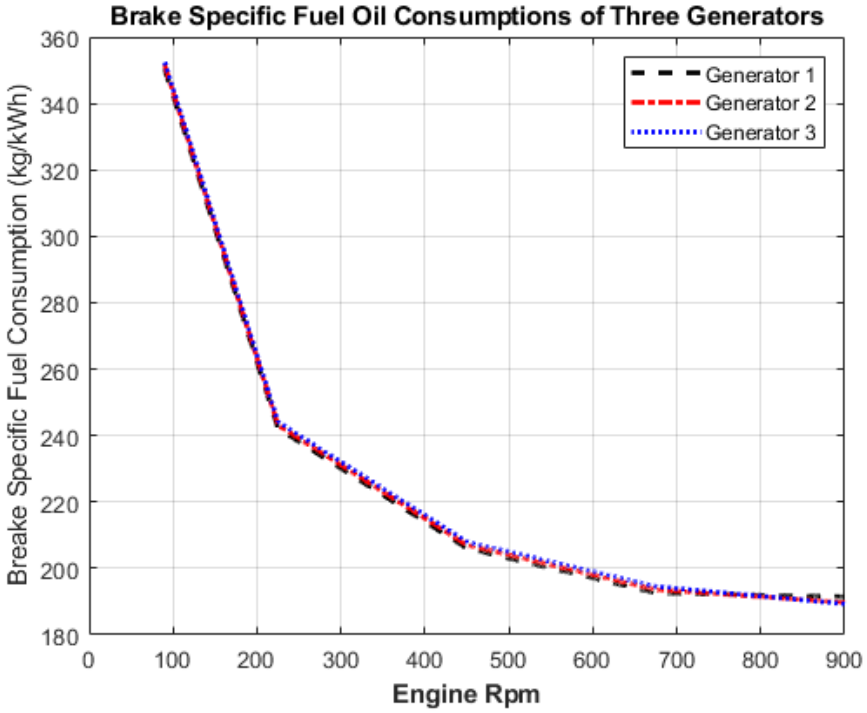


Figure 4.12 Brake-specific fuel oil consumptions of prime movers regarding engine rpm

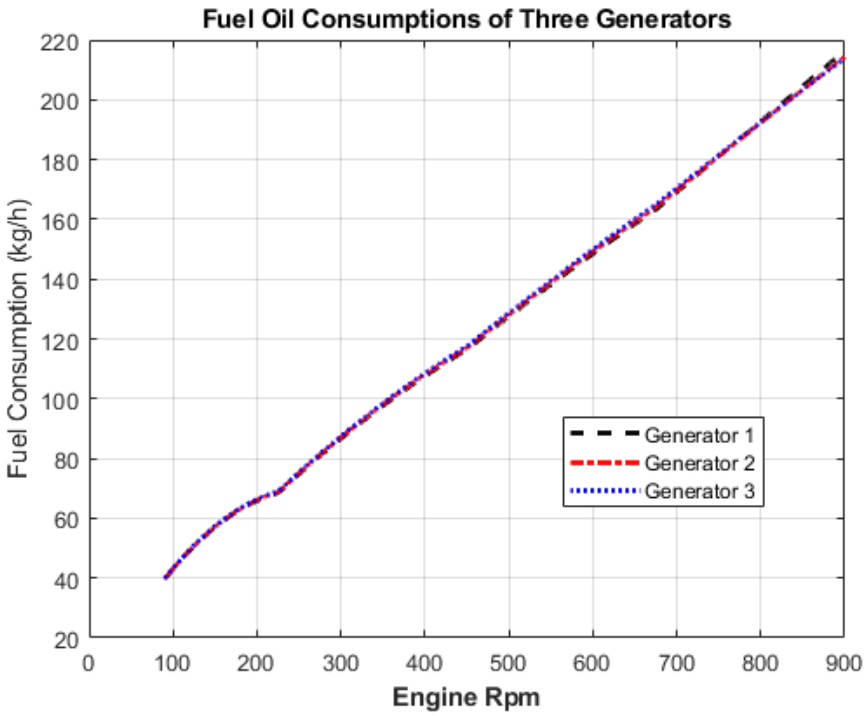


Figure 4.13 Fuel oil consumptions of prime movers depending on engine rpm

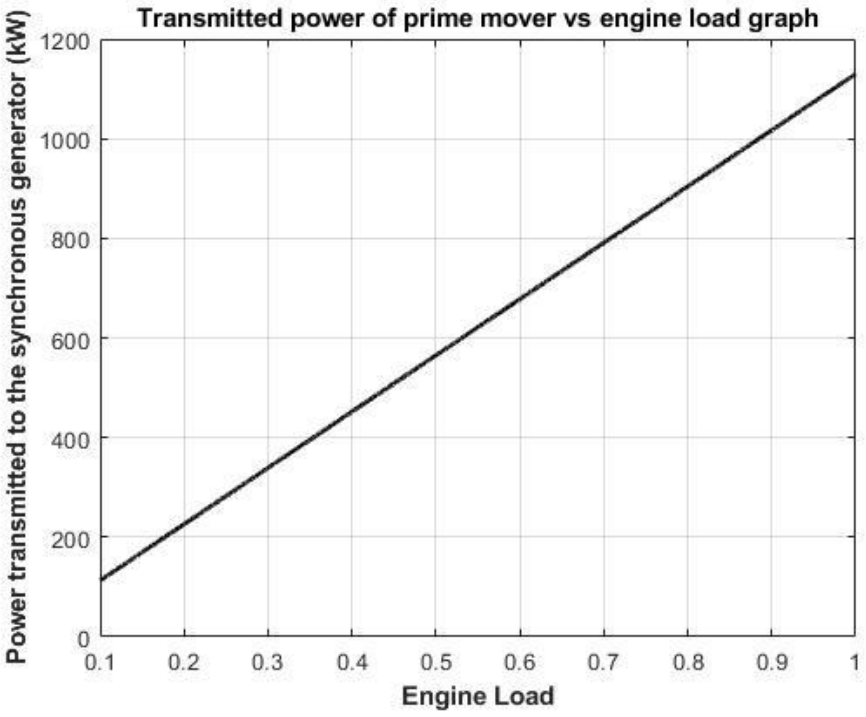


Figure 4.14 Transmitted power of prime mover vs engine load

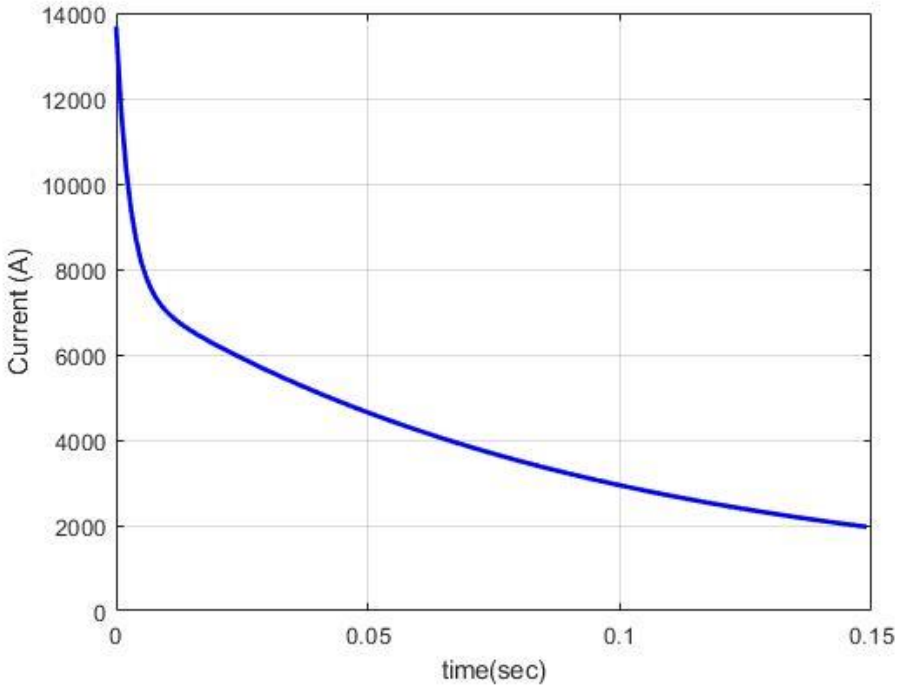


Figure 4.15 Transient current behavior when a fault occurs at the terminals of the generator

The utilization hours of the operation modes were calculated by the mathematical model. Figure 4.16 depicts the distribution of operation hours according to operation modes. The data contains 13169 hours of operation and 65% of these hours were spent during the navigation (8520.767 hours). The route of the ship involved many oceangoing voyages from the American continent to Europe or vice versa. The remaining 35% of the operation was spent in harbor or port operations. The total harbor time of the ship was 20% of all utilization time (2594.05 hours) which is a remarkably higher number for an oil/chemical tanker ship. However, the data collection process came across to Covid-19 pandemic thus, the ship remained at the harbor overly compared to the normal conditions. The results of the analysis should be evaluated by taking into consideration these two remarks. Figure 4.17 illustrates the FC distribution of the plant according to operation modes. The plant consumed 2731.118 t of fuel between 06/12/2019 and 07/06/2021. In addition, generators burnt HFO during the navigation and MGO in the harbor and port locations. The calculations demonstrated that HFO consumption was 1778.067 t during navigation and MGO consumption was 953.052 t.

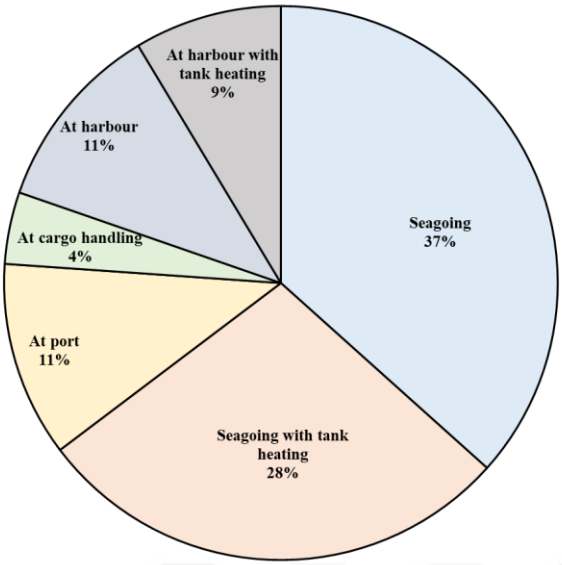


Figure 4.16 The distribution of utilization hours according to operation modes

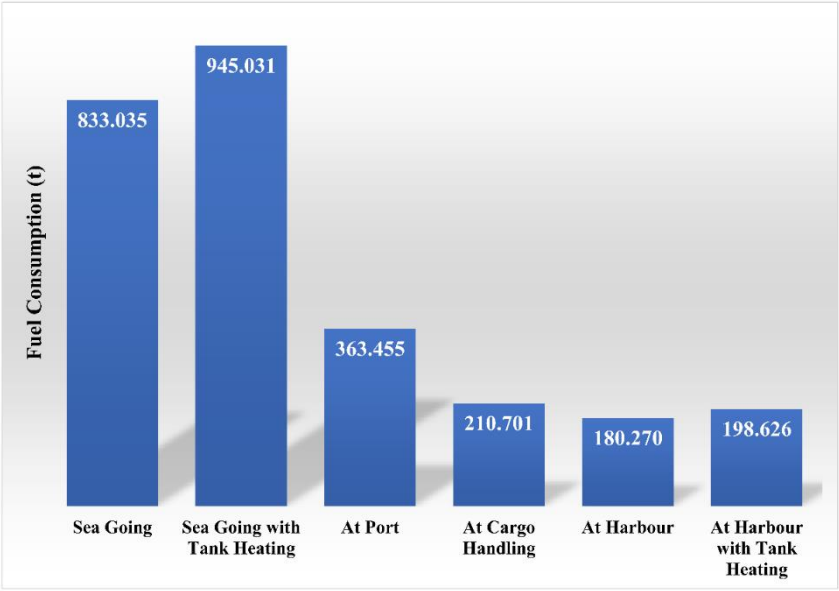


Figure 4.17 The distribution of FC according to operation modes

The emission production from the plant was calculated using the EF described in the previous chapter. Figure 4.18 illustrates the total pollutant amounts produced by the plant between the specified date range and Table 4.1 indicates the emissions according to operation modes. The plant produces 8592.38 t of CO_2 which is a remarkable amount compared to other pollutants. NO_x and SO_2 are the second and third highest generated pollutants respectively. The plant released 5536.9 t of CO_2, 44.46 t of SO_2, and 160.56 t of NO_x during the navigation since its voyage time is remarkably larger compared to port operations. During the harbor operations 1214.74

t of CO_2, 36.41 t of NO_x, and 3.79 t of SO_2 emissions were produced by marine diesel generators. The harbor time of the ship was greater than usual because of the pandemic conditions. Then finally, the generators 1840.75 t of CO_2, 55,18 t of NO_x, and 5.74 t of SO_2 in the port operations.

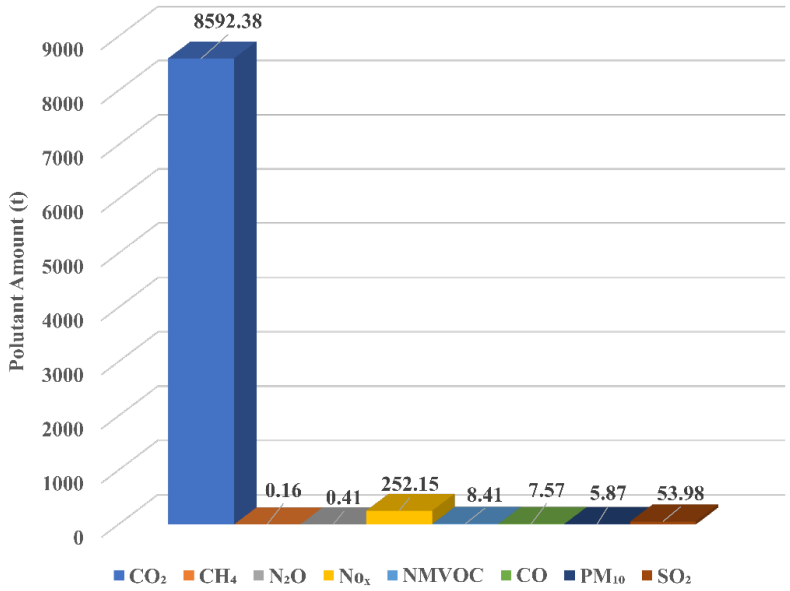


Figure 4.18 Total emissions from the plant.

Table 4.1 Emissions from diesel generators according to operation modes

Operation	CO_2	CH_4	N_2O	NO_x	NMVOC	CO	PM_{10}	SO_2
1	2594.07	0.05	0.12	75.22	2.57	2.31	2.32	20.83
2	2942.83	0.06	0.14	85.34	2.91	2.62	2.63	23.63
3	1165.24	0.02	0.05	34.93	1.12	1.01	0.35	3.63
4	675.51	0.01	0.03	20.25	0.65	0.58	0.20	2.11
5	577.95	0.01	0.03	17.32	0.56	0.50	0.17	1.80
6	636.79	0.01	0.03	19.09	0.61	0.55	0.19	1.99
Total	8592.38	0.16	0.41	252.15	8.41	7.57	5.87	53.98

4.3 Outcomes of the Hybrid Ship Power Distribution System Model

The proposed hybrid approach involves the battery addition to the plant. To select the ideal number of the batteries, battery brand, C-rates for charging and discharging processes, MADM methods were used, and their outputs compared. Using generators for charging is not profitable in operations that require only one generator. That's why, data set was constructed for operations 2, 3, and 4. The MADM methods were used

for these three data sets separately. The analysis results for each data set were compared. As a result of the analysis, if the combination selected in one data set was the highest in other data sets, that combination was added to the list. If there were differences in the number of parallel batteries of the combinations, it was checked whether that combination existed in each data set. The data set constraining the results were observed as the one belonging to operation 2. In other words, while the best combination in operation 2 was among the best in other datasets, the best in other operations were not included in the operation 2 datasets. However, all three methods tried finding similar CH-DH combinations of all three data sets. The difference was in the number of parallel batteries, which was adjusted for operation 2. In addition to the MCDA analysis, combinations that maximize the fuel-saving ratio were also added to the list. Table 4.2 demonstrates the results of the weight calculation using the objective methods. Table 4.3 depicts the top three combination picks of each method and the properties of the selected combinations.

The MCDA algorithms tend to find the DH and CH combinations between three and four hours. The battery numbers of three and four were ranked higher compared to others. Costs of these batteries were lower, and it is the factor of this phenomenon. Weights of the criterion were calculated and compared different objective weighting methods that use data to assess the importance of the data. The comparison and assessment resulted in choosing the Entropy method for the determination of weights. The method weighted the criterion equally. PROMETHEE technique prioritized the low weight and cost with a decent FS percentage. TOPSIS gave priority to high FS percentage with moderate cost and relatively higher weight. Its top pick was the third option of the PROMEETHE list. MOORA Ratio's highest pick was the same as TOPSIS and its second choice was the same with PROMETHEE. MOORA Ref Point ranked the highest a combination with high a FS percentage, a moderate weight, and a slightly higher cost. Its selection was the third option for PROMETHEE and MOORA Ratio and the second option for the TOPSIS. Combining this information, three battery set combinations were determined. Table 4.4 indicates the chosen combinations to add to the plant.

Table 4.2 Weight calculation results with objective weighting methods

Method	Operation 2 Data	Operation 3 Data	Operation 4 Data
Entropy Method	0.3329276	0.3322787	0.332119236
	0.335346729	0.33467145	0.33497496
	0.33172567	0.33304985	0.332905803
CRITIC Method	0.229699437	0.221510416	0.254467459
	0.426543028	0.4109568	0.302466254
	0.343757535	0.367532783	0.443066287
Standard Deviation Method	0.28679395	0.30062497	0.34034605
	0.33977781	0.37473927	0.34573753
	0.37342824	0.32463577	0.31391642

Table 4.3 Top three selections of MADM methods

Method	Battery No	DH	CH	Parallel Cells	Cost ($)	Weight (t)	FS%
PROMETHEE	3	3	3	190	425600	2.9792	4.38
	4	4	3	265	466400	4.24	5.16
	3	4	3	253	566720	3.96704	5.18
TOPSIS	4	4	3	265	466400	4.24	5.16
	3	4	3	253	566720	3.96704	5.18
	4	4	3	289	508640	4.624	5.28
MOORA Ratio	4	4	3	265	466400	4.24	5.16
	3	3	3	190	425600	2.9792	4.38
	3	4	3	253	566720	3.96704	5.18
MOORA Ref. Point	3	4	3	253	566720	3.96704	5.18
	3	3	3	253	566720	3.96704	4.78
	4	4	3	265	466400	4.24	5.16

Table 4.4 Battery combinations used in the plant

Combination	Battery No	DH	CH	Parallel Cells	Cost ($)	Weight (t)
C1	3	3	3	190	425600	2.9792
C2	3	4	3	253	566720	3.96704
C3	4	4	3	265	466400	4.24

When the hybrid model was run with combinations shown in Table 4.4, the mathematical model of the hybrid power plant calculated the total FC of combinations with different charging strategies between the specified date range and during the same operational schedule. Table 4.5 demonstrates the FC and FS of the combinations when generators were charging the batteries. Table 4.6 shows the same analogy for the scenario of usage of WHRS to charge the batteries.

The first charging strategy that involves the generators to charge batteries was not suitable for operations that require one generator. During the charging, the load of the system increases, and the second generator was needed to meet the increment.

Although, during the discharging process, the load and FC of the generators were lowered, using two generators for charging did not ensure a good amount of FS percentage. In addition, in the harbor, generator load was around 54% and battery support lowers the load to unwanted load regions for the generator. For these reasons, the first strategy was applicable during cargo loading/unloading operations and the navigation with a cargo requiring heating. The hybrid system can be used 43.67% of all operations equal to 5750.68 working hours because of the long voyages and harbor time. The harbor time was specifically higher for this ship because some parts of data collection have been carried through during the Covid-19 pandemic. Especially, in March and April 2020, the ship waited with or without the cargo in the harbor. On the other hand, even with a low usage rate, the system can save up to 8.415 % fuel depending on the chosen combination. This rate would be higher for the ships that visit the port areas more often or stay in these areas longer. The advantage of this charging is the ease of application. With low weights, volumes and costs, the systems can be installed for the tankers easily. However, it will be more efficient in the ships working frequently near coastal areas.

The second charging strategy adds an extra component to the system, but it solves the problem of the low usage rate of the hybrid system on the oceangoing vessels. The strategy involved a WHRS to charge batteries at the beginning of the navigation and after it assisted the working generator. During the navigation, WHRS used the WH from ME and DG, so it worked at a total capacity of 150 kW. In the harbor and port areas in other words, while the ME is not working, WHRS used WH from the working DG. Produced electricity was extended the discharge time of the batteries. During port operations, WHRS worked near to the full capacity due to the high number of working generators. Utilizing the charging process with this strategy increased the FS percentage potential up to 18.145 % that is an attention-grabbing enhancement. The WHRS used in the study has been used in maritime applications successfully with high efficiency and low prices.

Table 4.5 FC and FS of the hybrid plant when batteries are charged by generators

Combination	FC (t)	FS (t)	FS	FS (kg/h)
C1	2527.394	203.724	7.459%	35.426
C2	2495.748	235.370	8.618%	40.929
C3	2501.290	229.828	8.415%	39.965

Table 4.6 FC and FS of the hybrid plant when batteries are charged by WHRS

Combination	FC (t)	FS (t)	FS	FS (kg/h)
C1	2275.565	455.553	16.680%	34.593
C2	2236.567	494.551	18.108%	37.554
C3	2235.570	495.548	18.145%	37.630

The ER of each combination with different charging approaches was also calculated to highlight the environmental impact of the proposed system. Figure 4.19 indicates the FC distributions regarding operation modes for C1, C2, and C3 respectively when the generators charge to batteries. Since this charging strategy was not used in the operations that require one generator, the FC in operations 1, 5, and 6 remained the same compared to the normal operation. The FC reductions of combinations in operations 2, 3, and 4 are illustrated in Table 4.7. The FS ratio in operation 2, 13.922%, 16.079%, 15.713%, in operation 3, 14.151%, 16.249%, 15.906% and in operation 4, 9.837%, 11.562%, 11.166% for C1, C2 and C3 respectively for each operation. The FS ratios are remarkable for an operation that needs two generators.

Table 4.7 FS regarding operation modes when generators charge batteries (units are depicted in t)

Operation	FS C1	FS C2	FS C3
1	0.000	0.000	0.000
2	131.564	151.951	148.489
3	51.434	59.059	57.811
4	20.727	24.361	23.527
5	0.000	0.000	0.000
6	0.000	0.000	0.000

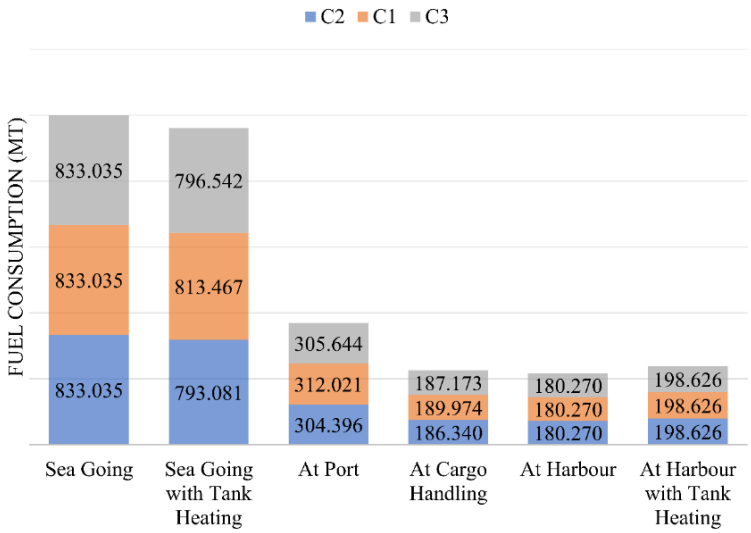


Figure 4.19 The distribution of FC regarding operation modes for each battery combination with generator charge

Emissions produced by the hybrid plant, are illustrated in Tables 4.8, 4.9, and 4.10 for each battery combination according to operation modes. Table 4.11 shows the emission reductions of the plant for operations 2, 3, and 4. Table 4.12 depicts the total emissions and emission reductions of each combination.

Table 4.8 Emissions of the hybrid plant with C1 generator charging (units are depicted in t)

Operation	CO_2	CH_4	N_2O	NO_x	NMVOC	CO	PM_{10}	SO_2
1	2594.07	0.05	0.12	75.22	2.57	2.31	2.32	20.83
2	2533.14	0.05	0.12	73.46	2.51	2.25	2.26	20.34
3	1000.34	0.02	0.05	29.99	0.96	0.86	0.30	3.12
4	609.06	0.01	0.03	18.26	0.59	0.53	0.18	1.90
5	577.95	0.01	0.03	17.32	0.56	0.50	0.17	1.80
6	636.79	0.01	0.03	19.09	0.61	0.55	0.19	1.99

Table 4.9 Emissions of the hybrid plant with generator charging (units are depicted in t)

Operation	CO_2	CH_4	N_2O	NO_x	NMVOC	CO	PM_{10}	SO_2
1	2594.07	0.05	0.12	75.22	2.57	2.31	2.32	20.83
2	2469.65	0.05	0.12	71.62	2.44	2.20	2.20	19.83
3	975.89	0.02	0.05	29.25	0.94	0.84	0.30	3.04
4	597.41	0.01	0.03	17.91	0.57	0.52	0.18	1.86
5	577.95	0.01	0.03	17.32	0.56	0.50	0.17	1.80
6	636.79	0.01	0.03	19.09	0.61	0.55	0.19	1.99

Table 4.10 Emissions of the hybrid plant with C3 generator charging (units are depicted in t)

Operation	CO_2	CH_4	N_2O	NO_x	NMVOC	CO	PM_{10}	SO_2
1	2594.07	0.05	0.12	75.22	2.57	2.31	2.32	20.83
2	2480.43	0.05	0.12	71.93	2.45	2.21	2.21	19.91
3	979.89	0.02	0.05	29.37	0.94	0.85	0.30	3.06
4	600.08	0.01	0.03	17.99	0.58	0.52	0.18	1.87
5	577.95	0.01	0.03	17.32	0.56	0.50	0.17	1.80
6	636.79	0.01	0.03	19.09	0.61	0.55	0.19	1.99

Table 4.11 Total emissions and ER of combinations with generator charging (units are depicted in t)

Pollutant	C1	ER with C1	C2	ER with C2	C3	ER with C3
CO_2	7951.346	641.037	7851.765	740.618	7869.215	723.168
CH_4	0.152	0.012	0.150	0.014	0.150	0.014
N_2O	0.379	0.031	0.374	0.035	0.375	0.034
NO_x	233.333	18.815	230.410	21.738	230.922	21.225
NMVOC	7.784	0.627	7.687	0.725	7.704	0.708
CO	7.001	0.564	6.913	0.652	6.929	0.637
PM_{10}	5.432	0.436	5.364	0.503	5.376	0.492
SO_2	49.971	4.011	49.349	4.633	49.457	4.526

The C2 provides the most ER and FS compared to other combinations. It reduces the CO_2 emission by 740.618 t which is a remarkable reduction in 1.5 years of operation. The reduction ratios can be upgraded by increasing the usage time of the hybrid plant. It can be ensured with the usage of the WHRS plant to charge the batteries. This charging strategy would raise the FS for operations requiring only one generator. During the navigation, WHRS can provide energy support for the plant. When the ME is not working, the DG WH extends the discharge time of batteries and supports the charging load. Figure 4.20 depicts the FC distributions regarding operation modes for C1, C2, and C3 respectively when the WHRS charges to batteries. The FS in t and ratios of combinations in operations 2, 3, and 4 are illustrated in Table 4.12.

Table 4.12 FS in regard of operation modes when the WHRS is used to charge batteries

Operation	FS C1	FS % C1	FS C2	FS % C2	FS C3	FS % C3
1	138.936	16.678%	145.118	17.420%	145.034	17.410%
2	111.468	11.795%	115.139	12.184%	115.404	12.212%
3	90.124	24.796%	100.145	27.554%	100.338	27.607%
4	45.920	21.794%	52.078	24.717%	51.948	24.655%
5	38.097	21.133%	43.048	23.880%	43.598	24.185%
6	31.009	15.612%	39.022	19.646%	39.227	19.749%

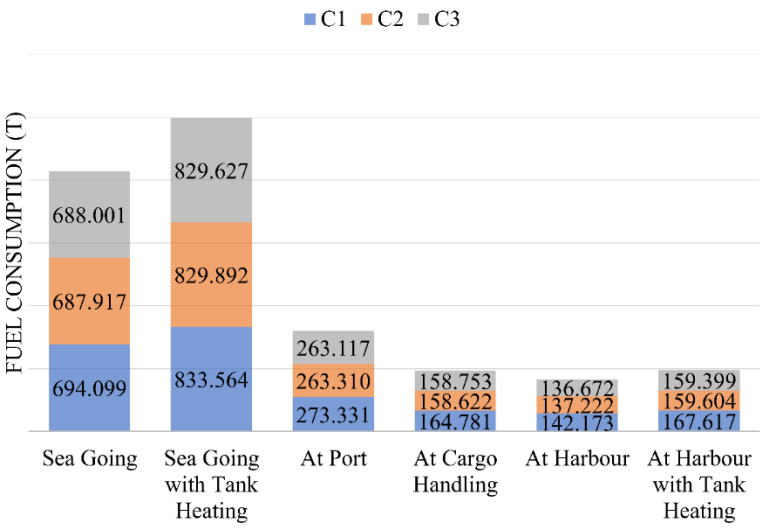


Figure 4.20 The distribution of FC regarding operation modes for each battery combination with WHRS charge

The FS was ensured for each operation mode with this charging strategy. Especially during the cargo loading-unloading operations up to 27.554% and 24.717% of fuel can be saved using the battery support and WHRS configuration. The support of the WHRS provided a remarkable FS when the ship is not carrying cargo requiring heating. In the normal navigation conditions up to 17.42 %, FS was ensured. Operation 2 requires two generators and 150 kW support reduced to the required number of working generators that caused FS. However, the remaining generator is required to work higher loads, or two generators are needed to run at moderate loads. Therefore, the Fs of the operation is slightly lower compared to other operations. In the harbor, WHRS neutralized the charging load that led to a remarkable FS because of the lower electrical load needs of operations 5 and 6. Tables 4.13, 4.14, and 4.15 provide the emission production information of the hybrid plant including WHRS for charging regarding operation modes. Table 4.16 indicates the total emissions generated by the plant for each battery combination and reduction amounts.

Table 4.13 Emissions of the hybrid plant with C1 WHRS charging (units are depicted in t)

Operation	CO_2	CH_4	N_2O	NO_x	NMVOC	CO	PM_{10}	SO_2
1	2161.42	0.04	0.10	62.68	2.14	1.92	1.93	17.35
2	2595.72	0.05	0.13	75.27	2.57	2.31	2.32	20.84
3	876.30	0.02	0.04	26.27	0.84	0.76	0.27	2.73
4	528.29	0.01	0.02	15.84	0.51	0.46	0.16	1.65
5	455.81	0.01	0.02	13.66	0.44	0.39	0.14	1.42
6	537.38	0.01	0.03	16.11	0.52	0.46	0.16	1.68

Table 4.14 Emissions of the hybrid plant with C2 WHRS charging (units are depicted in t)

Operation	CO_2	CH_4	N_2O	NO_x	NMVOC	CO	PM_{10}	SO_2
1	2142.17	0.04	0.10	62.12	2.12	1.91	1.91	17.20
2	2584.28	0.05	0.12	74.94	2.56	2.30	2.31	20.75
3	844.17	0.02	0.04	25.30	0.81	0.73	0.26	2.63
4	508.54	0.01	0.02	15.24	0.49	0.44	0.15	1.59
5	439.93	0.01	0.02	13.19	0.42	0.38	0.13	1.37
6	511.69	0.01	0.02	15.34	0.49	0.44	0.15	1.60

Table 4.15 Emissions of the hybrid plant with C3 WHRS charging (units are depicted in t)

Operation	CO_2	CH_4	N_2O	NO_x	NMVOC	CO	PM_{10}	SO_2
1	2142.44	0.04	0.10	62.13	2.12	1.91	1.91	17.20
2	2583.46	0.05	0.12	74.92	2.56	2.30	2.31	20.74
3	843.55	0.02	0.04	25.29	0.81	0.73	0.26	2.63
4	508.96	0.01	0.02	15.26	0.49	0.44	0.15	1.59
5	438.17	0.01	0.02	13.13	0.42	0.38	0.13	1.37
6	511.03	0.01	0.02	15.32	0.49	0.44	0.15	1.59

Table 4.16 Total emissions and ER of combinations with WHRS charging (units are depicted in t)

Pollutant	C1	ER with C1	C2	ER with C2	C3	ER with C3
CO_2	7154.916	1437.467	7030.795	1561.588	7027.615	1564.768
CH_4	0.137	0.027	0.134	0.030	0.134	0.030
N_2O	0.341	0.068	0.335	0.074	0.335	0.074
NO_x	209.821	42.326	206.131	46.017	206.036	46.112
NMVOC	7.009	1.403	6.889	1.523	6.886	1.526
CO	6.303	1.262	6.195	1.370	6.193	1.373
PM_{10}	4.972	0.895	4.917	0.951	4.915	0.952
SO_2	45.671	8.312	45.133	8.849	45.120	8.862

4.4 Results of Fuel Consumption and SoH Prediction

4.4.1 Results of the Fuel Consumption Prediction

FC was calculated based on operation modes and total operating hours in the simulation. To prepare the data for regression analysis, it was converted hourly. Fig. 4.21 depicts the plant's hourly FC increments throughout 13268 hours. The figure demonstrates that there is a linear relationship between FC and working hours in the data and the regression algorithms can achieve high R^2 scores Four suitable regression models were tried on the data. The goal of the regression analyses was to predict the future FC of the plant. The algorithm selection and comparison were carried out for the normal operation’s data. The most suitable model was used to estimate the FC of hybrid plants with different battery combinations and charging strategies. The

regression analyses were performed to highlight the environmental impact of the proposed methods for future periods. Train-test split was determined trials of various combinations on the forecasting algorithms used in this thesis. 80-20 split was the optimal choice due to these trials for each algorithm. The performance metrics were calculated for the test set.

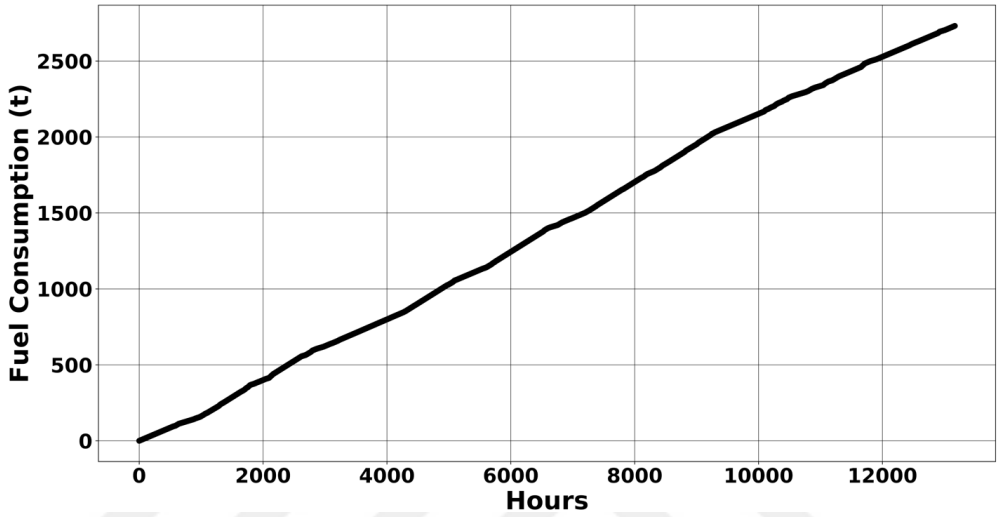


Figure 4.21 FC of the normal operation regarding operation hours

The first forecasting method tried on the data was time series analysis. The Figure demonstrates the time series data is non-seasonal and non-stationary. To assess these assumptions the ADF test was performed. The test results provided the p-value as 0.996 which is remarkably higher than the set value of 0.05. Figure 4.22 demonstrates the ACF and PACF plots of the data. There is no clear change in the ACF plot, however, PACF plots break after the lag of 2. To determine the correct model orders for the data "auto_arima" function from the "pmdarima" library in Python was used. This function offers the best model for time series by performing a stepwise search to minimize AIC. Table 4.17 demonstrates the search results of the model order.

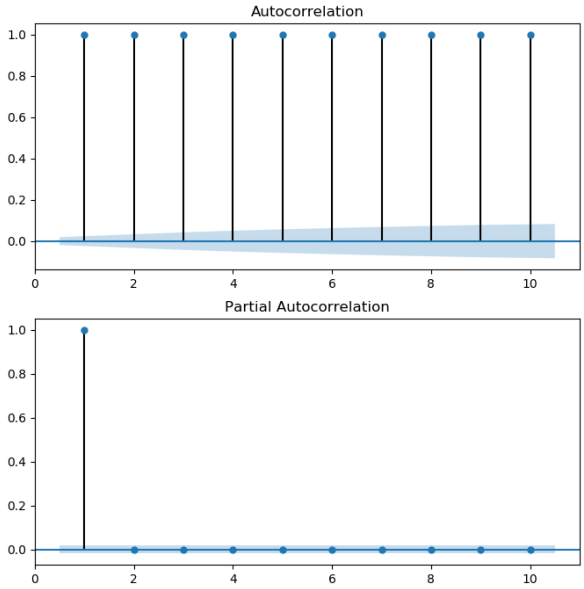


Figure 4.22 ACF and PACF plots of the hourly FC data

Table 4.17 Results of the ARIMA order search

Model	AIC	Time
ARIMA (1,2,1)	51212.835	0.61 sec
ARIMA (0,2,0)	49272.714	0.32 sec
ARIMA (1,2,0)	50766.121	0.24 sec
ARIMA (0,2,1)	51209.299	0.87 sec
ARIMA (2,2,1)	51210.978	1.33 sec
ARIMA (1,2,2)	51212.524	2.71 sec
ARIMA (0,2,2)	51213.135	2.12 sec
ARIMA (0,2,3)	51211.808	0.82 sec
ARIMA (1,2,3)	51209.992	0.96 sec
ARIMA (0,2,2)	51211.133	1.55 sec
Best model: ARIMA (0,2,2), Total fit time: 11.519 seconds		

After the determination of the model orders, ARIMA (0, 2, 2) was fitted to the dataset. Figure 4.23 depicts the analogy between actual data and predicted data by the ARIMA (0, 2, 2). The second regression algorithm was determined as OLS. The performance of various linear regression algorithms such as Ridge, Lasso, Elastic Net was evaluated, however, the parameter tuning for these methods resulted in the OLS being optimal. Figure 4.24 indicates the comparison between actual data and OLS predictions on test data. The third method is SVR and its fitting curve is shown in Figure 4.25. The various kernels were tried for observation and as expected, the linear kernel gave the best results in the SVR.

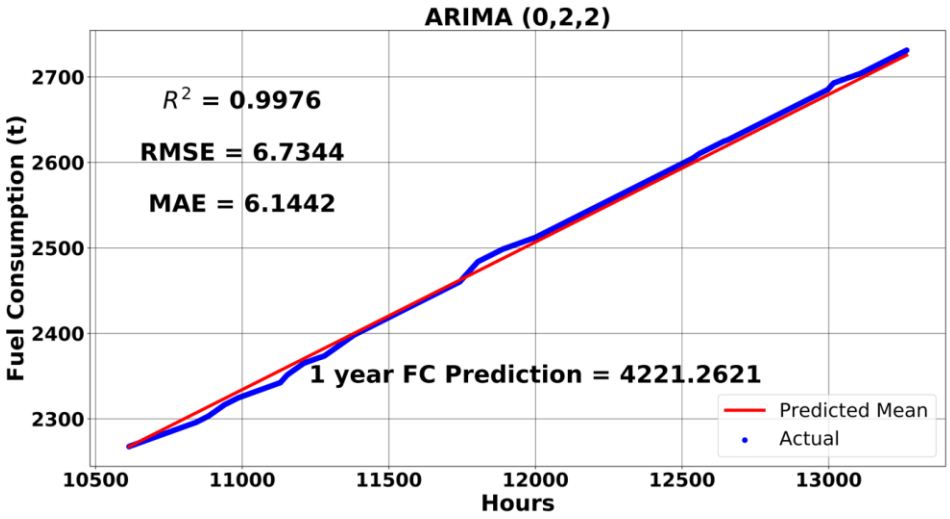


Figure 4.23 Analogy of actual and predicted data for ARIMA (0, 2, 2)

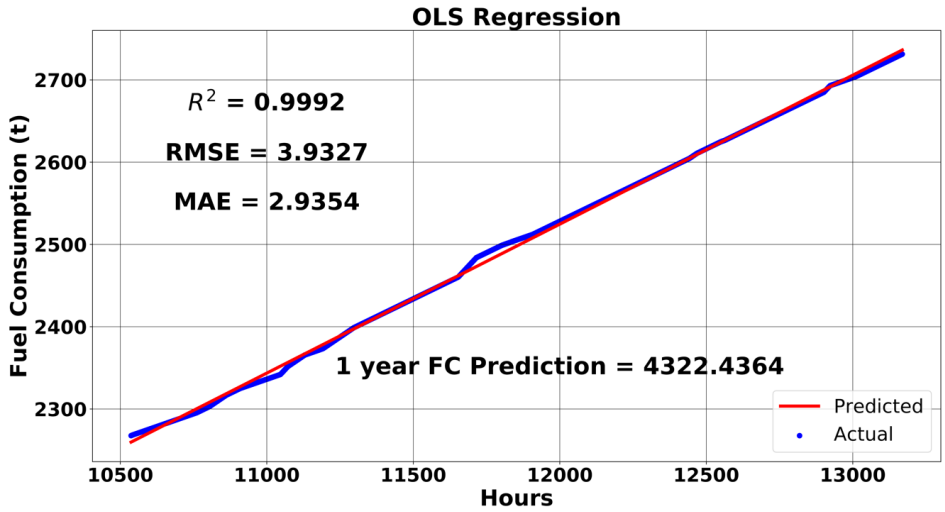


Figure 4.24 Analogy of actual and predicted data for OLS regression

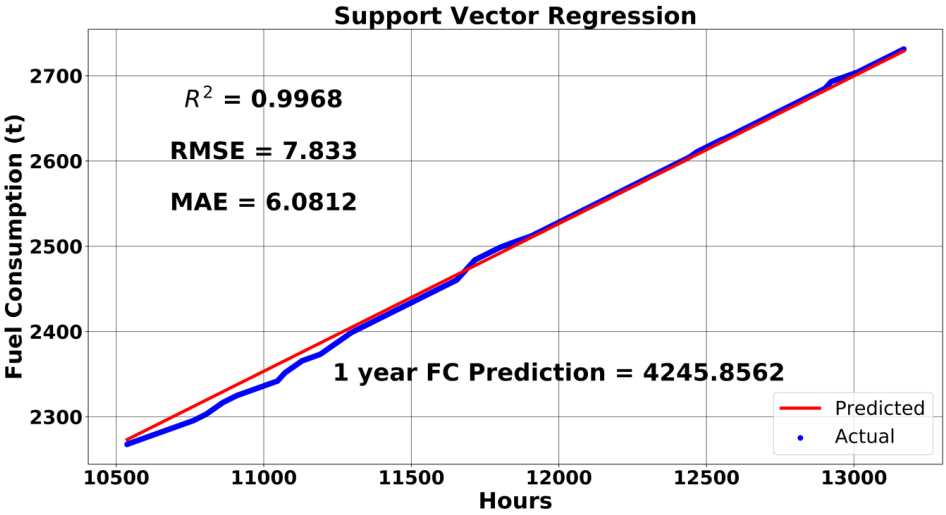


Figure 4.25 Analogy of actual and predicted data for SVR regression

The last regression technique used in the thesis is ANN. The parameters of the ANN were determined with trials. The FNN methodology was implemented, and the activation functions were the first trial subject. Between Sigmoid, Hyperbolic-tangent, Softmax, and Relu functions, Relu gave the lowest MAE and RMSE in the hidden layers. In the output layer, the Hyperbolic-tangent function was used. The batch size was 10 and the number of epochs was 50 for the optimal model. The number of neurons and input-output dimension were illustrated in Figure 3.18. Figure 4.26 demonstrates the comparison between actual and predicted data by the ANN. Table 4.18 illustrates the MAE, RMSE, R^2, and one-year predictions for each regression method.

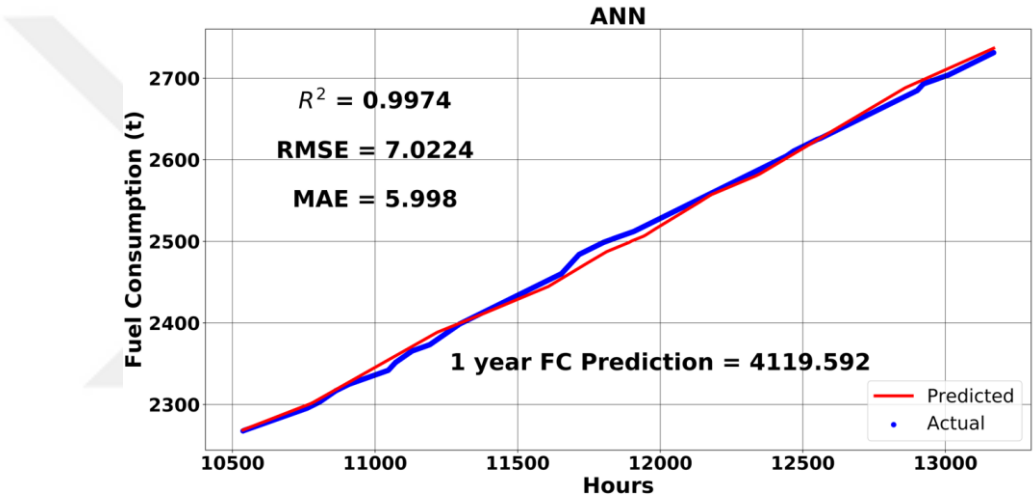


Figure 4.26 Analogy of actual and predicted data for ANN

Table 4.18 Model evaluation metrics and one-year FC predictions

Model	R-squared	RMSE	MAE	One-year FC Predictions (t)
OLS	0.9991	3.9326	2.9354	4322.43641
SVR	0.9965	7.833	6.0811	4245.8561
ARIMA	0.9976	6.7343	6.1442	4221.2621
ANN	0.9974	6.119	5.2387	4271.5566

Fitting curves depict that OLS has an overall the best curve fitting among other methods. Lower MAE and RMSE values also support the idea. In addition, OLS is the fastest and the most straightforward method that gives an advantage for selection. However, at the end of the data, the slope of the predicted line is higher than the actual line which results in higher future predictions compared to other techniques. A similar phenomenon is valid for ARIMA (0,2,2). Although its MAE is highest among the

others, a successful curve fitting can be observed from the figures. Nevertheless, its predicted data curve stays under the original data in the second part of the data which causes lower future forecasts. In addition, ARIMA's running time is the second highest after ANN. SVR's MAE and RMSE are particularly higher which seems to be caused at the beginning of the data. In the second part, SVR fits a near-perfect curve that conduces to efficient estimations but, the MAE and RMSE of the model are slightly over compared to the other regression techniques. Even though it is a complex methodology, the SVR model's computation time reduces remarkably with data standardization. ANN, on the other hand, has the highest R^2 score, and its future predictions and other evaluation metrics are decent. Nonetheless, ANN is not seeming to be the optimal choice from this data set. Its computation time is the markedly highest and it is more suitable for more complex datasets which have multiple inputs and uncertainty. For this dataset using OLS instead of other methods to forecast FC in future periods is more logical because of better performance metrics and computation time. One year later, after the end of the date range, the OLS model predicts 4322.43641042 t of total FC from the plant. Five-years, ten-years, and twenty-years estimations are 10684.86026, 18615.47205, and 34458.589 t respectively. Table 4.19 demonstrates the emission predictions of the periods using estimated data to highlight the environmental effect of the plant. The emission calculation of the forecasted FC is executed with an assumption that the route of the ship stays like in the simulation.

Table 4.19 Emission estimation of OLS (Units are depicted as t)

Pollutant	1-year	5-years	10-years	20-years
CO_2	13599.249	33616.707	58567.998	108413.613
CH_4	0.259	0.641	1.117	2.068
N_2O	0.648	1.603	2.792	5.169
NO_x	399.091	986.533	1718.767	3181.562
NMVOC	13.313	32.909	57.336	106.132
CO	11.973	29.597	51.565	95.450
PM_{10}	9.278	22.935	39.958	73.965
SO_2	85.368	211.026	367.656	680.557

OLS was used to predict how much potential battery configurations could have lowered FC and emissions in the future periods. Figure 4.27 depicts the actual and predicted data fitting curves of each combination's data set. Table 4.20 indicates the model assessment metrics of the OLS Table 4.21 demonstrates the total FC and FS of

each combination for future periods for each configuration. The predictions were made one, five, ten, and twenty years which was accepted system lifetime. Table 4.22 shows the future emission productions and Table 4.23 illustrates ERs of the hybrid plant when different battery combinations are used.

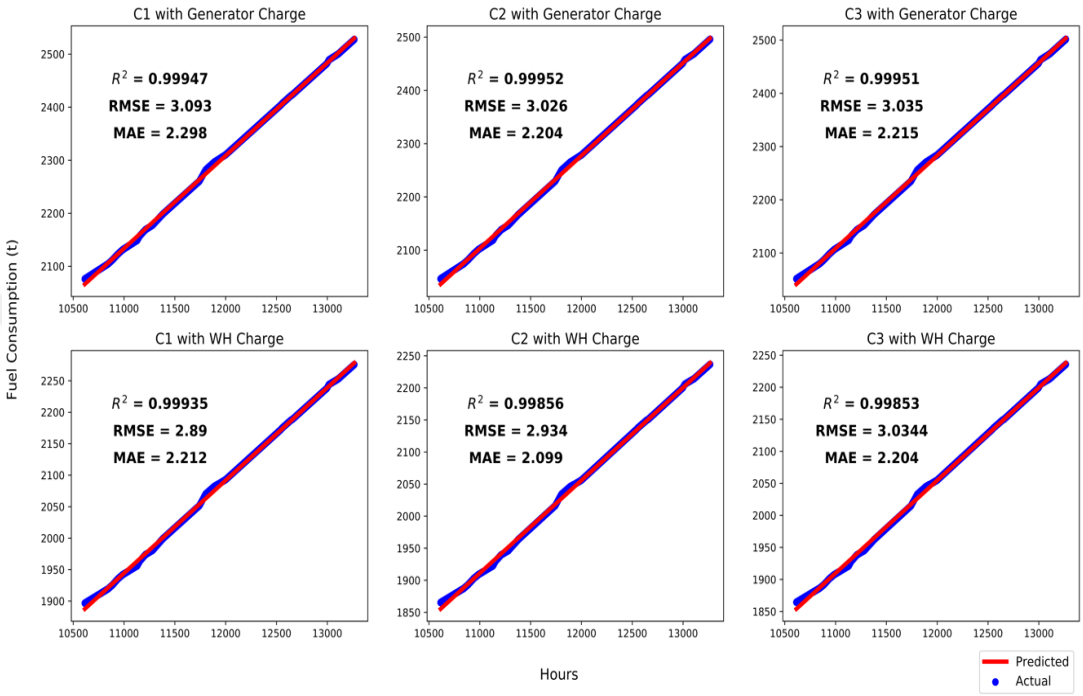


Figure 4.27 Analogy of FC actual and predicted data for hybrid plant combinations

Table 4.20 Performance metrics of OLS for hybrid plant FC estimation

Metric	C1	C2	C3	WHRS1	WHRS2	WHRS3
R^2	0.99947	0.99952	0.99951	0.99935	0.99856	0.99853
RMSE	3.093	3.026	3.035	2.890	2.934	3.044
MAE	2.298	2.204	2.215	2.112	2.099	2.204

Table 4.21 FC and FS of each combination in future periods

Period		C1	C2	C3	WHRS1	WHRS2	WHRS3
1 year	FC	4044.934	4006.484	4013.365	3554.678	3492.154	3492.514
	FS	277.502	315.953	309.071	767.759	830.282	829.922
5 years	FC	10189.820	10125.529	10137.582	8731.879	8575.452	8581.165
	FS	495.040	559.332	547.278	1952.981	2109.408	2103.695
10 years	FC	17849.277	17752.774	17771.274	15185.139	14911.664	14924.049
	FS	766.195	862.698	844.198	3430.333	3703.808	3691.423
20 years	FC	33150.702	32989.852	33021.230	28076.925	27569.620	27595.335
	FS	1307.888	1468.737	1437.359	6381.665	6888.969	6863.254

Table 4.22. Emissions from the hybrid plant in the future periods with different battery and charging combinations

Period	Emissions	C1	C2	C3	WHRS1	WHRS2	WHRS3
1 year	CO_2	12726.172	12605.199	12626.850	11183.727	10987.016	10988.148
	CH_4	0.243	0.240	0.241	0.213	0.210	0.210
	N_2O	0.607	0.601	0.602	0.533	0.524	0.524
	NO_x	373.469	369.919	370.554	328.203	322.431	322.464
	NMVOC	12.458	12.340	12.361	10.948	10.756	10.757
	CO	11.204	11.098	11.117	9.846	9.673	9.674
	PM_{10}	8.682	8.600	8.615	7.630	7.496	7.497
	SO_2	79.887	79.128	79.264	70.205	68.970	68.977
5 years	CO_2	32059.213	31856.939	31894.860	27472.238	26980.088	26998.062
	CH_4	0.611	0.608	0.608	0.524	0.515	0.515
	N_2O	1.528	1.519	1.521	1.310	1.286	1.287
	NO_x	940.826	934.890	936.003	806.214	791.772	792.299
	NMVOC	31.385	31.187	31.224	26.894	26.412	26.430
	CO	28.226	28.048	28.081	24.187	23.754	23.770
	PM_{10}	21.872	21.734	21.760	18.743	18.407	18.419
	SO_2	201.249	199.979	200.217	172.455	169.365	169.478
10 years	CO_2	56157.394	55853.779	55911.982	47775.483	46915.076	46954.043
	CH_4	1.071	1.065	1.066	0.911	0.895	0.895
	N_2O	2.677	2.663	2.666	2.278	2.237	2.239
	NO_x	1648.024	1639.114	1640.822	1402.044	1376.794	1377.937
	NMVOC	54.976	54.679	54.736	46.770	45.928	45.966
	CO	49.442	49.175	49.226	42.063	41.305	41.340
	PM_{10}	38.313	38.106	38.146	32.595	32.008	32.034
	SO_2	352.523	350.617	350.983	299.906	294.505	294.750
20 years	CO_2	104298.737	103792.672	103891.393	88335.620	86739.539	86820.443
	CH_4	1.989	1.979	1.981	1.685	1.654	1.656
	N_2O	4.973	4.948	4.953	4.212	4.135	4.139
	NO_x	3060.804	3045.953	3048.850	2592.342	2545.503	2547.877
	NMVOC	102.104	101.609	101.705	86.477	84.914	84.994
	CO	91.827	91.382	91.469	77.773	76.368	76.439
	PM_{10}	71.158	70.813	70.880	60.267	59.178	59.233
	SO_2	654.726	651.550	652.169	554.519	544.500	545.008

The FC predictions were carried out with an assumption that the route of the ship remains like the simulation conditions in the future periods. The utilization times and their percentages were illustrated in previous sections. The FC estimations about the hybridization of the ship power distribution system provided up to 1468.737 t of FS for the first charging strategy, 6888.969 of FS for the second strategy in the system lifetime. These savings can lead to lesser production of air pollutants based on fossil fuel usages. According to emission calculations shown in Tables 4.22 and 4.23, during the total lifetime of the plant, the battery pack addition alone can reduce up to 4620.941 t of CO2, 135.609 t of NOx, and 29.008 t of SO2. When the WHRS is added to the system, 21674.075 t of CO2, 636.059 t of NOx, and 136.057 t of SO2 can potentially

be reduced in 20 years. The emission reduction with the WHRS charge strategy is outstanding compared to generator charging for the selected ship. For a fast applicable system, the FS and ER ratios are satisfying according to calculations and forecasts. The WHRS addition increases these ratios remarkably due to providing higher utilization time.

Table 4.23. Emission reductions of hybrid plants in the future periods with various battery and charging combinations

Period	Emissions	C1	C2	C3	WHRS1	WHRS2	WHRS3
1 year	CO_2	873.077	994.050	972.400	2415.522	2612.233	2611.101
	CH_4	0.017	0.019	0.019	0.046	0.050	0.050
	N_2O	0.042	0.047	0.046	0.115	0.125	0.124
	NO_x	25.622	29.172	28.537	70.887	76.660	76.627
	NMVOC	0.855	0.973	0.952	2.365	2.557	2.556
	CO	0.769	0.875	0.856	2.127	2.300	2.299
	PM_{10}	0.596	0.678	0.663	1.648	1.782	1.781
	SO_2	5.481	6.240	6.104	15.163	16.398	16.391
5 years	CO_2	1557.494	1759.769	1721.847	6144.470	6636.619	6618.646
	CH_4	0.030	0.034	0.033	0.117	0.127	0.126
	N_2O	0.074	0.084	0.082	0.293	0.316	0.316
	NO_x	45.707	51.643	50.530	180.319	194.762	194.234
	NMVOC	1.525	1.723	1.686	6.015	6.497	6.479
	CO	1.371	1.549	1.516	5.410	5.843	5.827
	PM_{10}	1.063	1.201	1.175	4.192	4.528	4.516
	SO_2	9.777	11.047	10.809	38.571	41.661	41.548
10 years	CO_2	2410.604	2714.219	2656.016	10792.515	11652.922	11613.955
	CH_4	0.046	0.052	0.051	0.206	0.222	0.221
	N_2O	0.115	0.129	0.127	0.515	0.556	0.554
	NO_x	70.743	79.653	77.945	316.723	341.973	340.829
	NMVOC	2.360	2.657	2.600	10.565	11.408	11.370
	CO	2.122	2.390	2.338	9.502	10.260	10.225
	PM_{10}	1.645	1.852	1.812	7.363	7.950	7.924
	SO_2	15.132	17.038	16.673	67.749	73.150	72.906
20 years	CO_2	4114.876	4620.941	4522.220	20077.993	21674.075	21593.170
	CH_4	0.078	0.088	0.086	0.383	0.413	0.412
	N_2O	0.196	0.220	0.216	0.957	1.033	1.029
	NO_x	120.757	135.609	132.711	589.219	636.059	633.684
	NMVOC	4.028	4.524	4.427	19.656	21.218	21.139
	CO	3.623	4.068	3.981	17.677	19.082	19.011
	PM_{10}	2.807	3.153	3.085	13.698	14.787	14.732
	SO_2	25.831	29.008	28.388	126.038	136.057	135.549

4.4.2 Results of the SoH Prediction

The SoH of the batteries was computed in every iteration for each battery combination and charging strategy between the date range that the data is valid. The OLS regression was performed to determine the battery life of each situation using the calculated SoH. The battery life parameter is a key factor in economic feasibility analyses of the systems. Figure 4.28 demonstrates the actual and predicted data fitting curves of each combination's data set. Table 4.24 depicts the performance of the regression algorithm metrics and battery lives for each combination. Battery lifetimes are estimated slightly lower for the generator charging strategy. Since the electricity produced by WHRS during the loading and unloading operations support the batteries, the discharge operation of batteries can be done with lower C-rates. This situation led to an increment in the battery lifetimes when the WHRS is used in the system.

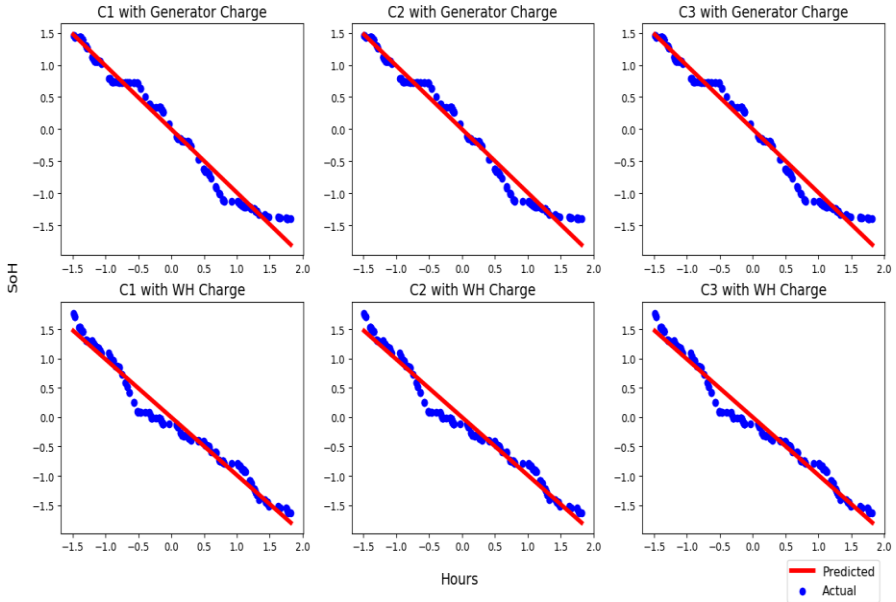


Figure 4.28 Analogy of SoH actual and predicted data for OLS

Table 4.24 Performance metrics of OLS for SoH Prediction and battery life regarding combinations

Charge Type	**Generator**			**WHRS**		
Combination	C1	C2	C3	C1	C2	C3
R^2	0.979	0.979	0.979	0.977	0.977	0.977
RMSE	0.003	0.003	0.003	0.002	0.002	0.002
MAE	0.003	0.002	0.002	0.002	0.002	0.002
SoH end of 1.5 years	0.925	0.936	0.936	0.944	0.952	0.952
Battery Life	3.910	4.550	4.550	5.600	6.550	6.540

4.5 Results of the Economic Analysis

The economic evaluation of the hybrid plant is required since different battery combinations selected by MCDA methods with two different charging strategies were modeled. The proposed systems' focuses were the lower weight and volume because of ease of the application onboard. Therefore, the main purpose of configurations is to support the ship electricity generation plant during the various operations. The simulation of the hybrid and normal plants calculated the FC of each combination with two charging strategies. Using the date-based fuel information, the total fuel price spent in the normal operation and hybrid operations was calculated. The fuel price of the normal operation was 1045916.457 USD, total electricity production was 13005724.85 kWh and electricity production cost (EPC) onboard was calculated as 0.080419697. The money spent on fuel, fuel cost reduction, investment costs, and maintenance costs of combinations were illustrated in Table 4.25. For the generator charge C1, C2, and C3, for the WHRS charge WHRS1, WHRS2, WHRS3 annotations were used. Battery costs were depicted in the previous section and WHRS costs were explained as 2000 USD/kW (Sachitanand, 2017; Pallis et al., 2021) explained in the previous chapter. Maintenance costs were 1.5% of the investment costs (Wei et al., 2019).

Table 4.25 Fuel, investment, and maintenance costs of combinations (Units are depicted as USD)

Combination	Fuel Cost	Fuel Cost Reduction	Investment Cost	Maintenance Cost
C1	970578.9909	75337.4661	425600	6384
C2	958922.0846	86994.37233	566720	8500.8
C3	960996.2634	84920.1935	466400	6996
WHRS1	860338.9674	185577.4896	725600	10884
WHRS2	843293.7308	202622.7262	866720	13000.8
WHRS3	842871.1441	203045.3129	766400	11496

EPC of each combination was calculated with the division of total fuel cost to total electricity production to observe how much a combination can lower the cost. Figure 4.29 indicates the EPC values for each combination. The lowest values were achieved with WHRS3 and WHRS2. LEC is another indicator of the economic analysis, and it was calculated for each battery set as well. Figure 4.30 demonstrates the LEC parameters and WHRS3 has the lowest value compared to others.

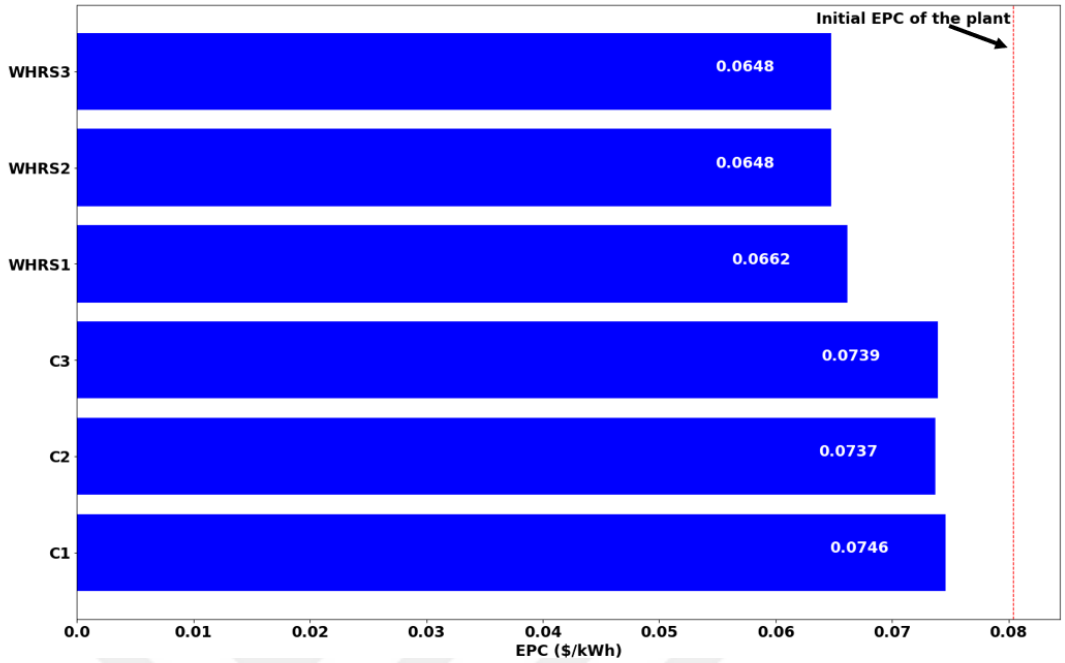


Figure 4.29 EPC of each combination

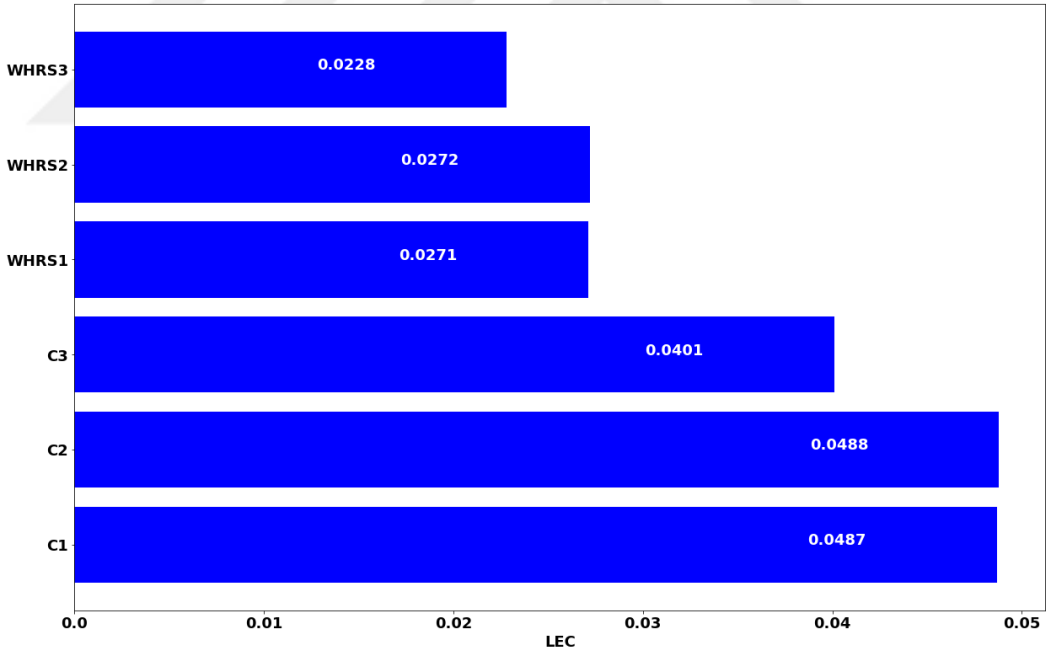


Figure 4.30 LEC of each combination

The LEC and EPC values indicated that the WHRS3 has the advantage compared to other combinations. However, the battery life and PBP is an indicator for this system. If the PBP is remarkably higher than battery life, it won't be a feasible system. In the economic analysis, it was assumed that when the SoH of batteries falls to 80%,

they are replaced with a new set. The possible variations of the fuel and battery prices in the future periods were disregarded for lifetime calculations. Figure 4.31 illustrates the PBP, and battery lives of each combination. Table 4.26 depicts the lifetime possible profits and losses.

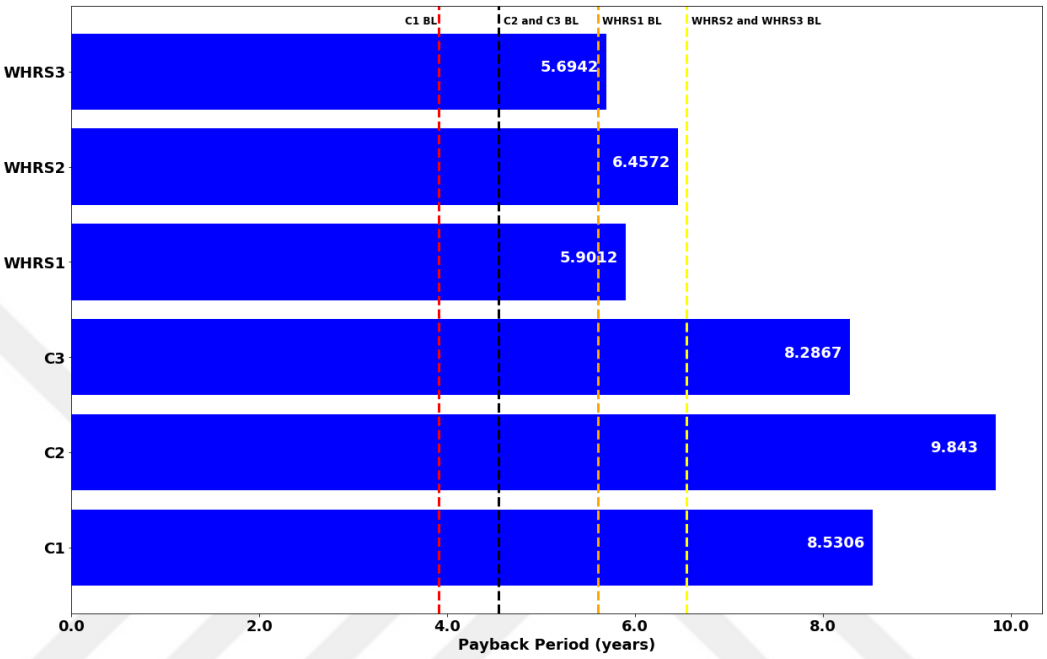


Figure 4.31 PBP of each combination

Table 4.26 Profits and losses of combinations during the system lifetime

Combination	Lifetime Profit/Loss	Interest Profit	Net Profit/Loss
C1	-1169087.705	93712.881	-1262800.586
C2	-1328491.656	124786.0994	-1453277.756
C3	-912614.0011	102696.6346	-1015310.636
WHRS1	945466.0116	159769.893	785696.1186
WHRS2	960765.8647	190843.1114	769922.7533
WHRS3	1272734.134	168753.6466	1103980.487

PBPs of WHRS charge and battery combinations vary between 5.5 and 6.5 years that complies with battery life estimations. Figure 4.31 demonstrates this phenomenon, the orange line is the battery life of WHRS1, and the yellow line indicates the battery lives of WHRS2 and WHRS3. This provides the lifetime profits for these combinations can be seen in Table 4.21. When the generators are used for charging, PBBs increase up to 10 years and battery lives are slightly lower compared to WHRS charging which makes the charging style non-profitable. In Figure 4.31, the red line represents the battery life for C1, and the black line is the battery life for C2 and C3. The most

applicable battery combination is C3 with WHRS charging support that was the top picks of TOPSIS and MOORA-Ratio. The generator charging strategy is not suitable for the oceangoing tanker vessel due to the low usage rate. This method can be more feasible for service vessels and ships that spent most of their time in port areas.

CHAPTER 5
CONCLUSIONS

The goal of the thesis was to evaluate the battery set addition to the ship power generation system to support the system with a cleaner energy system that can reduce fossil fuel-based emissions and provide economic profit. The main idea is to target loading and unloading operations that require running two or more generators. During these operations, additional power potential can be used to charge batteries. When the batteries are charged, they can provide the accumulated power to the system, and this can help to reduce the load and number of working generators. To carry through this analysis, the mathematical model of the plant was constructed in the MATLAB and Python environments. The required technical and operational data to form the model was collected from an oceangoing tanker. The selected ship type was determined as a tanker due to higher load demands during the cargo operations. Between the available dates, the model of the system was run, and the results of analyses were depicted and evaluated. To involve the battery support in the simulation, various batteries and their combinations were decided. Considering the limited space in a tanker ship, the battery set was designed to support rather than take on the entire system load. It was observed that a larger system can negatively impact the FC and CH-DH have an important role in both battery life and FS. Widely used MCDA methods were ranked every battery combination and as a result, three combinations were added to the model. Two different charging strategies were applied and the impact of each was assessed. The FS of each combination and related ER values were demonstrated and discussed. The FS and ER potentials were estimated using OLS determined with a detailed comparison. SoH of each battery was calculated for different charging strategies and predicted using OLS. Then finally economic analysis of the proposed system was performed to decide which charging strategy and battery combination are the most feasible.

The main conclusions derived from this thesis can be listed as:

- The utilization times of the ship were distributed as 65% navigation and 35% port and harbor operations. The shipping route was involved mainly

oceangoing voyages. In March and April 2020, the ship stayed in the harbor with the cargo because of the Covid-19 pandemic. During this process, the fuel prices were lowered significantly. These factors affected the outputs of the model calculations and the economic analysis.

- The electricity generation plant of the ship produced an attention-grabbing amount of emission for 1.5 years. For this ship, the air pollutants were mainly produced during navigation.
- Among the proposed battery charging methods, using generators as the source is not applicable for operations that require only one generator. Operations like cargo loading-unloading and navigation with heating requiring cargo need two or more generators and this charging strategy becomes useful. The larger battery plants than MCDA methods were found, which can negatively affect the FC. The optimal battery pack support was nearly 25% of a generator's total power. In addition, because of longer navigation and harbor times explained in the first item, the usage rate of the hybrid has decreased to 43.67%. The ratio was slightly higher than the port and harbor operations' ratio since the ship carried heating requiring cargo in a considerable amount of time. Despite the low usage time of the hybrid plant, the proposed charging strategy reduced the FC between 7.459% and 8.618% depending on the battery combination. The results complied with a similar study (Peralta et al., 2019) with the same charging strategy applied on a container vessel. These FS ratios led to lower emissions as well. This charging strategy can be more suitable for the ships that spent more time in port operations or service ships. The advantage of the strategy lies in the easy application, low space, and low cost. The selected battery plants occupy a place equal to a small room and their weights are very low compared to other types of machinery in the engine room. The costs and installation are not challenging. If the vessel's route and operations are suitable, it can provide more FS.
- The second charging strategy involves the addition of a WHRS to support generators for charging batteries. The selected WHRS is a commercial product that has been installed on ships. The other important specification of this system is the lower cost compared to traditional Organic Rankine Cycle-based

systems. The thesis focuses on the fast applicable FS strategies for the plant and the WHRS complies with this aim. The WHRS usage improved the FS up to 18.145% regarding the battery combination because the hybrid plant utilization time was increased to 100%. The WHRS addition provided a satisfactory improvement at a low cost. Another effect of WHRS usage can be seen on battery lifetimes. During the port and harbor operations, generators based on WH were used to produce electricity. This electricity was used to support battery charging and discharging periods. Thanks to additional power, batteries can be used at lower C-rates, or their discharge times were extended. This situation improved the battery life according to calculations and estimations.

- Although EPC was lowered slightly using generators for charging was not feasible for this ship type because of the aforementioned reasons. All three combinations caused financial losses due to higher PBPs and lower battery lifetimes. However, environmentally, they provided a considerable amount of ER. WHRS charging strategy for an oceangoing tanker was the economically applicable way to provide hybridization of the plant. All three combinations were economically feasible. PBBs of each combination were suitable with their battery lives so they ensured the profit. The third battery combination with WHRS charge selected by TOPSIS and MOORA-Ratio promised the most profit, FS and ER among all.
- The FC and ER estimations for the hybrid plant lifetime demonstrated that both charging strategies provide a remarkable positive environmental impact. The WHRS addition increases this benefit for this vessel. The environmental advantage can be increased with the green ports in the shore areas, but this approach needs more time and investment. The proposed strategies are currently available to apply onboard and lower emissions immediately.

The conclusions of this thesis. can be useful for:

- Shipowners and investors seeking to reduce shipping emissions to comply with the regulations.

- Researchers who deal with ship electricity generation plants and manufacturers of marine diesel generators.
- Researchers who are interested in the reduction of marine-based emissions.
- Authorities who deal with lowering the shipping emission in their responsible areas.

Some limitations and assumptions have existed for the study and the mathematical models. These are listed as:

- The operational load needs were gathered from the ship trials data, and they were assumed steady during the operations. The sudden load requirements or unsteady load changes were neglected. For example, during navigation, the fire pump can be operated, and it will increase the load of the generators. This kind of change was ignored for the lack of data.
- The maneuvering times and loads were neglected due to lack of information.
- The cargo discharge operations were limited to 24 hours according to the observations during the data collection process.
- The Pandemic conditions affected data collection and the simulation's calculations.

The recommendations for future studies on the topic of hybrid marine diesel generator plants are given below.

- In the thesis, the mathematical model was constructed using the electrical load tests from ship trials. The load of the system can be tracked in a sequence of times and the electrical load section can be simulated using this data in future studies.
- An oceangoing oil/chemical tanker was selected as a reference ship in the study. The chosen ship has limited port time and its utilization time was vastly passed during the navigation. Similar analyses can be carried out for a ship that spends more time in the port area or a service ship. The performance of the first charging strategy can more precisely be evaluated with such an investigation.
- The proposed system was designed for existing ships and its focus was a fast application and low required area. On the other hand, an analysis can be formed

about a larger battery support system for a ship that has the necessary space for the application.

- WHRS system was designed to utilize exhaust WH to generate electricity in the thesis. By considering other WH sources onboard, more electricity production can be achieved for this strategy. Especially, cruise ships have a great potential for this subject. An analysis of these subjects can be assessed in future studies.
- The suitable battery combination was determined firstly using MADM methods and then economic analysis yielded the best combination. A metaheuristic optimization algorithm that minimizes cost, weight, and FC can be used for this purpose.

REFERENCES

Al-Falahi, M., Tarasiuk, T., Jayasinghe, S., Jin, Z., Enshaei, H., & Guerrero, J. (2018). AC ship microgrids: control and power management optimization. *Energies*, *11*(6), 1458.

Al-suod, M. M. S., Alexander, U. O., & Olga, D. I. (2015). Optimization of the structure of diesel-generator units of ship power system. *International Journal of Advanced Computer Research*, *5*(18), 68.

American Bureau of Shipping. 2013. S*hip energy efficiency measures: Status and guidance.* Houston: ABS.

Anan, T., Higuchi, H., & Hamada, N. (2017). New artificial intelligence technology improving fuel efficiency and reducing CO_2 emissions of ships through use of operational big data. *Fujitsu Scientific & Technical Journal*. J, *53*, 23-28.

Ancona, M. A., Baldi, F., Bianchi, M., Branchini, L., Melino, F., Peretto, A., & Rosati, J. (2018). Efficiency improvement on a cruise ship: Load allocation optimization. *Energy Conversion and Management*, *164*, 42-58.

Ashari, M., & Nayar, C. V. (1999). An optimum dispatch strategy using set points for a photovoltaic (PV)–diesel–battery hybrid power system. *Solar Energy*, *66*(1), 1-9.

Attah, E. E., & Bucknall, R. (2015). An analysis of the energy efficiency of LNG ships powering options using the EEDI. *Ocean Engineering*, *110*, 62-74.

Awad M., & Khanna R. (2015) *Support vector regression in: Efficient learning machines.* Berkeley: Apress.

Bal Besikci, E., Arslan, O., Turan, O., et al., (2016). An artificial neural network based decision support system for energy efficient ship operations. *Computers & Operations Research. 66*, 393–401.

Baldi, F., Gabrielii, C., Melino, F., & Bianchi, M. (2015). A preliminary study on the application of thermal storage to merchant ships. *Energy Procedia*, *75*, 2169-2174.

Baldi, F., Ahlgren, F., Melino, F., Gabrielii, C., & Andersson, K. (2016). Optimal load allocation of complex ship power plants. *Energy Conversion and Management*, *124*, 344-356.

Bassam, A. M., Phillips, A. B., Turnock, S. R., & Wilson, P. A. (2017). Development of a multi-scheme energy management strategy for a hybrid fuel cell driven passenger ship. *International Journal of Hydrogen Energy*, *42*(1), 623-635.

Behzadian, M., Kazemzadeh, R. B., Albadvi, A., & Aghdasi, M. (2010). PROMETHEE: A comprehensive literature review on methodologies and applications. *European journal of Operational research*, *200*(1), 198-215.

Bellache, K., Camara, M. B., & Dakyo, B. (2015). Hybrid Electric Boat based on variable speed Diesel Generator and lithium-battery-using frequency approach for energy management. *In 2015 Intl Aegean Conference on Electrical Machines & Power Electronics (ACEMP), 2015 Intl Conference on Optimization of Electrical & Electronic Equipment (OPTIM) & 2015 Intl Symposium on Advanced Electromechanical Motion Systems (ELECTROMOTION)* (pp. 744-749). IEEE

Bialystocki, N., & Konovessis, D. (2016). On the estimation of ship's fuel consumption and speed curve: A statistical approach. *Journal of Ocean Engineering and Science*, *1*(2), 157-166.

Bilgili, L., Çelebi, U., Alkan, G., Caglak, S., & Koralturk, G. (2014). Comparison of different ship emission estimation methodologies for annual emission footprint and

reduction techniques of a bulk carrier. *Fresenius Environmental Bulletin, 23* (7), 1497-1509

Bilgili, L., & Çelebi, U. (2015). Emission estimation of cargo ships according to ship main dimensions and annual emission footprint calculation. *Fresenius Environmental Bulletin 24*(3), 1054-1062

Bolbot V, Trivyza NL, Theotokatos G, Boulougouris E, Rentizelas A, & Vassalos D. (2020) Cruise ships power plant optimisation and comparative analysis, *Energy 196*, 117061.

Boldea, I. (2015). *Synchronous generators* (2nd ed.). Boca Raton: CRC Press.

Box, G. E., Jenkins, G. M., Reinsel, G. C., & Ljung, G. M. (2015). *Time series analysis: forecasting and control*. New Jersey: John Wiley & Sons.

Brans, J. P., & De Smet, Y. (2016). PROMETHEE methods. *In Multiple criteria decision analysis* (pp. 187-219). New York: Springer.

Brauers, W.K.M., & Zavadskas, E.K. (2006). The MOORA Method and Its Application to Privatization in a Transition Economy. *Control and Cybernetics*, *35*(2), 445-469.

Brownlee J. (2017). *A Gentle Introduction to the Random Walk for Times Series Forecasting with Python*. Retrieved 22 January 2021, from https://machinelearningmastery.com/gentle-introduction-random-walk-times-series-forecasting-python/

Brownlee J. (2017). *White Noise Time Series with Python*. Retrieved 22 January 2021, from https://machinelearningmastery.com/white-noise-time-seriespython/#:~:text=A%20time%20series%20is%20white%20noise%20if%20the%20variables%20are,other%20values%20in%20the%20series.

Brownlee, J. (2020). *Introduction to time series forecasting with python: how to prepare data and develop models to predict the future*. New York: Machine Learning Mastery.

Chang, C. C. (2016). Causal analysis of carbon emissions, deadweight tonnage of global shipping fleet, fuel oil consumption, and economic activities in marine transportation. *Energy Sources, Part B: Economics, Planning, and Policy*, *11*(4), 303-308.

Chapman, S. (2005). Electric machinery fundamentals. New York: Tata McGraw-hill.

Cheng-Min F., & Wang R. (2001). Considering the financial ratios on the performance evaluation of highway bus industry, *Transport Reviews*, *21* (4), 449-467.

Cision. (2015). *Climeon's groundbreaking heat-power solution wins prestigious award for marine energy savings*. Retrieved May 29, 2021, from https://news.cision.com/climeon/r/climeon-s-groundbreaking-heat-power-solution-wins-prestigious-award-for-marine-energy-savings,c9872748.

Climeon, (2021). *How it works?* Retrieved 21, June 2021 from https://climeon.com/how-it-works/

Ekmekçioğlu, A. (2019). Ship emission estimation for Izmir and Mersin international ports–Turkey. *Journal of Thermal Engineering*, *5*(6), 184-195.

EC, (2020), 2019 A*nnual Report on CO_2 Emissions from Maritime Transport*. Retrieved September 24, 2021, from https://ec.europa.eu/info/sites/default/files/fueleu_maritime__green_european_maritime_space.pdf

Encyclopedia (2019). *Ordinary Least Squares Regression*. Retrieved September 24, 2021, from https://www.encyclopedia.com/social-sciences/applied-and-social-sciences-magazines/ordinary-least-squares-regression

Cahyagi, D., & Koenhardono, E. S. (2018). Study of shipboard power distribution system: Review on an aplication of ac zonal distribution. *IPTEK The Journal of Engineering*, *4*(1).

Capezza, C., Coleman, S., Lepore, A., Palumbo, B., & Vitiello, L. (2019). Ship fuel consumption monitoring and fault detection via partial least squares and control charts of navigation data. *Transportation Research Part D: Transport and Environment*, *67*, 375-387.

Cepowski, T., & Drozd, A. (2017). Interim fuel consumption estimation based on ship service parameters in real weather conditions with the use of ndCurveMaster curve fitting software. *Zeszyty Naukowe Akademii Morskiej w Szczecinie*.

Chai, T., and Draxler, R. R. (2014). Root mean square error (RMSE) or mean absolute error (MAE)? Arguments against avoiding RMSE in the literature. *Geoscientific model development*, *7*(3), 1247-1250.

Cheng, P., Liang, N., Li, R., Lan, H., & Cheng, Q. (2020). Analysis of Influence of Ship Roll on Ship Power System with Renewable Energy. *Energies*, *13*(1), 1.

Cooper, D. A. (2003). Exhaust emissions from ships at berth. *Atmospheric Environment*, *37*(27), 3817-3830.

Demirci, A., and Karagüzel, M. (2018). The evaluation of fishing vessels fuel consumption and pollutions emissions in the Iskenderun Bay. *Fresenius Environmental Bulletin*, *27*(1), 508-514.

Dolatabadi, A., Ebadi, R., & Mohammadi-Ivatloo, B. (2019). A two-stage stochastic programming model for the optimal sizing of hybrid PV/diesel/battery in hybrid electric ship system. *Journal of Operation and Automation in Power Engineering, 7*(1), 16-26.

Dragović, B., Tzannatos, E., Tselentis, V., Meštrović, R., & Škurić, M. (2018). Ship emissions and their externalities in cruise ports. *Transportation Research Part D: Transport and Environment, 61,* 289-300.

Dreyfus G. 2005. *Neural networks: methodology and applications*. Berlin: Springer Science & Business Media.

Ekmekçioğlu, A., Ünlügençoğlu, K., & Çelebi, U. B. (2021). Container ship emission estimation model for the concept of green port in Turkey. *Proceedings of the Institution of Mechanical Engineers, Part M: Journal of Engineering for the Maritime Environment,* 14750902211024453.

Elsayed, A. T., & Mohammed, O. A. (2015). A comparative study on the optimal combination of hybrid energy storage system for ship power systems. *In 2015 IEEE Electric Ship Technologies Symposium (ESTS)* (pp. 140-144).

Endresen, Ø., Sørgård, E., Behrens, H. L., Brett, P. O., & Isaksen, I. S. (2007). A historical reconstruction of ships' fuel consumption and emissions. *Journal of Geophysical Research: Atmospheres, 112*(D12).

Endresen, Ø., Bakke, J., Sørgård, E., Berglen, T. F., & Holmvang, P. (2005). Improved modelling of ship SO2 emissions—a fuel-based approach. *Atmospheric Environment, 39*(20), 3621-3628.

Eyring, V., Köhler, H. W., & Aardenne, J. van, Lauer, A., (2005). Emissions from international shipping: 1. The last 50 years. *Journal of Geophysical Research: Atmospheres, 110*(D17).

Fabozzi F.J, Focardi S.M, Rachev S.T., &. Arshanapalli B.G. (2014). *Model Selection Criterion: AIC and BIC*. New Jersey: John Wiley & Sons.

Fan, A., Wang, J., He, Y., Perčić, M., Vladimir, N., & Yang, L. (2021). Decarbonising inland ship power system: Alternative solution and assessment method. *Energy*, *226*, 120266.

Farag, Y. B., & Ölçer, A. I. (2020). The development of a ship performance model in varying operating conditions based on ANN and regression techniques. *Ocean Engineering*, *198*, 106972.

Frangopoulos, C. A. (2020). Developments, trends, and challenges in optimization of ship energy systems. *Applied Sciences*, *10*(13), 4639.

Gaber, M., Hamad, M. S., El-banna, S. H., & El-Dabah, M. (2021). An intelligent energy management system for ship hybrid power system based on renewable energy resources. *Journal of Al-Azhar University Engineering Sector*, *16*(60), 712-723.

Gaber, M., El-Banna, S., El-Dabah, M., & Hamad, M. (2021). Designing and implementation of an intelligent energy management system for electric ship power system based on adaptive neuro-fuzzy inference system (ANFIS). *Advances in Science, Technology and Engineering Systems Journal*, *6*(2), 195-203.

German–Galkin, S., Tarnapowicz, D., Matuszak, Z., & Jaskiewicz, M. (2020). Optimization to Limit the Effects of Underloaded Generator Sets in Stand-Alone Hybrid Ship Grids. *Energies*, *13*(3), 708.

Ghenai, C., Bettayeb, M., Brdjanin, B., & Hamid, A. K. (2019). Hybrid solar PV/PEM fuel cell/diesel generator power system for cruise ship: a case study in Stockholm, Sweden. *Case Studies in Thermal Engineering*, *14*, 100497.

Giannoutsos, S. V., & Manias, S. N. (2015). Energy management and D/G fuel consumption optimization in the power system of marine vessels through VFD-based process flow control. *In 2015 IEEE 15th International Conference on Environment and Electrical Engineering (EEEIC)* (pp. 842-850).

Gökdalay, M.H., (2009), "Havaalanlarının Performans Analizinde Bulanık Ölçütlü Karar Verme Yaklaşımı", *İstanbul Teknik Üniversitesi Mühendislik Dergisi*, *8* (6), 157-168.

Haseltalab, A., & Negenborn, R. R. (2017). Predictive on-board power management for all-electric ships with DC distribution architecture. *In Oceans 2017*-Aberdeen (pp. 1-8). IEEE.

Hu, Z., Jin, Y., Hu, Q., Sen, S., Zhou, T., & Osman, M. T. (2019). Prediction of fuel consumption for enroute ship based on machine learning. *IEEE Access*, *7*, 119497-119505.

Hu, Z., Zhou, T., Osman, M. T., Li, X., Jin, Y., & Zhen, R. (2021). A Novel Hybrid Fuel Consumption Prediction Model for Ocean-Going Container Ships Based on Sensor Data. *Journal of Marine Science and Engineering*, *9*(4), 449. MDPI AG.

Hulskotte, J. H. J., & Van Der Gon, H. D. (2010). Fuel consumption and associated emissions from seagoing ships at berth derived from an on-board survey. *Atmospheric Environment*, *44*(9), 1229-1236.

IMO, (2019), *IMO 2020 – cutting sulphur oxide emissions*. Retrieved September 24, 2021, from https://www.imo.org/en/MediaCentre/HotTopics/Pages/Sulphur-2020.aspx

IMO2, (2019), *Nitrogen Oxides (NOx) – Regulation 13*. Retrieved September 24, 2021, from https://www.imo.org/en/OurWork/Environment/Pages/Nitrogen-oxides-(NOx)-%E2%80%93-Regulation-13.aspx

IMO3, (2019) *Prevention of Air Pollution from Ships.* Retrieved September 24, 2021, from https://www.imo.org/en/OurWork/Environment/Pages/Air-Pollution.aspx

IMO4, (2014). *Third IMO Greenhouse Gas Study*. Executive summary and final report.

Işıklı, E., Aydın, N., Bilgili, L., & Toprak, A. (2020). Estimating fuel consumption in maritime transport. *Journal of Cleaner Production*, *275*, 124142.

Jaurola, M., Hedin, A., Tikkanen, S., & Huhtala, K. (2019). Optimising design and power management in energy-efficient marine vessel power systems: a literature review. *Journal of Marine Engineering & Technology*, *18*(2), 92-101.

Ji, C. (2021). Predicting Fuel Consumptions and Exhaust Gas Emissions for LNG Carriers via Machine Learning with Hyperparameter Optimization. *In SNAME 26th Offshore Symposium*. OnePetro.

Jia, J., & Dong, H. (2017). Research on ship power plant simulation system based on LabVIEW and MATLAB mixed programming. *In 2017 IEEE 2nd Information Technology, Networking, Electronic and Automation Control Conference (ITNEC)* (pp. 72-75). IEEE.

Karagiannidis, P., & Themelis, N. (2021). Data-driven modelling of ship propulsion and the effect of data pre-processing on the prediction of ship fuel consumption and speed loss. *Ocean Engineering*, *222*, 108616.

Karagiannidis, P., Themelis, N., Zaraphonitis, G., Spandonidis, C., & Giordamlis, C. (2019). Ship Fuel Consumption Prediction using Artificial Neural Networks. *In*

Proceedings of the Annual meeting of marine technology conference proceedings, Athens, Greece (pp. 46-51).

Karatug, Ç., & Durmusoglu, Y. (2020). Design of a solar photovoltaic system for a Ro-Ro ship and estimation of performance analysis: A case study. *Solar Energy*, *207*, 1259-1268.

Kasuya, E. (2019). *On the use of r and r squared in correlation and regression* (Vol. 34, No. 1, pp. 235-236). Hoboken: John Wiley & Sons, Inc.

Kee, K. K., Simon, B. Y. L., & Renco, K. H. Y. (2018). Prediction of ship fuel consumption and speed curve by using statistical method. *Journal of Computer Science & Computational Mathematics*, *8*(2), 19-24.

Kesgin, U., & Vardar, N. (2001). A study on exhaust gas emissions from ships in Turkish Straits. *Atmospheric Environment*, *35*(10), 1863-1870.

Kim, K. J., Lee, S. D., Jun, C. H., Park, K. M., & Byeon, S. S. (2017). A statistical procedure of analyzing container ship operation data for finding fuel consumption patterns. *The Korean Journal of Applied Statistics*, *30*(5), 633-645.

Kim, K.-S., & Roh, M.-I. (2020). ISO 15016:20S15-Based Method for Estimating the Fuel Oil Consumption of a Ship. *Journal of Marine Science and Engineering*, *8*(10), 791. MDPI AG.

Kim, Y.-R., Jung, M., and Park, J.-B. (2021). Development of a fuel consumption prediction model based on machine learning using ship in-service data. *Journal of Marine Science and Engineering*, *9*, 137.

Kingma, D. P., & Ba, J. (2014). Adam: A method for stochastic optimization. *arXiv*, 1412.6980.

Kirchgässner, G., & Wolters, J. (2007). *Introduction to modern time series analysis*. Berlin: Springer Science & Business Media.

Kistner, L., Bensmann, A., & Hanke-Rauschenbach, R. (2021). Optimal Design of Power Gradient Limited Solid Oxide Fuel Cell Systems with Hybrid Storage Support for Ship Applications. *Energy Conversion and Management*, 243, 114396.

Konur, O., Saatcioglu, O. Y., Korkmaz, S. A., Erdogan, A., & Colpan, C. O. (2020). Heat exchanger network design of an organic Rankine cycle integrated waste heat recovery system of a marine vessel using pinch point analysis. *International Journal of Energy Research*, *44*(15), 12312-12328.

Köseoğlu B. (2015). *Port modeling and applying optimization techniques* (book in Turkish). İzmir: Dokuz Eylul University.

Krause, P. C., Wasynczuk, O., Sudhoff, S. D., & Pekarek, S. (2002). *Analysis of electric machinery and drive systems* (2nd Ed.). New York: IEEE press.

Kumar, R., & Fozdar, M. (2017). Optimal sizing of hybrid ship power system using variants of particle swarm optimization. *In 2017 Recent Developments in Control, Automation & Power Engineering (RDCAPE)* (pp. 527-532). IEEE.

Kundakci, N. (2016). Combined multi-criteria decision making approach based on MACBETH and MULTI-MOORA methods. *Alphanumeric Journal*, *4*(1), 17-26.

Kusakana, K., & Vermaak, H. J. (2014). Hybrid diesel generator/renewable energy system performance modeling. *Renewable energy*, *67*, 97-102.

Kuzu, S. L., Bilgili, L., & Kilic, A., (2021). Estimation and dispersion analysis of shipping emissions in Bandirma Port, Turkey. *Environment, Development and Sustainability*, *23*(7), 10288-10308.

Lai, K., & Illindala, M. S. (2017). Design and planning strategy for energy storage system in a shipboard dc hybrid power system. *In 2017 IEEE/IAS 53rd Industrial and Commercial Power Systems Technical Conference (I&CPS)* (pp. 1-9). IEEE.

Lan, H., Bai, Y., Wen, S., Yu, D. C., Hong, Y. Y., Dai, J., & Cheng, P. (2016). Modeling and stability analysis of hybrid pv/diesel/ess in ship power system. *Inventions*, *1*(1), 5.

Lan, H., Wen, S., Hong, Y. Y., David, C. Y., & Zhang, L. (2015). Optimal sizing of hybrid PV/diesel/battery in ship power system. *Applied energy*, *158*, 26-34.

Le, L. T., Lee, G., Kim, H., & Woo, S. H. (2020). Voyage-based statistical fuel consumption models of ocean-going container ships in Korea. *Maritime Policy & Management*, *47*(3), 304-331.

Lee, J. B., Roh, M. I., & Kim, K. S. (2021). Prediction of ship power based on variation in deep feed-forward neural network. *International Journal of Naval Architecture and Ocean Engineering*, *13*, 641-649.

Leloup, R., Roncin, K., Behrel, M., Bles, G., Leroux, J. B., Jochum, C., & Parlier, Y. (2016). A continuous and analytical modeling for kites as auxiliary propulsion devoted to merchant ships, including fuel saving estimation. *Renewable Energy*, *86*, 483-496.

Lepore, A., dos Reis, M. S., Palumbo, B., Rendall, R., & Capezza, C. (2017). A comparison of advanced regression techniques for predicting ship CO_2 emissions. *Quality and Reliability Engineering International*, *33*(6), 1281-1292.

LGChem (2014) *Product Specification, Rechargeable Lithium Ion Battery Model: INR18650 MJ1 3500mAh.* Retrieved June 7, 2021, from https://birikimpilleri.net/Resim/900817503007_1.pdf

LGResu (2021), *RESU10H Prime*. Retrieved June 7, 2021, from https://www.lgessbattery.com/eu/home-battery/product-info.lg

Li J., Han Y., Mao G., and Wang P. (2020) Optimization of exhaust emissions from marine engine fueled with LNG/diesel using response surface methodology, Energy Sources, Part A: Recovery, *Utilization, and Environmental Effects*, *42*:12, 1436-1448,

Li, X., Zhu, Y., Zuo, Y., Li, T., & Chen, C. P. (2019). Prediction of ship fuel consumption based on broad learning system. *In 2019 International Conference on Security, Pattern Analysis, and Cybernetics (SPAC)* (pp. 54-58). IEEE.

Liu, J., & Duru, O. (2020). Bayesian probabilistic forecasting for ship emissions. *Atmospheric Environment*, *231*, 117540.

Lu, Z., Wang, X., & Xiao, J. (2021). Multi-Objective Optimization Method for Hybrid Ship Power System Capacity. *International Core Journal of Engineering*, *7*(5), 356-363.

Lundh, M., Garcia-Gabin, W., Tervo, K., & Lindkvist, R. (2016). Estimation and optimization of vessel fuel consumption. *IFAC-PapersOnLine*, *49*(23), 394-399.

M.A.N (2020). *CEAS (Computerized Engine Application System) engine calculation*. Retrieved October 20, 2020, from https://www.man-es.com/marine/products/planning-tools-and-downloads/ceas-engine-calculations

MarineTraffic, (2021) *Prevention of Air Pollution from Ships.* Retrieved September 24, 2021, from https://www.marinetraffic.com/en/ais/home/centerx:-12.0/centery:24.9/zoom:4

McGeorge, H. D. (1998). *Marine auxiliary machinery* (7th Ed.). Oxford: Elsevier.

Mersin, K., Alkan, G., & Mısırlıoğlu, T. (2017). A new method for calculating fuel consumption and displacement of a ship in maritime transport. *Cogent Engineering*, *4*(1), 1415107.

Mills, T. C. (2019). *Applied time series analysis: A practical guide to modeling and forecasting*. London: Academic Press.

Miola, A., & Ciuffo, B. (2011). Estimating air emissions from ships: Meta-analysis of modelling approaches and available data sources. *Atmospheric Environment*, *45*(13), 2242-2251.

Molicel (2018) *Approval sheet lithium-ion rechargeable battery*. Retrieved June 7, 2021, from https://birikimpilleri.net/Resim/900375503001_2.pdf.

Moreira, L., Vettor, R., & Guedes Soares, C. (2021). Neural Network Approach for Predicting Ship Speed and Fuel Consumption. *Journal of Marine Science and Engineering*, *9*(2), 119.

Motley, M. R., Nelson, M., & Young, Y. L. (2012). Integrated probabilistic design of marine propulsors to minimize lifetime fuel consumption. *Ocean Engineering*, *45*, 1-8.

Nichols, C. R., & Williams, R. G. (2009). *Encyclopedia of marine science*. Infobase Publishing: New York.

Nishida, T., Waseda, T., Katori, M., & Ohuchi, K. (2011). Optimization of integrated weather routing systems for sailing cargo ships. *In The Twenty-first International Offshore and Polar Engineering Conference*. International Society of Offshore and Polar Engineers.

Norstad, I., Fagerholt, K., & Laporte, G. (2011). Tramp ship routing and scheduling with speed optimization. *Transportation Research Part C: Emerging Technologies*, *19*(5), 853-865.

Nuchturee, C., Li, T., & Xia, H. (2020). Energy efficiency of integrated electric propulsion for ships–A review. *Renewable and Sustainable Energy Reviews*, *134*, 110145.

Odu, G. O. (2019). Weighting methods for multi-criteria decision making technique. *Journal of Applied Sciences and Environmental Management*, *23*(8), 1449-1457.

Omar, N., Monem, M. A., Firouz, Y., Salminen, J., Smekens, J., Hegazy, O., & Van Mierlo, J. (2014). Lithium iron phosphate-based battery–Assessment of the aging parameters and development of cycle life model. *Applied Energy*, *113*, 1575-1585.

Oways, (2019), *Electrical Distribution*. Retrieved September 28, 2021, from https://owaysonline.com/electrical-distribution/

Ovrum, E., & Bergh, T. F. (2015). Modelling lithium-ion battery hybrid ship crane operation. *Applied Energy*, *152*, 162-172.

Oztemel E. (2016). *Yapay sinir ağları* (4th ed) (book in Turkish). İstanbul: Ozkaracan Publishing, Papatya Bilim.

Özbek, A. (2015). Akademik birim yöneticilerinin moora yöntemiyle seçilmesi: Kırıkkale üzerine bir uygulama. *Erciyes Üniversitesi Sosyal Bilimler Enstitüsü Dergisi*, *1*(38), 1-18.

Pallis, P., Varvagiannis, E., Braimakis, K., Roumpedakis, T., Leontaritis, A. D., & Karellas, S. (2021). Development, experimental testing and techno-economic assessment of a fully automated marine organic rankine cycle prototype for jacket cooling water heat recovery. *Energy*, *228*, 120596.

Panasonic (2021) *Specifications for NCR18650GA*. Retrieved June 7, 2021, from https://birikimpilleri.net/Resim/900095503030_1.pdf

Peralta, P., César, O., Vieira, G. T., Meunier, S., Vale, R. J., Salles, M. B., & Carmo, B. S. (2019). Evaluation of the CO_2 Emissions Reduction Potential of Li-ion Batteries in Ship Power Systems. *Energies*, *12*(3), 375.

Perez, H. M., Chang, R., Billings, R., & Kosub, T. L. (2009). Automatic identification systems (AIS) data use in marine vessel emission estimation. *In 18th Annual International Emission Inventory Conference* (Vol. 14, p. e17).

Phua M.H. & Minowa M., (2005). A GIS-Based Multi-Criteria Decision-Making Approach to Forest Conservation Planning at A Landscape Scale: A Case Study in The Kinabalu Area, Sabah, Malaysia. *Landscape and Urban Planning*, 71: 207–222.

PowerXtra (2021), *Power-Xtra PX18650-32E - 3.7V 3200 Mah Li-ion Battery- 3C*. Retrieved June 7, 2021, from https://birikimpilleri.net/Resim/900600503339_1.pdf

Prpić-Oršić, J., and Faltinsen, O. M. (2012). Estimation of ship speed loss and associated CO2 emissions in a seaway. *Ocean Engineering*, *44*, 1-10.

Prpić-Oršić, J., Vettor, R., Faltinsen, O. M., & Soares, C. G. (2016). The influence of route choice and operating conditions on fuel consumption and CO 2 emission of ships. *Journal of Marine Science and Technology*, *21*(3), 434-457.

Pulkrabek, W. W. (2004). *Engineering fundamentals of the internal combustion engine* (2nd Ed.). London: Pearson.

Qiu, Y., Yuan, C., Tang, J., & Tang, X. (2019). Techno-economic analysis of PV systems integrated into ship power grid: A case study. *Energy Conversion and Management*, 198, 111925.

Radan, D., Johansen, T. A., Sorensen, A. J., & Adnanes, A. K. (2005). Optimization of load dependent start tables in marine power management systems with blackout prevention. *WSEAS Transactions on circuits and systems, 4*(12), 1861-1866.

Reis, M. S., Rendall, R., Palumbo, B., Lepore, A., & Capezza, C. (2020). Predicting ships' CO2 emissions using feature-oriented methods. *Applied Stochastic Models in Business and Industry*, *36*(1), 110-123.

Roh, Gilltae, Hansung Kim, Hyeonmin Jeon, & Kyoungkuk Yoon (2019). Fuel Consumption and CO_2 Emission Reductions of Ships Powered by a Fuel-Cell-Based Hybrid Power Source. *Journal of Marine Science and Engineering 7*, 230.

Sachitanand R. (2017) *Cheaper than solar PV? Why low temperature heat power makes sense.* Retrieved 18 October 2021 from https://climeon.com/cheaper-than-solar-pv-why-low-temperature-heat-power-makes-sense/.

Safaei, A. A., Ghassemi, H., & Ghiasi, M. (2019). VLCC's fuel consumption prediction modeling based on noon report and automatic identification system. *Cogent Engineering*, *6*(1), 1595292.

Salvi J. (2019). *Significance of ACF and PACF Plots in Time Series Analysis*. Retrieved 22 January 2021 from https://towardsdatascience.com/significance-of-acf-and-pacf-plots-in-time-series-analysis-2fa11a5d10a8

Ship&Bunker, (2021). *World Bunker Prices*. Retrieved 25 September 2021 from https://shipandbunker.com/prices.

Saxena, S., Hendricks, C., & Pecht, M. (2016). Cycle life testing and modeling of graphite/LiCoO2 cells under different state of charge ranges. *Journal of Power Sources, 327*, 394-400.

Seddiek, I. S., & Elgohary, M. M. (2014). Eco-friendly selection of ship emissions reduction strategies with emphasis on SOx and NOx emissions. International *Journal of Naval Architecture and Ocean Engineering*, *6*(3), 737-748.

Shannon, C. E. (1948). A mathematical theory of communication. *The Bell system technical journal*, *27*(3), 379-423.

Sharp, T. (2020). *An Introduction to Support Vector Regression (SVR).* Retrieved 18, October 2021 from https://towardsdatascience.com/an-introduction-to-support-vector-regression-svr-a3ebc1672c2

Shao, W., Zhou, P., & Thong, S. K. (2012). Development of a novel forward dynamic programming method for weather routing. *Journal Of Marine Science and Technology*, *17*(2), 239-251.

Shumway, R. H., & Stoffer, D. S. (2017). *Time series analysis and its applications: with R examples*. Berlin: Springer.

Simonsen, M., Walnum, H. J., & Gössling, S. (2018). Model for estimation of fuel consumption of cruise ships. *Energies*, *11*(5), 1059.

Sirimanne, S. N., Hoffman, J., Juan, W., Asariotis, R., Assaf, M., Ayala, G., & Youssef, F. (2019). *Review of maritime transport*. Retrieved 14 December 2021 from https://unece.org/fileadmin/DAM/cefact/cf_forums/2019_UK/PPT_L_L-UNCTAD-RMT.pdf.

SMA, 2021, *Sunny Central Storage*. Retrieved 21, June 2021, from https://www.sma.de/en/products/battery-inverters/sunny-central-storage-1900-2200-2475-2900.html

Soba, M., & Eren, K. (2011). Topsis yöntemini kullanarak finansal ve finansal olmayan oranlara göre performans değerlendirilmesi, şehirlerarasi otobüs sektöründe bir uygulama *Sosyal Ekonomik Araştırmalar Dergisi* , *11* (21) , 23-40 .

Styhre, L., Winnes, H., Black, J., Lee, J., & Le-Griffin, H., (2017). Greenhouse gas emissions from ships in ports – Case studies in four continents. *Transportation Research Part D: Transport and Environment*, *54*, 212-224.

Şenkayas, H., & Hekimoğlu, H. (2013). Çok kriterli tedarikçi seçimi problemine PROMETHEE yöntemi uygulaması. *Verimlilik Dergisi*, *2013*(2), 63-80.

Tang, D., Yan, X., Yuan, Y., Wang, K., & Qiu, L. (2015). Multi-agent based power and energy management system for hybrid ships. *In 2015 International Conference on Renewable Energy Research and Applications (ICRERA)* (pp. 383-387). IEEE.

Taylor, D. A. (1996). Introduction to marine engineering (2nd Ed.). Oxford: Butterworth-Heinemann.

Tesla (2019), *Powerwall*. Retrieved June 7, 2021, from, https://www.tesla.com/sites/default/files/pdfs/powerwall/Powerwall%202_AC_Datasheet_en_northamerica.pdf

Tian, Z., Zeng, W., Gu, B., Zhang, Y., & Yuan, X. (2021). Energy, exergy, and economic (3E) analysis of an organic Rankine cycle using zeotropic mixtures based on marine engine waste heat and LNG cold energy. *Energy Conversion and Management*, *228*, 113657.

Tichavska, M., & Tovar, B. (2015). Port-city exhaust emission model: An application to cruise and ferry operations in Las Palmas Port. *Transportation Research Part A: Policy and Practice*, *78*, 347-360.

Tien-Anh, T. (2021). Comparative analysis on the fuel consumption prediction model for bulk carriers from ship launching to current states based on sea trial data and machine learning technique. *Journal of Ocean Engineering and Science*. 6(4), 317-339

Tillig, F., & Ringsberg, J. W. (2019). A 4 DOF simulation model developed for fuel consumption prediction of ships at sea. *Ships and Offshore Structures, 14*(1), 112-120.

Trebuňa, P., Halčinová, J., Fil'o, M., & Markovič, J. (2014). The importance of normalization and standardization in the process of clustering. *In 2014 IEEE 12th International Symposium on Applied Machine Intelligence and Informatics (SAMI)* (pp. 381-385). IEEE.

Trivyza, N. L., Rentizelas, A., & Theotokatos, G. (2018). A novel multi-objective decision support method for ship energy systems synthesis to enhance sustainability. *Energy Conversion and Management*, *168*, 128-149.

Trozzi, C., (2010). Emission estimate methodology for maritime navigation. *In 19th International emission inventory conference*, San Antonio, USA.

Uyanik, T., Karatug, Ç., & Arslanoglu, Y. (2020). Machine learning approach to ship fuel consumption: A case of container vessel. *Transportation Research Part D: Transport and Environment*, *84*, 102389.

UNCTAD, (2018), *Review of Maritime Transport*. Retrieved 14 December 2021 from https://unctad.org/system/files/official-document/rmt2018_en.pdf.

Wang, S., Ji, B., Zhao, J., Liu, W., & Xu, T. (2018). Predicting ship fuel consumption based on LASSO regression. *Transportation Research Part D: Transport and Environment*, *65*, 817-824.

Wang, Z., Yang, Z., & Xiao, S. (2021). Research on Energy Efficiency Design Index Calculation Method for the Hybrid Ship. *Journal of Physics: Conference Series 2029* (1), 012087

Wei, F., Senchuang, G., & Zhonghe, H. (2019). Economic analysis of Organic Rankine Cycle (ORC) and Organic Rankine Cycle with internal heat exchanger (IORC) based on industrial waste heat source constraint. *Energy Procedia*, *158*, 2403-2408.

Wen, S., Lan, H., Hong, Y. Y., David, C. Y., Zhang, L., & Cheng, P. (2016). Allocation of ESS by interval optimization method considering impact of ship swinging on hybrid PV/diesel ship power system. *Applied Energy*, *175*, 158-167.

Winnes, H., Styhre, L., & Fridell, E. (2015). Reducing GHG emissions from ships in port areas. *Research in Transportation Business & Management*, *17*, 73-82.

Willmott, C. J., & Matsuura, K., (2005). Advantages of the mean absolute error (MAE) over the root mean square error (RMSE) in assessing average model performance. *Climate research*, *30*(1), 79-82.

Woodyard, D. (2009). *Pounder's marine diesel engines and gas turbines* (9th ed.). London: Butterworth-Heinemann.

Xie, G. (2011). Optimal preliminary propeller design based on multi-objective optimization approach. *Procedia Engineering*, *16*, 278-283.

Vittinghoff, E., Glidden, D. V., Shiboski, S. C., & McCulloch, C. E. (2006). *Regression methods in biostatistics: linear, logistic, survival, and repeated measures models*. New York: Springer.

Yan, J. (2021). The impact of climate policy on fossil fuel consumption: Evidence from the Regional Greenhouse Gas Initiative (RGGI). *Energy Economics*, 105333.

Yan, R., Mo, H., Wang, S., & Yang, D. (2021). Analysis and prediction of ship energy efficiency based on the MRV system. *Maritime Policy & Management*, 1-23.

Yang, L., Chen, G., Rytter, N. G. M., Zhao, J., & Yang, D. (2019). A genetic algorithm-based grey-box model for ship fuel consumption prediction towards sustainable shipping. *Annals of Operations Research*, 1-27.

Yao, S., Zhang, Y., & Yu, X. (2018). Thermo-economic analysis of a novel power generation system integrating a natural gas expansion plant with a geothermal ORC in Tianjin, *China. Energy*, *164*, 602-614.

Yau, P. S., Lee, S. C., Corbett, J. J., Wang, C., Cheng, Y., & Ho, K. F. (2012). Estimation of exhaust emission from ocean-going vessels in Hong Kong. *Science of the Total Environment*, *431*, 299-306.

Yüksel O. & Köseoğlu B. (2019) Modelling and performance prediction of a centrifugal cargo pump on a chemical tanker, *Journal of Marine Engineering & Technology*. *19*(4), 278-290.

Zardari, N. H., Ahmed, K., Shirazi, S. M., & Yusop, Z. B. (*2015). Weighting methods and their effects on multi-criteria decision-making model outcomes in water resources management*. New York: Springer.

Zhu, Y., Zhou, S., Feng, Y., Hu, Z., & Yuan, L. (2017). Influences of solar energy on the energy efficiency design index for new building ships. International Journal of *Hydrogen Energy*, *42*(30), 19389-19394.

Zhou, T., Hu, Q., Hu, Z., & Zhen, R. (2021). An adaptive hyper parameter tuning model for ship fuel consumption prediction under complex maritime environments. *Journal of Ocean Engineering and Science*. In Press, Journal Pre-proof.

Zhu, Y., Zuo, Y., & Li, T. (2021). Modeling of ship fuel consumption based on multisource and heterogeneous data: case study of passenger ship. *Journal of Marine Science and Engineering, 9(3)*, 273.

Zou, Z. H., Yi, Y., & Sun, J. N. (2006). Entropy method for determination of weight of evaluating indicators in fuzzy synthetic evaluation for water quality assessment. *Journal of Environmental Sciences, 18(5)*, 1020-1023.

.